

Formation of Methane and Carbon Dioxide Hydrates in Bulk and in Porous Media

Proefschrift

ter verkrijging van de graad van doctor
aan de Technische Universiteit Delft,
op gezag van de Rector Magnificus prof. ir. K.C.A.M. Luyben,
voorzitter van het College voor Promoties,
in het openbaar te verdedigen op woensdag 9 mei 2012 om 10:00 uur

door

Yuanyuan HE

Ingenieur in Applied Earth Science
geboren te GuanSu, China

Dit proefschrift is goedgekeurd door de promotor:

Prof.dr. P.L.J. Zitha

Copromotor:

Dr.ir. E.S.J. Rudolph-Flöter

Samenstelling promotiecommissie:

Rector Magnificus	voorzitter
Prof. dr. P.L.J. Zitha	Technische Universiteit Delft
Dr. ir. E.S.J. Rudolph-Flöter	Technische Universiteit Delft
Prof. dr. M. Golombok	Technische Universiteit Eindhoven, Shell Global Solutions B.V
Prof. dr. A. Graue	University of Bergen, Norway
Prof. dr. ir. T.J.H. Vlugt	Technische Universiteit Delft
Prof. dr.W.R. Rossen	Technische Universiteit Delft
Prof. dr. J. Bruining	Technische Universiteit Delft
Prof. dr. ir. Jansen	Technische Universiteit Delft

The research reported in this thesis has been sponsored by Shell International Exploration and Production B.V.

Typeset with L^AT_EX. Printed by WÖHRMANN PRINT SERVICE
Cover design: Fengbo ZHANG
ISBN: 978-94-6203-033-6

Copyright © 2012, Yuanyuan He, Delft, The Netherlands.
All rights reserved. No part of this book may be reproduced or transmitted in any form or by any means, electronic or mechanical, including photography, recording, or any information storage and retrieval system, without prior written permission of the author.

*To my family,
who love and support me
in every possible way*

Samenvatting

Gashydraatvorming is een kristallisatieproces. Dit proces bestaat uit twee fases, respectievelijk nucleatie (de vorming van nucleatie kernen) en hydraatgroei (de groei van kleine nucleatiekernen tot grote hydraatkristallen). Deze twee fases van het kristallisatieproces worden in het binaire systeem gekenmerkt door de nucleatietijd en de halfwaardetijd. De resultaten laten een afname zien in nucleatietijd naar mate oververzadiging en roersnelheid toenemen. Bovendien vermindert de nucleatietijd als gevolg van het geheugeneffect wanneer de experimenten worden uitgevoerd met ‘gebruikt’ water. Dit geheugeneffect is beschreven door andere auteurs [98, 149] en kan worden verklaard door het bestaan van (water) hydraatstructuren na dissociatie van gashydraten. De structurering van de watermoleculen is waarschijnlijk gewaarborgd door de overvloed aan waterstofbruggen in de waterfase bij lage temperaturen door de aanwezigheid van opgeloste gastmoleculen.

De tweede fase, de daadwerkelijke groei van gashydraten, bleek ongevoelig te zijn voor veranderingen in de mate van oververzadiging. De groei neemt toe met een verhoging van de roersnelheid; echter, het geheugeneffect van water heeft een licht negatief effect op de groei van het gashydraat. Daarom is niet nucleatie, maar kristalgroei de snelheidslimiterende stap tijdens gashydraatvorming. Uit experimenten in het binaire systeem bleek ook, dat, bij gelijke mate van oververzadiging, de kristalgroei van CO_2 hydraten sneller is dan van CH_4 hydraten. Dit wijst erop dat, kinetisch gezien, de vorming van CO_2 hydraten gunsitiger is dan de vorming van CH_4 hydraten. Bevindingen resulterend van experimenten in het ternaire systeem ondersteunen deze theorie.

In het ternaire systeem blijken bij iedere geteste initiële druk CO_2 moleculen makkelijker te vangen in kooien van watermoleculen dan CH_4 moleculen (Hoofdstuk 4). Ondanks dat de CH_4 concentratie in de gevormde gashydraten toeneemt met de initiële druk, bevatten de ontstane gashydraten nog steeds meer CO_2 dan CH_4 . De formatie van methaanhydraat bij lage druk (lager dan de evenwichtsdruk van de $H - Lw - V$ curve voor het $CH_4 + H_2O$ systeem) wordt bevestigd. Dit betekent dat de aanwezigheid van een ‘makkelijker’ gashydraatvormer, zoals CO_2 , er voor kan zorgen dat de CH_4 hydraat wordt gestabiliseerd. Experimenten, waarbij van een gasmix van 50/50 CH_4/CO_2 gashydraten worden gevormd, lieten zien dat de hoogste CH_4 en CO_2 scheidings efficiëntie wordt behaald bij een druk lager dan 3.5 MPa. Hierbij wordt in de gasfase een verandering van 18% van de initiële CH_4 molfractie gevonden.

Bulkexperimenten hebben tastbaar bewijs geleverd dat CH_4 in de al gevormde methaanhydraten kan worden uitgewisseld met CO_2 zonder dat er dissociatie van de gashydraten optreedt (Hoofdstuk 4). Echter, de vervanging vindt plaats op een zeer geringe diepte, vlakbij het scheidingsvlak tussen de gasfase en de gashydraten. Hierdoor functioneren CO_2 -rijke hydraatlagen als een schild en

belemmeren verdere penetratie van CO_2 in dieper gelegen methaanhydraatlagen en werken de migratiestroom van CH_4 naar de gasfase tegen. Ten gevolge hiervan is het noodzakelijk dat eerst dissociatie van de CO_2 hydraatlagen plaats vindt, alvorens er CH_4 vrij kan komen uit de lager gelegen gashydraatlagen. Als gevolg is een lagere druk dan de evenwichtsdruk nodig voor de dissociatie van de CH_4 hydraten.

De CO_2 hydratvorming werd ook bestudeerd in een kern bestaand uit gelijkde glazen kralen (Hoofdstuk 5). De vorming van gashydraat in dit poreuze medium werd voornamelijk waargenomen in het bovenste gedeelte van de horizontaal gepositioneerde kern waar gas en connaat water zich bevinden. In het onderste gedeelte van de kern, voornamelijk gevuld met de CO_2 verzadigde waterige vloeibare fase, werd een lokale distributie van gashydraatvorming geconstateerd, die moeilijk te detecteren valt op CT beelden. Drie verschillende regimes konden onderscheiden worden in het proces van gashydraat vorming: een reactie gelimiteerd regime, een diffusie gelimiteerd regime en een pre-evenwichtsregime. Uit de data komt naar voren dat de temperatuur en de snelheid waarmee het gas geïnjecteerd wordt weinig invloed hebben op de vorming van gashydraten.

Modelleren en numerieke simulaties van gelijktijdige methaanwinning en CO_2 injectie in een klasse II gashydraat accumulatie hebben aangetoond dat door injectie van CO_2 de productie van CH_4 stijgt in vergelijking tot de methaanproductie door alleen drukvermindering (Hoofdstuk 6). In het beste geval nam de totale CH_4 productie toe met 60% door de injectie van CO_2 . Ook kan uit de experimenten worden geconcludeerd dat CO_2 op een efficiënte wijze kan worden opgeslagen in de vorm van hydraten. Slechts 2 mol% van het geïnjecteerde CO_2 werd hergeproduceerd. Uit de simulaties blijkt dat CO_2 hydraten zich direct onder de lagen met CH_4 hydraten vormen; de warmte die vrij komt bij deze CO_2 hydraten formatie versterkt de verdere dissociatie van CH_4 gashydraten.

Acknowledgement

After more than four years of fight, I finally come to this last stage of my PhD. It is tough period but I'm happy that I managed. This is all because the people who helped and supported me during these years. I would like to address my greatest appreciation to them.

I would like to thank my promoter, Prof. Pacelli Zitha. I have been worked with you for more than 5 years since the last year of my master. your supervision guided and supported me through the whole project. I have learnt great deal from you not only on the subject, but also on other aspects, such as, writing, speaking and social skills. You trained me to be more confident and positive. When I was writing my final thesis, your strict requirements have improved my reasoning and writing greatly. I would never regret that I have chosen this subject and worked with you. I would also like to express my great thanks to Dr. Susanne Rudolph. Your daily supervision and support helped me a lot. I enjoyed very much the brainstorming discussions with you. Many new ideas were popped up and questions were solved during our meetings. You have taken care of every little details of my research and provided me with every possible help you could.

Beside my supervisors, I would also like to thank all my committee members for your precious time and carefully reading of my thesis. Particularly, I would like to address my gratitude to Prof. Michael Golombok. Thanks for introducing me some experts in my research area and inviting me to visit the Shell laboratory. I'm grateful for your suggestions and ideas that improved my final work. Of course, I would not forget your efforts on helping me to look to the future.

My research involved a lot work with experiments. Behind every data point, many names are concealed. I would like to express my thanks to Henk van Asten for saving me (many times) from frustrating repairing work of the set-ups. I will always remember your timely help. I enjoyed working with you. Henny van der Meulen, thank you for assembling my set-up and teach me some techniques on tubing connection. I will remember the 3 quarters turn of the nuts. I would like to thanks Frans Riem Vis for designing the set-ups for me. I want to thank Karel Heller and Gerard Mathu for helping me with experimental work, Adri Maijaar and Ellen Meijvogel for helping me with the CT-Scans, Joost Meel for microscopic experimental tests and Wim Verwaal for consulting the applications of Micro CT-Scan.

I should thank Roel Huneker, Medet Bazil and Mark Loerakker for your contributions to my project, and also thanks Mark for translating the summary of the thesis for me. Mariette van Tilburg: thank you very much for checking the language errors of my thesis. Your considerate and detailed comments improved the quality of my thesis. I need to express my thanks to Fengbo Zhang, a friend I never met, who designed the nice cover of my thesis.

I should also thank Prof. FAN Shuanshi and Prof. UCHIDA Takashi, although we only met during conference, but the nice discussion we had bring me some new knowledge and ideas. And I'm thankful for the papers you had send to me.

I need to thank my friends, without them my life in Holland will be so pale that I could not bear. Olivia, Farzad, Juan Carlos, and Mankit, I know some of you might not have change to see this again but the time we have spend together was joyful. Christiaan Shoemaker, thank you for helping me with all the research related or non-related problems (such as the tax form). Talking with you is a lot of fun, I just hope that we did not cause too much noise in our office. ZHOU Feng, QING Wenting, MAO Ronghai, LAI Fuqing, ZHOU Jian, MENG Chunfang and WANG Xiaoxi, it was a pleasure to know you all. The warmth of Chinese community in this faculty made me feel I'm not fighting along. I wish you all have a prosperous future and I hope we could work together again. I should thank DONG Yufei, GUO Hua and FAN Huajun you help me a lot during my study. You always offer your hands whenever I had questions or doubts. Without your warm-hearted help, my PhD life will be more painful.

ZHAO Yi, you are the best roommate I ever had (which made it difficult for me to find another one). Thank you for being there with me when I'm sick at 2 am. I wish you a good luck for your graduation. XIA Lei, YU Miao, MAO Ziqian, JIN MingLiang, SHUI Lingling, LUI Jun, LI Nan, RAO Xiangyu, LI Rui, JIU Qianqian and LI Sha, it was a pleasure to know you through LI Chen. Your multi-discipline background broadens my knowledge. Particularly, I enjoyed our trips, diners and chats together.

At Last, I want to express my most ardent love and gratitude to my parents. You never required me to do anything, jet you always love me and support me unconditionally. All these years, you worried about my health, cared about my everyday life and encouraged me to go through harsh time. Your warmth and care is my strength. Without you, I will never become who I am and even walk this far in my life. LI Chen, marring you is another achievement that I made in these years. You are my friend, my teammate and my love. Thanks for the light and happiness you bring into my life and all the supports you gave me.

Yuanyuan HE

April, 2012

Contents

1	Introduction	1
1.1	Gas Hydrates	1
1.2	Occurrence of Natural Gas Hydrates	2
1.3	Motivation and Objective	3
1.4	Scope and Approach	3
1.5	Organisation of the Thesis	4
2	Theoretical Background	7
2.1	Structure of Gas Hydrate	7
2.2	Phase Behaviour	9
2.2.1	Phase Diagrams	9
2.2.2	Thermodynamic Model	10
2.3	Kinetics of Hydrate Formation	12
2.3.1	Nucleation and Crystal Growth	12
2.3.2	Hydrate Formation and Dissociation	13
2.3.3	Kinetics Model	14
2.4	Hydrates in Porous Media	16
2.4.1	Phase Equilibria in Porous Media	16
2.4.2	Hydrate Formation in Porous Media	17
2.5	Hydrate Applications	18
2.5.1	Gas Hydrate in Flow Assurance	18
2.5.2	Hydrates for Gas Transport	19
2.5.3	Gas Hydrate as Energy Source	19
2.6	Summary	20
3	Single Gas Hydrate	23
3.1	Introduction	23

CONTENTS

3.2	Background	24
3.2.1	Phase Behaviour	24
3.2.2	Hydrate Formation Kinetics	26
3.3	Experiments	28
3.3.1	Materials	28
3.3.2	Experimental Set-up	28
3.3.3	Experimental Procedure	29
3.4	Results and Discussion	30
3.4.1	Reference Experiment	30
3.4.2	Influence of Water Quality	31
3.4.3	Comparison of CO_2 and CH_4 Hydrate Formation	33
3.4.4	Effect of Stirring	37
3.5	Conclusions	39
4	Hydrate Formation and Exchange in Ternary Systems	41
4.1	Introduction	41
4.2	Phase Behaviour	42
4.2.1	Binary System	42
4.2.2	Ternary System $CO_2 + CH_4 + H_2O$	43
4.2.2.1	Contribution Factors	44
4.3	Experiments	46
4.3.1	Materials	46
4.3.2	Experimental Set-up	46
4.3.3	GC Analysis	47
4.3.4	Experimental Procedure	49
4.3.4.1	Gas Hydrate Formation with CH_4 and CO_2 Mix- tures	49
4.3.4.2	Exchange of CH_4 with CO_2 in Methane Hydrates	50
4.4	Results and Discussion	50

4.4.1	Gas Hydrate Formation Kinetics in Ternary System	50
4.4.2	Exchange of CH_4 by CO_2 in Methane Hydrates	58
4.4.2.1	Methane Hydrates Formation	58
4.4.2.2	$CH_4 - CO_2$ Exchange Process	58
4.4.2.3	Gas Hydrate Dissociation	61
4.5	Conclusions	63
4.5.1	Formation Kinetics of Ternary System	63
4.5.2	Exchange of Methane by CO_2 within gas hydrates	64
5	Gas Hydrate Formation in Porous Media	65
5.1	Introduction	65
5.2	Experiments	66
5.2.1	Material	66
5.2.2	Experimental Set-up	67
5.2.3	Determination of Porosity and Permeability	68
5.2.4	X-ray CT Imaging	69
5.2.5	Experimental Procedure: Without CT-Scan	70
5.2.6	Experimental Procedure: With CT-scan	72
5.3	Results and Discussion	72
5.3.1	Gas Hydrate Formation in Porous Media	72
5.3.2	Influence of gas injection rate	77
5.3.3	Influence of Initial Pressure	82
5.3.4	Influence of Relaxation Time	84
5.3.5	Gas Hydrate Visualisation by X-Ray CT	85
5.4	Conclusions	88
6	Enhanced Gas Hydrate Production	91
6.1	Introduction	91
6.2	Model	92

CONTENTS

6.2.1	Hydrate Reservoir Model	93
6.2.2	Components and Phases	94
6.2.3	Hydrate Saturation and Permeability	95
6.2.4	Reaction Kinetics	97
6.3	Results and Discussion	99
6.3.1	Base Case	99
6.3.2	Enhanced Gas Recovery	102
6.3.2.1	Thermal Stimulation Combined with Depressurisation	103
6.3.2.2	CO_2 Injection Combined with Depressurisation	105
6.4	Summary and Conclusions	109
7	Summary and Outlook	111
A	Appendix-Ternary System	115
A.1	Contribution Factor	115
B	Appendix-Porous Media	119
B.1	Preparation of the synthetic glass beads core	119
B.2	Error Analysis on X-ray CT Images	120
B.3	Temperature Influence on Gas Hydrate Formation in Porous Media	122
C	Appendix-Simulations	125
C.1	Kinetics Equation	125
C.2	Correlations	127
C.2.1	Viscosity	127
C.2.2	Heat Capacity	128
C.2.3	Relative Permeability	128
D	Appendix-Micro Cell	131
D.1	Microcell Experiments	131

1

Introduction

Natural gas hydrates, also known as burning ice, are potentially significant energy resources. The extraction of gas containing essentially methane from natural gas hydrate accumulations can provide large amounts of cleaner fossil fuels than coal to meet the growing energy demand. For decades, efforts were devoted to understand the behaviour of gas hydrates. In this chapter, basic information relate to gas hydrates will be given and the scope of the research will be outlined.

1.1 Gas Hydrates

Clathrate gas hydrates are ice-like crystalline compounds formed at low temperatures and high pressures, where (small) gas molecules are held within a cage-like structure formed by water molecules. The entrapped gas molecules are the guest molecule and the water molecules are the host molecules.

Gas hydrates were first identified in 1810 by Sir Humphrey Davy [38]¹. While working with mixtures of chlorine and water he noted the formation of an ice-like solid, which occurred above the freezing temperature of water. However, it is believed that other scientists, including Priestley [66], may have observed hydrates earlier than Davy. Faraday continued with Davy's research on dissociation of hydrates under high temperatures [38]. Hydrates remained a curiosity throughout the 19th century; researchers were mainly interested in which gases form hydrates and at which conditions (pressure and temperature) hydrates could form. Villard [135] discovered several gases that form hydrates, including CH_4 , C_2H_6 and C_3H_8 . De Forcrand and co-workers [111] determined the formation conditions of over 15 hydrate forming gases.

¹The references of this thesis are organised by the name of the author alphabetically

1.2 Occurrence of Natural Gas Hydrates

Natural gas hydrates are found in environments where gas and water are present at low temperatures and high pressures. In 1965, Makogon [74] announced the discovery of gas hydrate in permafrost regions of the former Soviet Union. Since then the research on production of natural gas from hydrates has been carried out. In 1998, a test well was drilled for tentative production in the Mallik field in Canada [111]. Until now, several other natural gas hydrate accumulations were found based on the results of seismic mapping, logging, well drilling and core sampling. These data allow the determination of the thickness and the lateral spreading of gas hydrate layers. Figure 1.1 shows the worldwide distribution of proven and possible gas hydrate reservoirs [70]. Most of the observed reserves are at continental margins and in permafrost regions.

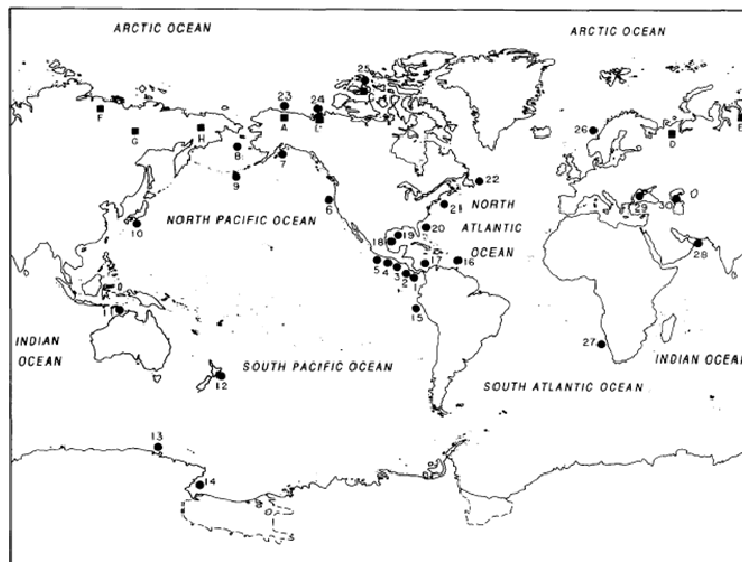


Figure 1.1: The distribution of proven and possible natural gas hydrate accumulations around the globe. The dots represent hydrate accumulations at continental margins. The squares represent accumulations in permafrost regions. [70]

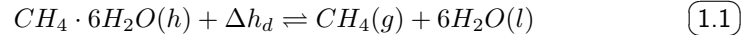
Natural gas hydrates found in the sub-sea occur either as large bulk masses on the seafloor, or within the sediments either in a thin layer or in a randomly distributed hydrate accumulation.

There have been many estimates of the total amount of gas hydrate reserves in the world. These estimations are based on global geological surveys (by using seismic, acoustic methods etc.) and data from test wells. The amount of natural gas hydrate reserves showed a clear diminishing trend over the last few decades.

In the 1980's, the hydrates reserves were estimated to be between $10^{17} - 10^{18} sm^3$ ² while in the 1990's, the estimated hydrates amount has decreased to $10^{16} sm^3$ [70]. In a recent report [41, 113], gas hydrate reserves ranged from 10^{14} and $10^{15} sm^3$. Milkov [81] estimated the global gas hydrate reserves to be in the range of 1 to $5 \times 10^{15} sm^3$. He stated that this value appears to be a good estimation based on the data from drilling and the hydrates concentration determinations from core samples. It is generally accepted that the amount of energy contained in natural gas hydrates is at least twice the amount of available energy of all conventional fossil fuels combined [111].

1.3 Motivation and Objective

Natural gas hydrates are an unconventional energy resource for which no commercial production were made. New production methods need to be developed to extract natural gas from hydrates. The distinctive feature of gas hydrate reservoirs compared to conventional gas reservoirs, is that the production of natural gas involves not only the two phase flow towards the well but also requires a controlled dissociation (Equation 1.1) of the gas hydrates to unlock the gas.



where Δh_d is the specific heat for dissociation.

Three main production methods from gas hydrate reservoirs emerged from research done to date namely, depressurisation, thermal stimulation and chemical injection. More recently, a new method consisting of simultaneous injection CO_2 and production of natural gas from hydrates was proposed [97]. The advantage of this method is that methane can be produced and used as energy source while at the same time CO_2 is stored in the sub-sea sediments such as sandstone reservoirs.

This study mainly aimed to answer the question of whether it is feasible to replace CH_4 in the natural gas hydrates with CO_2 . This process should be possible from a thermodynamic perspective (see Chapter 2). However, whether it will be feasible in terms of kinetics remains an open question. Thereby, the focus of this research is to gain understanding on hydrate behaviour at the typical conditions encountered in sub-sea hydrate accumulations.

1.4 Scope and Approach

To achieve the above mentioned objectives, this research focused on the kinetics of the formation and dissociation of methane and carbon dioxide hydrates.

² sm denotes the cubic meters at standard condition

CHAPTER 1. INTRODUCTION

The laboratory experiments were carried out at various conditions with CO_2 and/or CH_4 . Formation and dissociation of gas hydrates were performed in bulk (only water and CO_2 and/or CH_4) and in porous media. In the bulk environment, 4 systems were investigated: two binary systems of $CO_2 + H_2O$ and $CH_4 + H_2O$, ternary system of $CO_2 + CH_4 + H_2O$ and $CH_4 + CO_2$ gas hydrate replacement system.

The aim of study these binary systems is to investigate gas hydrate formation with single guest molecules and identify the differences on CO_2 and CH_4 hydrate formation kinetics. The ternary system of $CO_2 + CH_4 + H_2O$ gives insight in the competitive behaviour of CO_2 and CH_4 in the hydrate formation process. With these 3 systems mentioned above, we can answer the question: which gas hydrate is more favourable in terms of formation kinetics. This is the key issue in this thesis and the basis for further investigations. The last system studied by experiment is a special system which contains initially solid CH_4 hydrates and CO_2 . With this system the possibility of methane replacement by CO_2 in solid gas hydrate condition is investigated.

Reservoir modelling and simulation studies were performed to prove and test new strategies which can enhance the methane production from hydrate reservoirs. The reservoir model was a real scale class 2 type of hydrate reservoir. Simulations with depressurisation as a production method were used as a reference case to evaluate the performance of a combined production by thermal stimulation or CO_2 injection.

1.5 Organisation of the Thesis

The remaining thesis is organised in 6 chapters:

Chapter 2 provides an overview on relevant literature. Theory and background on gas hydrates are given including the structure of gas hydrates and the phase diagrams of the interested systems.

Chapter 3 gives the results of bulk studies for the two binary systems ($CO_2 + H_2O$ and $CH_4 + H_2O$). The gas hydrates formation kinetics in these binary systems were investigated in detail. The gas hydrates were formed separately in bulk under various initial pressures and stirring rates. Thereby, nucleation and hydrate growth processes were characterised for CH_4 and CO_2 hydrate formation. The results of the two hydrate forming systems were compared.

Chapter 4 presents and discusses the results of the bulk studies for two types of experimental studies, gas mixtures and gas hydrate exchange. The first study focused on kinetics of gas hydrate formation in the ternary system $CH_4 + CO_2 + H_2O$. The second study concerned the exchange of CH_4 with CO_2 within the stable methane hydrates.

1.5. ORGANISATION OF THE THESIS

Chapter 5 reports the study of the behaviour of CO_2 hydrate formation in porous media. Formation rates were investigated by varying temperatures, initial pressures, and gas injection rates. X-ray computed tomography images of the hydrate-bearing core were acquired and analysed.

Chapter 6 is devoted to reservoir modelling and numerical simulations on gas hydrate production methods. In particular, the enhanced methane production by CO_2 injection was examined.

Chapter 7 presents the main conclusions of this thesis and gives an outlook on future research.

2

Theoretical Background

The research on gas hydrate is broad, but in general it can be organised in the following main topics: gas hydrate structure, phase behaviour, kinetics of hydrates and hydrates in porous media. This chapter provides an overview of gas hydrate research focusing on the above mentioned topics and gives the theoretical background needed for understanding the thesis.

Section 2.1 discusses the existing gas hydrate structures and forms a basis for understanding the contents of Chapters 3 and 4. Section 2.2 reviews the basic thermodynamic concepts for understanding the gas hydrate equilibrium conditions mentioned in all experimental work. Section 2.3 and Section 2.4 provide the related work on formation of gas hydrates in bulk (Chapter 3) and in porous media (Chapter 5) respectively. Section 2.5 mentions the application fields of gas hydrate technology (Chapter 6).

2.1 Structure of Gas Hydrate

The most common microscopic gas hydrate structures are known as structure *I*, *II* and *H* [58]. Von Stackelberg [137, 138, 139], Müller [138, 139] and Claussen [22, 23, 24] confirmed the *I* and *II* clathrate structure by X-ray diffraction experiments. The structure *H* was discovered 20 years later by Ripmeester et al. [99].

In Figure 2.1, the water cavities, the basic unit of gas hydrate structures are shown. 5^{12} means the cavity is formed by 12 pentagons and $5^{12}6^2$ means the cavity is organised by 12 pentagons and 2 hexagons. Clearly $5^{12}6^2$ cavity is larger than 5^{12} . Structure *I* was formed by 2 small cavities (5^{12}) and 6 medium cavities ($5^{12}6^2$). Gas molecules such as CH_4 , CO_2 and H_2S normally form structure *I* hydrates. Larger molecules e.g. C_3H_8 , forms structure *II* hydrates. Butane (C_4H_{10}) and larger hydrocarbons can form Structure *H* with small gas molecule

CHAPTER 2. THEORETICAL BACKGROUND

such as CH_4 . This type of structure is rarely found in nature except in the Gulf of Mexico.

Even though it seems that the water cavities are formed by a well-defined amount of water molecules, Nikitin [95] stated that the cage structures of crystal hydrates are in fact non-stoichiometric¹.

Recently, new trigonal gas hydrate structures other than the classical structures *I*, *II* and *H* were identified; an unusual cavity was named T cavity ($4^15^106^3$) [130].

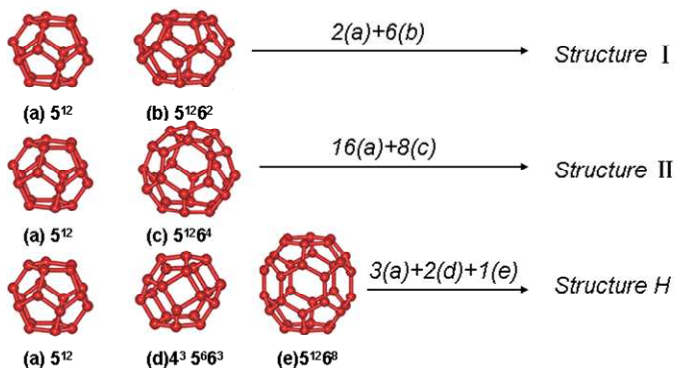


Figure 2.1: The water cavities arrangement to form structure I, II and H gas hydrates.

The crystal lattice of the gas hydrate cavities is formed due to hydrogen bonds between water molecules. Each water molecule can bond to four other water molecules, resulting in a cavity structure. The cavities are larger than the basic unit of ice crystals (I_h), allowing gas molecules to be trapped inside. The stability of hydrate cavities is maintained by van der Waals interactions between the water lattice and the trapped gas molecules, in addition, the hydrogen bonds between the water molecules.

Not all gases are suitable guest molecules. According to Jeffery [57], gas molecules should fulfil two basic requirements to form hydrates. Firstly, the guest molecule should not contain a strong or moderately strong hydrogen bonds (e.g. HF). Secondly, the guest molecule should be small enough to be caged. It is estimated that the size of a guest molecule should be between 0.35 and 0.90 nm [111]. Too small molecules can hardly be captured in the hydrate cages. When the molecule to cavity diameter ratio (D_g/D_c) is smaller than 0.77, the guest-host attractive forces are too weak to keep the guest molecule within the cavity. Clearly, above the upper bound ratio of one, the guest molecule cannot fit into the cavity without

¹Non-stoichiometric compounds are chemical compounds with an elemental composition that cannot be represented by a ratio of well-defined natural numbers, and therefore violate the law of definite proportions [43]

distortion of the lattice. For gas mixtures, mixed hydrate structures are likely to form.

2.2 Phase Behaviour

2.2.1 Phase Diagrams

With the aid of phase diagrams the phase behaviour can be visualised. The P-T diagram gives the temperature and pressure region where the different phases coexist. With the help of the Gibbs phase rule [40], it can be determined how many phases can coexist simultaneously. This is determined based on the degrees of freedom.

In the gas hydrate system, e.g. binary system consisting of gas and water, possible occurring phases are: the vapour phase (V), the aqueous liquid phase (L_w), Ice (I), the liquefied phase containing mainly the guest molecule component (L_g) and the hydrate phase (H). Consequently, three-phase consistence lines can be determined, namely, $H - V - L_w$, $H - V - I$, $H - L_g - L_w$ and $H - L_g - I$. The phase lines join at quadruple points, where four phases coexist.

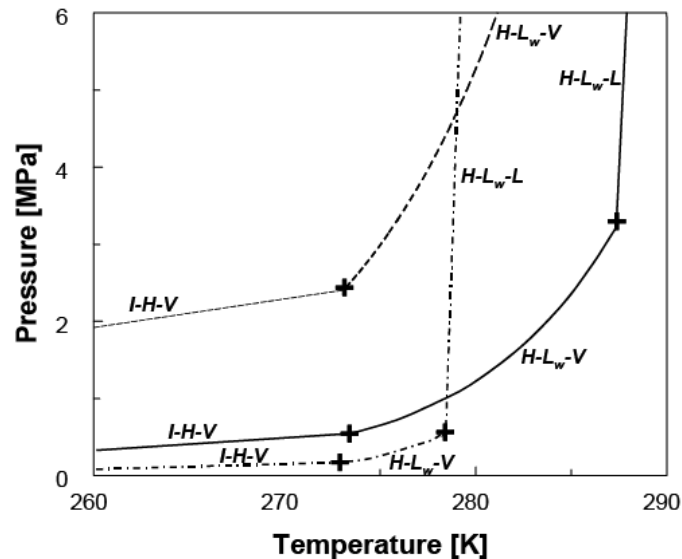


Figure 2.2: An example of the P-T phase diagram for the binary system: $CH_4 + H_2O$ (dashed line), $C_2H_6 + H_2O$ (solid line) and $C_3H_8 + H_2O$ (dash dotted line). The quadruple point is indicated with cross signs [134].

Since 1940's several research groups have determined the phase equilibrium be-

CHAPTER 2. THEORETICAL BACKGROUND

haviour of system forming gas hydrates. Data on the $H - L_w - V$ phase equilibrium line of methane and water system have been reported by Deaton et al. [27], Marshall et al. [77, 104], de Roo et al. [103] and Thakore and Holder [122]. Equilibrium data for carbon dioxide and water can be found in Deaton et al. [27], Larson et al. [71], Robinson et al. [101], Ng et al. [92] and Yang et al. [148]. These experimental studies were used to generate the phase diagrams used in this study.

Although this work does not deal with guest molecules other than CH_4 and CO_2 , reliable equilibrium data can be found for ethane, [100, 27, 53, 54, 92], propane [82, 27, 122, 101], nitrogen [133, 77, 104] and also for various gas mixtures [58, 107].

A detailed explanation regarding the phase equilibrium, especially related to experimental conditions can be found in Chapter 3 for the binary systems and in Chapter 4 for the ternary systems.

2.2.2 Thermodynamic Model

In 1959, van der Waals and Platteeuw published a comprehensive thermodynamic model describing the phase behaviour of gas hydrate forming systems [28]. The van der Waals and Platteeuw model was developed based on statistical thermodynamics. The model provides acceptable predictions of gas hydrate equilibrium conditions. As one of the first models, it forms the basis for more sophisticated models.

In the Van der Waals and Platteeuw's model, the gas hydrate equilibrium state was described by equating the chemical potentials of water in the liquid phase and the hydrate phase as follows:

$$\mu^W = \mu^H \quad or \quad (2.1)$$

$$\Delta\mu^W = \Delta\mu^H \quad (2.2)$$

where $\Delta\mu^W$ is the difference of the chemical potential of water in the aqueous phase between the state which is to be described (μ^W) and its reference state, namely the empty cavity (μ^β), $\Delta\mu^H$ is the difference of the chemical potential of water in the hydrate phase between the actual state to be described (μ^H) and the reference state, also the empty cavity (μ^β).

Based on statistical thermodynamics the latter chemical potential difference can be described by:

$$\Delta\mu^H = -RT \sum_{j=1}^2 v_j \ln \left(1 - \sum_i \vartheta_{ij} \right) \quad (2.3)$$

where μ^β is the chemical potential of water for empty cavities, i stands for the types of guest molecules, j denote the types of cavity, v_j is the ratio of j cavity to the number of guest molecules in hydrate phase² ϑ_{ij} represents the occupation of i type guest molecule in j types cavity.

In this model, it was assumed that the entrapment of guest molecules into the cavity can be described by Langmuir-type of equation [28]. The gas hydrate formation is considered as gas adsorbed on a solid surface. The probability of a single molecule adsorbed into a certain cavity (ϑ_{ij}) is described by:

$$\vartheta_{ij} = \frac{C_{ij}f_i}{1 + \sum_i C_{ij}f_i} \quad (2.4)$$

where C_{ij} is the Langmuir constant, f_i is the gas phase fugacity of i type guest molecules. It describes the affinity of a gas molecule occupying a single cavity. The value of the Langmuir constant depends on the potential interaction between the lattice and the guest molecules [53] (Equation 2.5).

$$C_{ij} = \frac{4\pi}{k_B T} \int_0^{R-a} \exp \left[-\frac{\omega(r)}{k_B T} \right] r^2 dr \quad (2.5)$$

where, $\omega(r)$ is interaction potential energy, k_B is the Boltzmann constant, R is the cavity radius.

In the original van der Waals and Platteeuw model, the Langmuir constant was calculated using a Lennard-Jones 12-6 potential function. It was proven that using Lennard-Jones 12-6 potential gives satisfactory results for systems containing monatomic gases (e.g. Ar) or CH_4 . However, for anisotropic molecules (such as CO_2) the Kihara potential is more accurate. The Kihara potential (Equation 2.6) accounts for the fact that molecules are not spherical and consequently the minimum attractive energy does not always occur in the middle between two molecules [80].

$$\omega(r) = 2z\varepsilon \left[\frac{\sigma^{12}}{R^{11}r} \left(\delta^{10} + \frac{a}{R} \delta^{11} \right) - \frac{\sigma^6}{R^5 r} \left(\delta^4 + \frac{a}{R} \delta^5 \right) \right] \quad (2.6)$$

The difference of the chemical potential of water in the aqueous phase ($\Delta\mu^w$) in Equation 2.1 satisfies the following differential equation [53].

² j stands for either small, medium or large cavity. For example, V_j for small cavity (5^{12}) in structure I is 1/23 for medium cavity ($5^{12}6^2$) V_j is 3/23

$$d\left(\frac{\Delta\mu^W}{RT}\right) = -\left(\frac{\Delta h^W}{RT^2}\right)dT + \left(\frac{\Delta V^W}{RT}\right)dP \quad (2.7)$$

where, the chemical potential difference ($\Delta\mu^W$) is a function of the enthalpy (Δh^w) and the volume (ΔV^w) differences.

Holder et al. [53] suggested to integrate Equation 2.7 assuming an ideal liquid phase. This leads to Equation 2.8:

$$\frac{\Delta\mu^W}{RT} = \frac{\Delta\mu_0^W}{RT_0} - \int_{T_0}^T \frac{\Delta h^W}{RT^2} dT + \int_0^P \frac{\Delta V^W}{RT} dP - \ln X^W \quad (2.8)$$

The first term on the right hand side is the chemical potential difference between the empty water cage and the reference condition. The second term gives the temperature dependency of the enthalpy at a constant pressure. The third term gives the change of the partial molar volume when integrating from atmospheric pressure to equilibrium pressure. X is the mole fraction of water in the liquid phase. In the case that hardly any gas has been dissolved in the aqueous phase as e.g. for $CH_4 + H_2O$ system, the mole fraction of water is nearly equal to one.

During the recent two decades, the model was improved by different research groups, e.g. Sloan [112] and Bishnoi [13]. Tohidi et al. [125] developed a model to predict the inhibition effect of electrolytes on gas hydrate formation. New modifications based on the van der Waals and Platteeuw model are proposed by Chen et al. [17, 18] assuming that the gas hydrate formation is a quasi-chemical process combined with gas adsorption. Duan et al. [31] proposed a method to compute the Langmuir constant from an angle-dependent intermolecular potential functions. The estimation of gas hydrates equilibrium has been developed into commercial programs e.g. CSMHYD (Colorado School of Mines), STFlash (Shell) and CSMGem (Ballard et al. [7])

2.3 Kinetics of Hydrate Formation

2.3.1 Nucleation and Crystal Growth

The formation of gas hydrates bears similarity to crystallisation processes. In this work, this theory was applied to interpret the results in the bulk. The crystallisation can be separated in two stages [89]. The first stage is the formation of crystal nuclei. The second stage is the growth of these small nuclei into larger crystals. The two processes are called nucleation and gas hydrate or crystal growth respectively.

2.3. KINETICS OF HYDRATE FORMATION

The driving force of the gas hydrate formation is supersaturation [89] which can also be expressed in terms of overpressure [34]. The driving force relaxes during nucleation and crystal growth, until the system finally reaches its equilibrium state which is described by a minimum energy. The time elapsed between the creation of supersaturation and the formation of a new phase is the induction time [33]. It is mainly a function of temperature and supersaturation.

Experimentally, the occurrence of hydrates can be detected by several ways, including direct visual inspection, increases in turbidity, and decreases in the refractive index. Vysniauskas and Bishnoi [141, 142], Skovborg [110] detected the gas hydrate formation in a sealed reactor by measuring the pressure depletion. Englozos [34, 35] tracked gas hydrate formation by monitoring the amount of gas consumed during this process. Because it is an exothermic process, the hydrate formation can also be detected by an increase of the temperature in a thermally insulated system [114, 120]. Other methods for detecting the formation of hydrates involve X-ray [67], neutron diffraction [51, 106, 116, 39], NMR [44, 6, 37, 36], Raman Spectroscopy [119, 64] and Powder X-ray Diffraction [120]. In this work, the pressure decay was used as indication for occurrence of gas hydrate crystals.

2.3.2 Hydrate Formation and Dissociation

The main interest in this work is to investigate the formation and dissociation of gas hydrates. Knox et al [65] investigated the kinetics of propane hydrate formation with the attempt to desalinate water. The gas hydrates were removed from the salted water. The rate of hydrate formation was determined by the mass of the solid crystals removed from the liquid phase. Barrer et al [8, 9] investigated the gas hydrate formation from ice particles at low temperatures. The experiments revealed that increase initial pressure can enhance the formation rate while increasing temperature can hinder the formation. Makogan [73] investigated the nucleation phenomenon of gas hydrate formation and reported that the nucleation rate is controlled by pressure, temperature and degree of supercooling (driving force). Vysniauskas and Bishnoi [141, 142] used a semi-batch stirred tank reactor to carry out methane and ethane hydrate formation experiments at temperatures ranging from 284 K to 294 K and pressures range of 3 to 10 MPa. The gas hydrate formation rate was directly determined from the gas consumption. Skovborg et al [110] quantified the induction times for the gas hydrate formation with methane, ethane and a mixture of the two gases. Their data indicated that the induction time is strongly dependent on the stirring rate and the driving force³. However, the data on the stirring rate influence was not discussed in detail.

Several researchers have done studies to either visualise or quantify the formation

³Driving force can be supercooling, over-pressure or supersaturation which increases the potential of the system for gas hydrate to occur.

CHAPTER 2. THEORETICAL BACKGROUND

of hydrates in the ocean. Brewer et al. [14] performed a sub-sea experiment with seawater at 910 m depth and a temperature of 277 K. Methane and CO_2 was circulated from bottom of a column to the top for gas hydrates formation. Their experiment showed over 85 days, CH_4 hydrates complete fills up the column while the injected liquid CO_2 only forms a hydrate skin at the bubble interface. Hester et al. [52] performed a similar experiment with Brewer et al. in the ocean introducing a modified Raman apparatus to detect hydrate formation. Gas spectra obtained from these experiments showed agreement with laboratory measurements at same conditions. Clarke and Bishnoi [21, 19] determined hydrate particle size in order to determine the growth and dissociation rate. They found that the formation rate for CO_2 hydrates is lower than for CH_4 . The lowest CO_2 formation rate occurs at a temperature of 277K.

The history of solution can influence the nucleation rate [89]. Parent and Bishnoi [98] studied the induction times for methane hydrates using pre-treated water at three different temperatures. They found that when water is kept at room temperature for 24 hours, the induction time is much longer than when water was kept at lower temperatures (275K). The experiment of Zatsepina et al. [149] revealed that addition of even a small amount of recently thawed water reduces the nucleation time of CO_2 hydrates compared to experiments with ‘untreated’ distilled water. However, Sloan [59] showed that the memory effect vanishes if water was warmed up to temperatures over 297 K.

The study on formation of gas hydrates covers many fields, however, most of the research were carried out in isobaric conditions [34, 35, 33]. The effects of supersaturation, stirring rate and water memory on nucleation time and hydrate growth time were not systematically investigated.

2.3.3 Kinetics Model

The kinetics of gas hydrate formation and decomposition is a new topic compared to the gas hydrate phase behaviour. It has become the main focus of gas hydrate research in recent decades. Vysniauskas and Bishnoi (1983) [141] developed and tested a semi-empirical kinetics model to describe methane hydrate formation. Their model is based on their gas hydrate formation data at a constant pressure. Hydrate formation rate (R^*) was determined from gas consumption rate.

$$R^* = Aa_s \exp\left(-\frac{\Delta E}{RT}\right) \exp\left(-\frac{a}{\delta T^b}\right) P^\gamma \quad (2.9)$$

where R^* represents the gas consumption rate during hydrate formation. A is pre-exponential constant, a_s is effective surface area of gas water interface, ΔE is activation energy of gas hydrate formation, a and b are empirical constants to account for the effect of supercooling to consumption rate.

2.3. KINETICS OF HYDRATE FORMATION

Englezos et al. (1987) [34] proposed a model to describe the kinetics of hydrate formation based on the standard crystallisation theory. Additionally, the model accounts for the mass transfer of gas through the surrounding liquid phase and the interface between liquid and hydrate phase. This is called the two film model which considers two continuous steps for hydrate growth: diffusion of the dissolved gas from the aqueous solution to the liquid-hydrate (crystal) interface and the subsequent adsorption of gas molecules into water cavity of gas hydrates (See Figure 2.3).

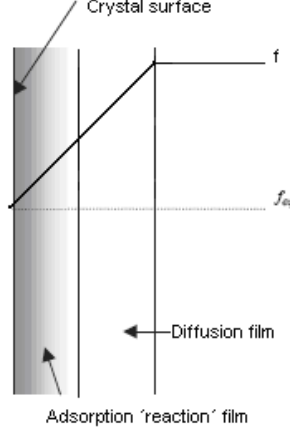


Figure 2.3: Illustration of the two-film theory. The first film is dissolution film, the second film is adsorption film [35].

In the model it is assumed that no mass is accumulated in the diffusion layer, thus the rates for those two steps are identical. The growth rate per hydrate particle in terms of the overall driving force is defined as:

$$\left(\frac{dn}{dt}\right)_p = kA_p(f - f_{eq}) \quad (2.10)$$

where dn/dt is the time derivative of the amount of guest molecules, k is the gas hydrate formation rate parameter, A_p is the surface area of hydrate particles, f_{eq} is the fugacity of the guest molecules in the gas phase at equilibrium condition.

The global gas hydrate formation rate (R_y) is obtained by integrating the growth rate per particle over the total number of particles, assuming that the particles are spherical, the nucleation is homogeneous (see Equation 2.11).

$$R_y = \int_0^\infty \left(\frac{dn}{dt}\right)_p \phi(r, t) dr = 4\pi k \mu_2 (f - f_{eq}) \quad (2.11)$$

where, $\phi(r, t)$ is the crystal size distribution, r is the diameter of hydrate particles,

K is formation rate parameter.

The two-film theory describes the gas transport from the gas phase into the liquid phase and finally in the crystal surface. Assuming quasi-steady state transport conditions and no accumulation within the films, the mass conservation of guest molecules can be expressed as:

$$D \frac{d^2 c}{dy^2} = 4\pi K \mu_2 (f - f_{eq}) \quad (2.12)$$

This model is valid only when the gas hydrate formation rate is constant. Englezos et al. [35] modified this model later by adding a mixing rule allowing the description of the gas hydrate formation kinetics for methane and ethane mixtures.

Dholabhai (1993) [29, 30] further extended the model of Englezos et al. allowing the description of methane hydrate formation in electrolyte solutions. The model of Kawamura et al. [62] describes the growth kinetics of CO_2 hydrates below the freezing temperature of water. In this model, it is assumed that the active surface for hydrate formation does not change over time. This model shows agreement with experimental data for 70-80% of the total process. However, if the system is close to equilibrium, e.g. when the formation rate slows down tremendously, the match of the model with the experiment data was not satisfactory.

2.4 Hydrates in Porous Media

Compared with bulk conditions the behaviour of natural gas hydrate in sub-sea sediments are much less understood. Research on the phase behaviour and kinetics of hydrate growth in porous media started only recently. Reliable methods for examining hydrates in porous media are still under development.

2.4.1 Phase Equilibria in Porous Media

The equilibrium conditions of hydrate forming system in porous media differ from the conditions in the bulk. Possible reasons are: 1) interactions between the fluid molecules and the hydrophilic mineral surface, and 2) the energy required to maintain capillary equilibrium [25].

Handa and Stupin [48] determined the $H - L_w - V$ equilibrium pressure and temperature in a synthetic porous media with very small pore size ($7.0 \times 10^{-3} \mu m$). The $H - L_w - V$ equilibrium pressure of CH_4 hydrates in porous media is 20-100% higher than in the bulk phase.

Uchida et al. [128] found that the $H - L_w - V$ equilibrium temperature of methane hydrates is lower in confined small pores than in the bulk. They argued that this temperature shift is due to the changes in the activity of water in small pores. Later on, Uchida et al. [129] investigated the inhibition effects on methane hydrate dissociation in a silica sand pack, sandstone, clay and glass beads. They also analysed the pore effect by changing the water saturation of the porous media. They found that for sandstone ($\phi = 0.17$ pore diameter of $100 \mu m$), the offset of the $H - L_w - V$ temperature is only 0.5 K. Therefore, when changing the water saturation, the equilibrium temperature did not show significant changes.

Turner et al. [127, 126] performed a study on methane hydrate formation in sandstone. They concluded that with a pore radius larger than $0.06 \mu m$, the shift of the $H - L_w - V$ equilibrium curve with respect to the bulk phase $H - L_w - V$ curve can be neglected. According to Anderson et al. [2] for pore size larger than $3.1 \times 10^{-2} \mu m$ the $H - L_w - V$ conditions in the porous media and in the bulk can be assumed to be identical [3].

The small pore sizes mentioned above may occur in clay type of sediments. In typical sandstones the porosity is around 15-25% and the pore size is ranging from 50-150 μm [145]. For coarse siltstone pore size ranging from 1-10 μm and for shale is 0.05-1 μm [91]. Therefore, it can be assumed that the gas hydrate equilibrium conditions in sandstone are not significantly affected by the pore size.

2.4.2 Hydrate Formation in Porous Media

The study on formation and dissociation of gas hydrates in porous media is essential in many fields such as production of natural gas from gas hydrate bearing reservoirs and in environmental issues (i.e. carbon sequestration). Yet, research in this area has started rather late and the focus is quite diverse. The porous media used for experiments varied from glass beads, silica gels or other synthetic porous materials to loose sand packs or core samples from natural gas hydrate-bearing layers.

Dvorkin et al. [32] proposed four possible locations for hydrate distributions in pore space. Gas hydrate may float in pore fluid, fill pore space, surround and cement grain or cement grain contact only. Following the work of Dvorkin et al., several authors attempted to probe these gas hydrate locations in pores.

Tohidi et al. [123, 124] used a 2-D glass micro model to simulate the pore channels and observed gas hydrate formation by microscope. They claimed that hydrate crystals preferably form in pore centres. Therefore permeability is reduced due to clogging of pores.

Stern et al. [117] showed that methane hydrates cement the ice grains in a system containing only vapour and solid phases. Weite et al. [143, 144] stated that in partially saturated sand packs, the liquid water which surrounding the grain is

CHAPTER 2. THEORETICAL BACKGROUND

replaced with the solid gas hydrates, so that the grains are locked in their position.

Buffett and Zatsepina [15] reported a set of gas hydrate experiments with sand packs filled with CO_2 saturated water. The hydrate formation was detected by resistivity change and temperature increase. They showed that gas hydrates could be formed in porous media from dissolved gas.

Spangenberg [115] performed similar experiments with glass-beads packs. Methane saturated water was prepared and then charged to the core from the bottom to create upward flow. The experiment was terminated due to blockage of the flow by hydrate formation. The results showed a complete blockage of porous media occurring after 60 days.

Graue et al. [44] conducted core-flood experiments where CO_2 was injected in the cores containing methane hydrates. 3D Magnetic Resonance Imaging (MRI) shown that exposure of the methane hydrate to CO_2 resulted in release and production of methane. The authors also conducted thermodynamic simulations based on Phase Field Theory [69] and found good agreement with experiments.

These above mentioned laboratory hydrate research in porous media provide information on the distribution of the gas hydrates in pores and how gas hydrate reservoirs originated. However, the formation kinetics and the parameters which could influence the gas hydrate formation in the porous media have not been studied in detail.

2.5 Hydrate Applications

Due to their special chemical-physical properties, gas hydrates can be applied in many fields including potentially flow assurance, gas storage and transportation, gas separation, refrigeration and in other fields concerning pipeline safety, energy extraction and carbon sequestration. Some of the technologies have already reached maturity and have been applied in industry. A brief review of these technologies is given below.

2.5.1 Gas Hydrate in Flow Assurance

In the 1930's Hammerschmidt discovered that blockage in high-pressure pipelines was due to the formation of gas hydrates [47]. Consequently, interests of research was focused on avoiding gas hydrates formation during gas transportation through pipelines.

Extensive works (i.e. Jacoby [56], Katz et al. [61], Makogon [73], Ng and Robinson [93], Nielson [94] and Chen [17]) were devoted to the prevention of gas hydrate formation following the discovery of Hammerschmidt. Several chemicals includ-

ing alcohol, glycol and salt were identified to have a thermodynamic inhibition effect on gas hydrates. Their presence in water shifts the hydrate equilibrium line to higher pressures at a certain temperature (or temperature depression at a certain pressure). Experiments show that alcohol and glycol are the most effective gas hydrates inhibitors [111].

In the recent flow assurance studies, the focus has been on the inhibition of the gas hydrates formation rate. This includes the anti-agglomerant (AAs) and the kinetic hydrate inhibitor (KHIs) [4]. The AAs prevent the agglomeration of hydrate crystals while KHIs can prolong the nucleation time substantially.

Koh and co-workers [68] conducted research with gas hydrates containing THF (Tetrahydrofuran) and three different chemical additives: N-vinylpyrrolidone, VC-713 terpolymer and quaternary ammonium bromide (QAB). Results indicated that VC-713 is highly effective on controlling the onset of gas hydrate formation. QAB showed a better control of the gas hydrate formation rate in 27:1 (water/QBA)solutions. Daraboina et al. [26] investigated the influences of polyvinylpyrrolidone (PVP), type III antifreeze protein (AFP) and a proprietary commercial chemical (HIW85281) on gas hydrate growth. They concluded that PVP is the least effective in formation control.

2.5.2 Hydrates for Gas Transport

In 1942, Benesh [11] proposed using the gas hydrates to store natural gas. Gas storage and transportation in the form of hydrates has the advantage of a smaller storage space and lower pressures. These are favourable in terms of safety compared to compressed natural gas (CNG). However, this concept requires that gas hydrates are kept at low temperatures during transportation. Additionally, the energy density is low compared to liquified natural gas (LNG). A number of research groups investigated the possibilities to improve the economics of gas storage in the form of hydrates, to compete with liquified natural gas (LNG). Berner [12] evaluated the conceptual design for shipment of gas hydrates. Gudmundsson et al. [46] proposed using ice barriers to protect hydrates from dissociation so that the storage temperature can be increased. Gudmundsson and Borrehaug [45] estimated the cost of gas transportation in hydrates and stated that in offshore applications, natural gas hydrate (NGH) technology is expected to have much lower costs than gas-to-liquid (LNG) technologies.

2.5.3 Gas Hydrate as Energy Source

There are three main methods to produce and recover natural gas from hydrate deposits: 1) depressurisation, 2) thermal stimulation and 3) inhibitor injection. A detailed discussion on these production methods can be found in Chapter 6.

CHAPTER 2. THEORETICAL BACKGROUND

Many of the proposed recovery procedures involve one of these methods or their combinations [58, 73]. Here only a general overview of the related research is provided.

Several modelling and numerical simulation studies on gas hydrate dissociation and production have been performed. Holder et al. [54] investigated the contribution of hydrates during gas production in a Class 1⁴ hydrate reservoir (free gas zone below the hydrate zone). Their study indicated that gas hydrate decomposition contributed up to 30% of the total gas production. McGuire [79] reported a study on the feasibility of applying thermal stimulation and hydraulic fracturing to hydrate bearing reservoirs.

In the last three decades, several numerical simulators have been developed allowing the modelling of gas production from hydrate reservoirs. Sawyer et al. [105] reported a summary where ten types of numerical models were compared including the simulators TOUGH-EOSHYDR developed by Moridis et al. 1998 [83] and Shell simulator MoRes by Swinckels et al. 2000 [121]. They stated that both simulators are robust in their mathematical formulation to solve fully coupled mass and energy balance equations that yield pressure, temperature, and saturation distributions over time.

In 2005, TOUGH-Fx/HYDRATE simulator was released. It is a modification based on the EOSHYDR module. Moridis et al. [85, 88, 87, 84] have reported several simulation results for different types of gas hydrate reservoirs by using TOUGH-Fx/HYDRATE. They found that the gas production is strongly affected by permeability, initial hydrate saturation, the thickness of the water zone and the initial temperature and pressure in the hydrate zone. Uddin et al. [132, 131] studied various gas production strategies using reservoir simulator CMG STARS. According to their results, steam and thermal stimulation at both field and laboratory scale showed good performance. They focused on the possibility of CO_2 sequestration and potential to enhance CH_4 recovery. Their results have shown that CO_2 can form in the reservoir within a specific pressure and temperature range. However, the specific methods to increase the gas production from hydrate reservoir was not discussed in detail.

2.6 Summary

In order to place this work in its own context we provided a brief summary of the state of the art of research in gas hydrates and then describe the scope of the thesis. The conditions under which gas hydrates are formed have been established by experimental and modelling studies. It is commonly accepted that gas hydrates form mainly three types of crystal structures (structure *I*, *II* and

⁴Class 1 hydrate reservoir is one of the geology setting of typical natural gas hydrate reservoirs. Noted here not to confuse with the Structure of the hydrates.

H). The size of gas molecules determines the structure of gas hydrates. Phase equilibria data for gas hydrates were obtained by many researchers and the phase behaviour of hydrate forming systems has been described with some success by the thermodynamic model of Holder et al. [53]. The behaviour of hydrates in porous media having extremely small pores was found to be notably different than that of hydrates formed in bulk ($H - L_w - V$ equilibrium pressures and temperatures are found at lower temperatures and higher pressures in porous media). However, for the typical pore sizes characteristic of hydrate-bearing sediments no apparent differences were found between hydrates formed in bulk and porous media [126].

The formation of gas hydrates can be separated into two steps, namely nucleation and crystal growth. The growth of hydrate crystals under isobaric conditions was satisfactorily described by the kinetics model for hydrate formation developed by Englezos et al. [35]. Several researchers have shown that gas hydrates can be formed in porous media either with free gas overlaying water or with water and dissolved gas [15, 115]. Also the formation of hydrates in porous media appeared to be consistently slower than in bulk conditions.

Although much research was devoted to gas hydrates as surveyed in this chapter, many questions about the formation of gas hydrates remain open. These questions concern the kinetics behaviour of gas hydrates at various conditions. The influence of the physical parameters on the nucleation and crystal growth processes were not studied systematically. The knowledge on hydrate formation with gas mixtures and the hydrate occupation in mixed gas hydrates was also lacking. The studies concerning the replacement of CH_4 by CO_2 within methane hydrates and the hydrate formation kinetics in porous media was scarce.

This thesis aims to gain more insight on the time-dependent formation and dissociation process of gas hydrates in binary systems (Chapter 3), ternary systems in the bulk (Chapter 4) and a binary system in porous media (Chapter 5). Numerical simulation and modelling (Chapter 6) provide information to evaluate the methane production by CO_2 injection into gas hydrates reservoirs. The results of this work can contribute to the technical and engineering challenges in gas production from hydrate bearing reservoirs, gas separation, carbon sequestration, flow assurance (avoiding plugging of gas pipelines), gas storage and transportation.

3

Single Gas Hydrate

This chapter presents the results of the experimental study on the kinetics of gas hydrate formation of systems containing water and either carbon dioxide or methane. The experimental data were interpreted in terms of nucleation and crystal growth. (This chapter is adapted from publication [50])

3.1 Introduction

In order to keep CO_2 footprint as small as possible when recovering gas from natural gas hydrates, the idea arose to combine the production of gas from methane hydrates with the sequestration of CO_2 in the form of gas hydrates [97]. The CO_2 and CH_4 hydrate formation and dissociation kinetics in their respective binary system is essential. In the past, studies mainly focused on the thermodynamics of gas hydrate forming systems. Research on the actual gas hydrate formation has only been done by a limited number of research groups (see Chapter 2). The effect of parameters i.e. driving force, stirring rate and memory of water on gas hydrate crystallisation process were not been systematically studied.

In this chapter, gas hydrate formation in the systems $CO_2 + H_2O$ and $CH_4 + H_2O$ has been studied experimentally, keeping the temperature and the total amount of water and gas in the system constant. The data were interpreted in terms of nucleation and crystal growth processes. The effect of supersaturation, agitation and water quality on the nucleation and growth of gas hydrates were investigated in detail.

3.2 Background

3.2.1 Phase Behaviour

The pressure-temperature diagrams for the $CH_4 + H_2O$ and $CO_2 + H_2O$ system are shown in Figure 3.1 and 3.2, respectively [134]. Both CH_4 and CO_2 form the same type of gas hydrate structure (structure *I*) with water. The solid lines in the graph represent the different phase coexistence lines of the binary systems. The dashed-lines depict the equilibrium lines for pure water. The dotted-dashed line depicts the phase equilibrium line of either pure methane or carbon dioxide. The phases are denoted as follows: *H*: hydrate phase; L_w : aqueous liquid phase; L_g : liquid phase rich in CO_2 or CH_4 ; *I*: ice, *V*: vapour phase which is commonly rich in CO_2 or CH_4 . *CP* is the critical point of CO_2 or CH_4 . *Q* is the quadruple point at which four phases coexist.

For the investigation of the kinetics of hydrate formation the three-phase coexistence lines, for which one of the phases is the hydrate phase, is basic. As shown in Figure 3.1 and 3.2, there are several of these three-phase coexistence lines namely $H-L_g-V$, $H-L_w-V$, $H-I-V$, $H-I-L$ and $H-L_g-L_w$.

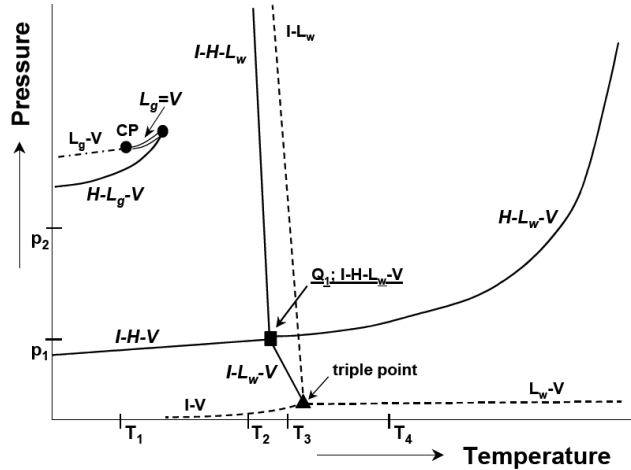


Figure 3.1: Phase diagram of the binary system methane and water. The critical temperature of the guest molecule (methane) is lower than the triple point temperature of pure water [134].

The experiments presented here were performed at a constant temperature of 276.15 K and initial pressures varying between 2.5 MPa and 7.0 MPa. In the experiments, the temperature was slightly lower than those temperatures typically encountered in hydrate bearing sediments. In natural gas hydrate reservoirs the temperature normally ranges from 278K to 285K. However, choosing a higher

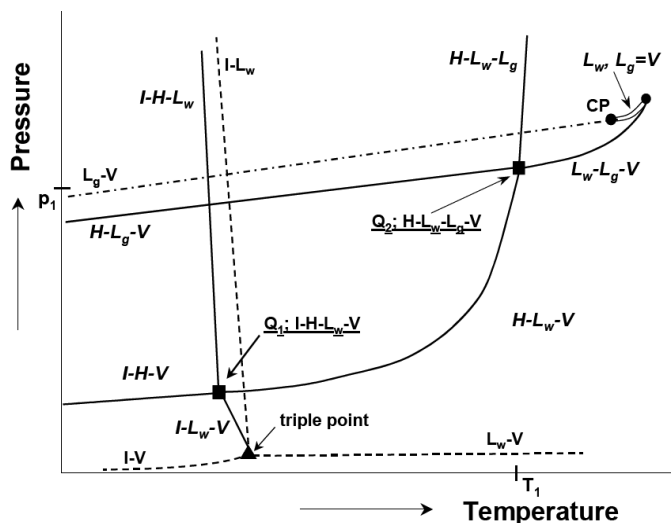


Figure 3.2: Phase diagram of the binary system of carbon dioxide and water. The critical temperature of the guest molecule (carbon dioxide) is higher than the triple point temperature of pure water [134].

temperature for the experiments would require higher pressures to meet the stability criteria for methane hydrates, making the experiments much harder to handle. It is believed that the behaviour at the temperature chosen for the experiments will not differ substantially from the behaviour at real reservoir conditions. This is because for both cases, the pressure and temperature conditions are within the same phase region between the $H - L_w - V$ and $H - L_g - V$ equilibrium lines (L_g for liquid CO_2).

The phase behaviour of the systems $CO_2 + H_2O$ (Figure 3.2) and $CH_4 + H_2O$ (Figure 3.1) differs considerably. For the methane system, only the three-phase coexistence line $H - L_w - V$ is found. While for the carbon dioxide system, additionally the three-phase coexistence line $H - L_g - V$ occurs at higher pressures. In Figure 3.3 the phase diagram of the $CO_2 + H_2O$ system is shown, with an indication of the experimental window. The $H - L_w - V$ line describes the three-phase equilibrium between the CO_2 -rich gas phase, the hydrate phase and the aqueous liquid phase. The $H - L_g - V$ line represents the phase equilibrium curve between the gas phase, the liquid phase rich in CO_2 and the hydrate phase. This line actually indicates at which conditions the CO_2 condensates. In this work, the interest is in the formation of CH_4 and CO_2 hydrates from the gas phase. Therefore, the initial pressures of CO_2 were always kept above the $H - L_w - V$ equilibrium curve but below the $H - L_g - V$ curve to avoid appearance of liquid CO_2 which would make the interpretation and comparison of the experimental data rather difficult.

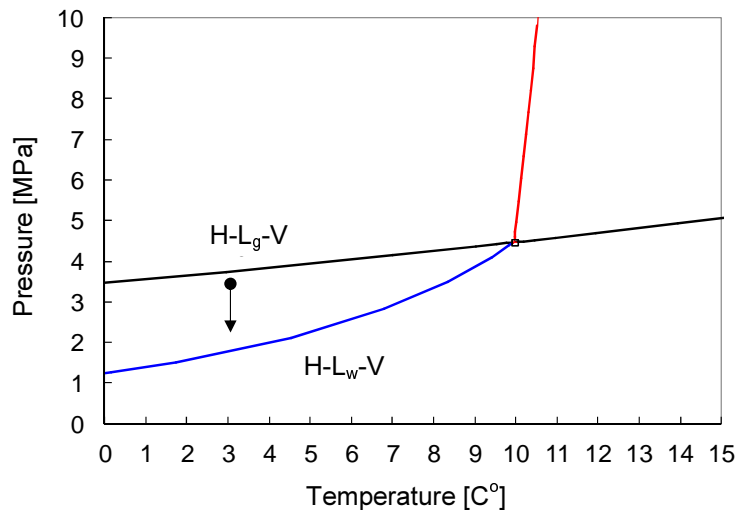


Figure 3.3: Schematic P, T phase diagram of the binary system $CO_2 + H_2O$. The round dot shows the maximum initial pressure used for the CO_2 experiments. The arrow indicates the range in which the initial pressure was varied for the experiments. L_g indicates liquid CO_2 .

3.2.2 Hydrate Formation Kinetics

As discussed in Chapter 3, the formation of gas hydrates can be described as a crystallisation process [33]. The driving force of the gas hydrate formation is determined by the supersaturation of the gaseous component in the aqueous liquid phase. A supersaturated solution means that the concentration of the solute (dissolved component) in the liquid phase is higher than its solubility (at equilibrium). The supersaturation of the solute decreases during the formation of the gas hydrates and the system approaches equilibrium. In this work, the classical crystallisation theory [89] was applied to describe the gas hydrate formation. The actual crystallisation is divided into the nucleation and the crystal growth processes. Unfortunately, the definitions of these two processes as found in literature are not completely unique.

The nucleation stage forms the first stage in which very small hydrate nuclei are formed in the supersaturated solutions; in the second stage those nuclei grow into larger sizes, the gas hydrate crystals.

The induction time (t_{ind}) is the time between the creation of the supersaturated solution and the occurrence of the first gas hydrate crystals. It is defined by Myerson as [89]:

$$t_{ind} = t_{tr} + t_n + t_g \quad (3.1)$$

where, t_{tr} is the time to reach steady-state nucleation; t_n is the time for the actual nucleation and t_g is the time for crystals to reach detectable sizes. However, these three periods cannot be clearly distinguished in the experiments. In this work, the induction time is defined as the sum of the times described above plus the time necessary to dissolve the gas in the aqueous phase. It can be expressed as:

$$t_{ind} = t_{tr} + t_n + t_g + t_d \quad (3.2)$$

To investigate the second stage of the crystallisation, i.e. the actual hydrate growth, the change in the supersaturation with respect to time was monitored by determined pressure data. It is believed that the gas molecules used for gas hydrate formation originate from two sources: 1) the gas dissolved in the aqueous phase and 2) the gas in the vapour phase [66]. The autoclave used to study the formation of gas hydrates do not enable the determination of the origins of the gas trapped in the hydrates. The pressure decline determined in the gas phase is caused by both sources. A decrease of pressure indicates that gas is transferred from gas phase either into the liquid aqueous phase or directly into the solid hydrate phase. At the end of an experiment, all water molecules initially present were consumed to form gas hydrates, so that no aqueous liquid phase was present. This means that all gas that was dissolved in the aqueous phase was eventually incorporated into the gas hydrates.

For a better comparison of the experimental results of the two binary systems, the degree of supersaturation, and not the absolute supersaturation, was used. The kinetics of the crystal growth is deduced from the change of the degree of supersaturation as a function of time, within the period from the beginning of the crystal formation to the equilibrium state. The degree of supersaturation S at constant temperature is defined as:

$$S(t) = P(t)/P_{eq} - 1 \quad (3.3)$$

where P_{eq} is the equilibrium pressure at a given temperature, i.e. the final pressure of an experimental run. Obviously, a degree of supersaturation of zero means that the initial pressure and the equilibrium pressure are equal, and thus there is no driving force for gas hydrate formation.

For a better comparison of the formation rates, the half-decay time was used. The half decay time can be described as the time for which the pressure has decreased by 50% over the total pressure decrease (See also Figure 3.5).

3.3 Experiments

3.3.1 Materials

Carbon dioxide (99.7 mol% purity, Linde Gas) and methane (99.99 mol% purity, Linde Gas) were supplied from a gas cylinder with a pressure of 5.0 and 10.0 MPa respectively. The water used was double distilled water. Before each experiment, new water was charged into the autoclave. The water was not exchanged for the experiments studying the influence of the water quality.

3.3.2 Experimental Set-up

The set-up used to do the experiments is shown in Figure 3.4. The set-up was designed to study the gas hydrate formation and dissociation at constant temperature. It consists of a high pressure autoclave, a mechanic stirrer, a gas supply system and a data acquisition system.

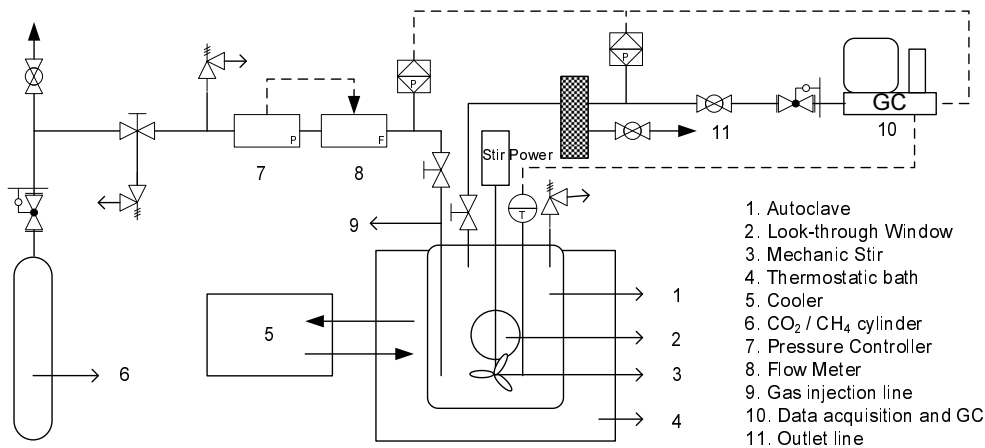


Figure 3.4: Schematic of experimental set up (from Shell Global Solutions)

The autoclave has an inner volume of 430 ml and can withstand pressures up to 10.0 MPa. There are two visualisation windows to observe the gas hydrate formation inside the cell. The maximum operating pressure was set to 8.0 MPa using a safety valve. For the experiments performed with carbon dioxide the initial pressure varied between atmospheric and 3.5 MPa. For the experiments with methane initial pressures up to 7.5 MPa were applied. For all experiments, the temperature was kept constant at 276.15 K with the help of a thermostatic water bath. To ensure proper mixing of the supplied gas and water in the cell, a mechanic stirrer (manufactured by Premex Reactor AG, Lengnau, Switzerland)

was used. Maximal dispersion of the gas in the water was achieved by a unique design of the impeller, allowing recirculation of the gas from the gas phase above the liquid phase into the liquid phase. Due to the rotation of the stirrer a lower pressure at the tip of the impeller is induced. This pressure difference forces the gas into the small holes at the top of the shaft. The gas is transported through the hollow shaft towards the dispersion ports located at the tips of the impellers. The interface between the liquid and the gas phase is constantly renewed due to this kind of stirrer. The higher the stirring speed, the lower the pressure at the tip of the impeller, and the better the dispersion of the gas in the liquid. A pressure-regulated flow meter is connected to the inlet to control the flow and the pressure in the cell during injection of the gas. During an experimental run the pressure in the autoclave is determined with the help of a Keller digital manometer with an accuracy of 0.1 kPa. The temperature is monitored using a thermocouple with an accuracy of 0.1 K. Temperature and pressure data are collected and transmitted to a computer.

3.3.3 Experimental Procedure

Each experiment was carried out with controlled procedures as described below. The summarised experimental steps and parameters needed to be determined is listed in Table 3.1.

First, the autoclave was charged with a known amount of distilled water sufficient to form hydrates with all the injected gas. In this study it was assumed that the molar ratio of water and gas is 6:1 in the gas hydrates [58]. This ratio (w/g) is called hydration number¹, by assuming this hydration number, it can be ensured that enough water is added to the autoclave to capture the gas molecules. Water loading is done manually and outside the cooling bath by opening the top cover of the autoclave. Before charging the water, the autoclave is rinsed with distilled water to make sure that no hydrate crystals or other impurities are present. Then the cell is sealed and immersed in the thermostatic bath to cool down to the desired temperature. To remove air from the system the autoclave is flushed carefully with either carbon dioxide or methane at atmospheric pressure. Therefore, water was saturated with the respective gas at atmospheric pressure. The flushing was done within a short time, so that the amount of gas dissolved in the aqueous liquid phase can be ignored.

When the temperature stabilised, gas was injected into the autoclave up to the desired initial pressure. This pressure was higher than the equilibrium pressure at the given temperature [147]. The gas was injected at maximum flow rate to minimise any gas hydrate formation during injection. Gas hydrate formation during

¹The hydration number depends on the occupation of the hydrate cavities. When the cavities are completely filled by guest molecules, hydration number can be assumed to be 6. When cavities are not completely filled the hydration number can be larger e.g. 7.3 or 20.

CHAPTER 3. SINGLE GAS HYDRATE

injection would make it impossible to reliably determine the supersaturation and induction times.

When the desired initial pressure was established, the system was closed and ready for the first experiment. During an experimental run, the overall composition of the system remained constant; meaning the total amount of moles of water and CO_2 or CH_4 in the system was fixed. The pressure in the gas phase was monitored as function of time. The actual gas hydrate formation can be visualised through two sapphire windows. The experiment was stopped when the pressure was constant or its decay was less than 5 kPa/hr . At the end of an experiment the water in the autoclave was completely used to form gas hydrates and no liquid phase was present.

After the experiment was finished, the pressure in the autoclave was released by venting the gas via the outlet line (see No. 11 in Figure 3.4), achieving the dissociation of the gas hydrates.

Table 3.1: Summary of the important experimental steps for the bulk experiments

Step	Description	Determined Parameters
step 1	Load water	m_w
step 2	Start cooling, stirrer	T
step 3	Inject gas	P_{in} , T
step 4	Close valves	P(t), T(t), P_{eq}
step 5	Dissociation	-

Two different series of experiments were conducted. First, experiments with different initial pressures using either fresh distilled water or ‘used’ water to study the influence of the supersaturation and the quality of the water on the kinetics of hydrate formation. Secondly, experiments were done at one initial pressure with different stirring speed to study the influence of gas dispersion in the aqueous phase.

3.4 Results and Discussion

3.4.1 Reference Experiment

Figure 3.5 shows pressure as a function of time obtained from a typical hydrate formation experiment in this study. The pressure declined in two steps: first, the pressure decreased slightly from the highest value (i.e, 3.0 MPa) when injection stopped, to the initial pressure of the experiment, i.e, 2.8 MPa. This normally takes a few minutes; in this case, it was 3 minutes. After the first pressure decline, the pressure remained at this plateau value for about 12 minutes. Then the pressure diminished continuously to the equilibrium pressure of 1.9 MPa.

The first pressure decrease corresponds to the dissolution of CO_2 in the aqueous phase. The plateau pressure indicates the formation of the gas hydrate nuclei and thus describes the induction process. According to the definition (see Equation 3.2), it can be inferred that the induction time is 15 minutes (3 minutes for dissolution and 12 minutes plateau) for this specific experiment.

The second pressure decay is attributed to the growth of the gas hydrates. The corresponding half-decay time ($t_{1/2}$) was determined to be about 6 minute for this experiment.

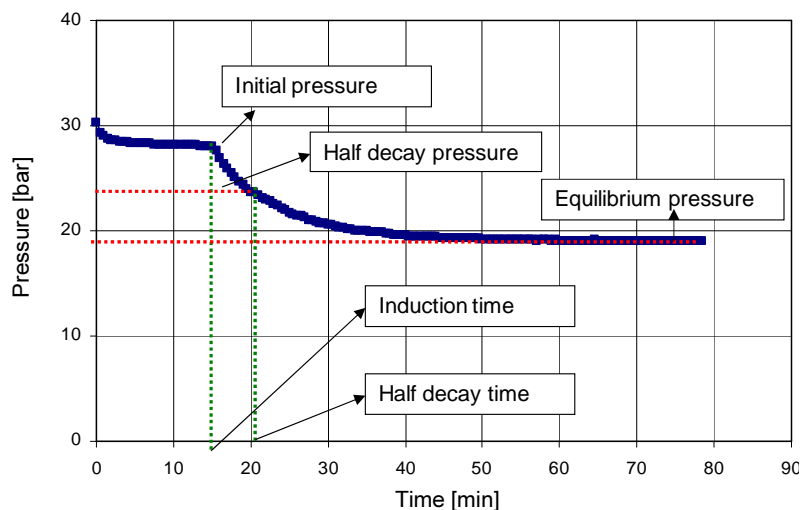


Figure 3.5: Pressure profile during gas hydrates formation experiment at 276.15 K with CO_2 . The initial pressure, half decay pressure and equilibrium pressure for the crystal growth process are indicated in the graph.

3.4.2 Influence of Water Quality

As mentioned in Chapter 2, the quality of the water (or more accurately the history of water) can influence the kinetics of gas hydrate formation. This is often referred to as the ‘memory’ effect. In order to study this effect, several experiments were done with CO_2 using either ‘fresh’ or ‘used’ water and various initial pressures at a constant temperature of 276.15 K. The ‘fresh’ water was double-distilled water preserved at room temperature and had previously never been used for hydrate formation. While the ‘used’ water experienced one or more cycles of the gas hydrate formation and dissociation process. This water was repeatedly used immediately after the hydrates were completely dissociated.

Figure 3.6 shows the determined induction times (t_{ind}) as a function of the degree of supersaturation for both ‘fresh’ and ‘used’ waters. For ‘fresh’ water, the in-

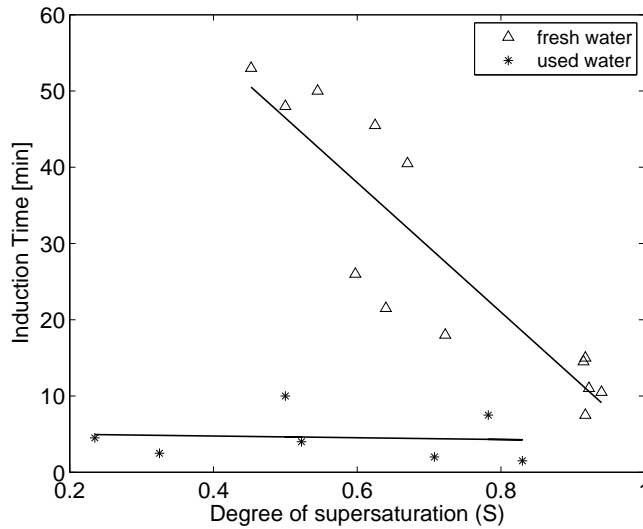


Figure 3.6: Influence of water quality (‘fresh’ and ‘used’ water) on the induction time of gas hydrate formation for the system $CO_2 + H_2O$ at a constant temperature of 276.15 K. The induction time is given as a function of supersaturation (initial pressure). Lines are drawn to guide the eye.

duction time decreases almost linearly with increasing degrees of supersaturation (or initial pressure). While for ‘used’ water the induction time remains almost constant around a low value of 5 minutes. It can be clearly seen that the induction time for ‘used’ water is shorter than for ‘fresh’ water at the same degree of supersaturation. A possible explanation is that after the gas hydrates have been dissociated, the hydrogen bonds between the water molecules and residue hydrate structures remain in the liquid. With the presence of these structures, gas hydrate nuclei formation is much faster. Similar behaviour was observed for the formation of ice [118]. These residue water structures enhance the nucleation of crystals.

Figure 3.7 shows the half-decay time as a function of the degree of supersaturation for ‘fresh’ and ‘used’ water. It can be seen that the quality of water appears to have less influence on the gas hydrate crystal growth than on the induction time. This is in agreement with the work of Lee et al. [72] for structure H gas hydrates. Lee found that the induction time was shortened by the memory effect but does not change the gas consumption rate². The ‘fresh’ water data scatters, this might be due to the random occurrence and distribution of the hydrate crystals during the formation process. The half-decay time increases with increasing supersaturation (initial pressure) for both ‘fresh’ and ‘used’ water. However, the

²In the work of Lee et al., the gas hydrate formation was characterised by the gas consumption rate

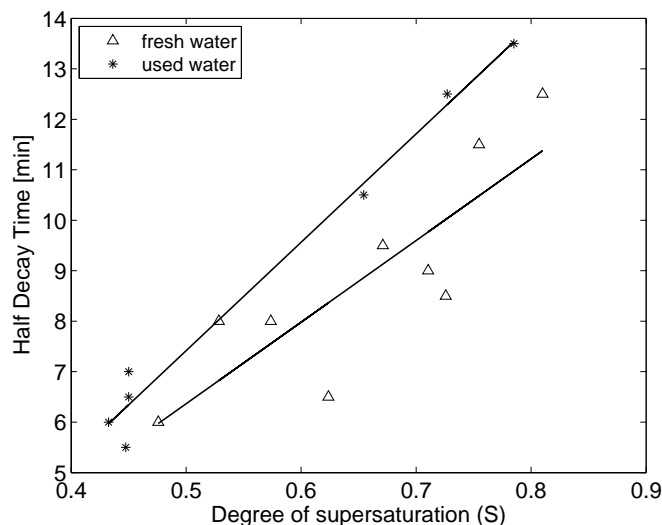


Figure 3.7: Influence of water quality (‘fresh’ and ‘used’ water) on the half decay time of gas hydrate formation for the system $CO_2 + H_2O$ at a constant temperature of 276.15 K. The half decay time is given as a function of degree of supersaturation. Lines are drawn to guide the eye.

half-decay time for ‘used’ water is even longer than for ‘fresh’ water at the same degree of supersaturation. This suggests that the gas hydrate formation in ‘used’ water is even slower than gas hydrate formation in ‘fresh’ water. The presence of residual water structures (due to hydrogen bonding) in the experiments with ‘used’ water does not promote the growth of gas hydrates in the bulk phase. The growth of hydrates after nuclei have been formed, is mainly due to the agglomeration of nuclei and small crystals into larger crystal particles. Therefore, the presence of residual structures have less influence in this process. Introducing hydrogen-bonded water structures will shorten the nucleation time, but will not enhance the growth of gas hydrate crystals. However, compare Figure 3.6 with Figure 3.7, it can be seen that the induction time is much longer than the half decay time and the influence of water quality to the induction time outweighs the influence on half decay time.

3.4.3 Comparison of CO_2 and CH_4 Hydrate Formation

Figure 3.8 shows the induction time as a function of the initial pressure and degree of supersaturation for the systems with either CO_2 or CH_4 . As already shown in Figure 3.6, the induction time diminishes with increasing initial pressure (or degree of supersaturation). Higher supersaturation create a stronger driving force for gas hydrate nucleation. Because of the difference of the phase behaviour

CHAPTER 3. SINGLE GAS HYDRATE

of the systems with CO_2 and CH_4 , the induction time data cannot be directly compared at a given initial pressure (see also Figure 3.8A). The induction time for the carbon dioxide system approaches zero for initial pressures larger than 4.0 MPa, while for methane this happens at a much higher pressure of about 5.5 MPa. Therefore, the induction time is given as function of the degree of supersaturation (as shown in Figure 3.8B).

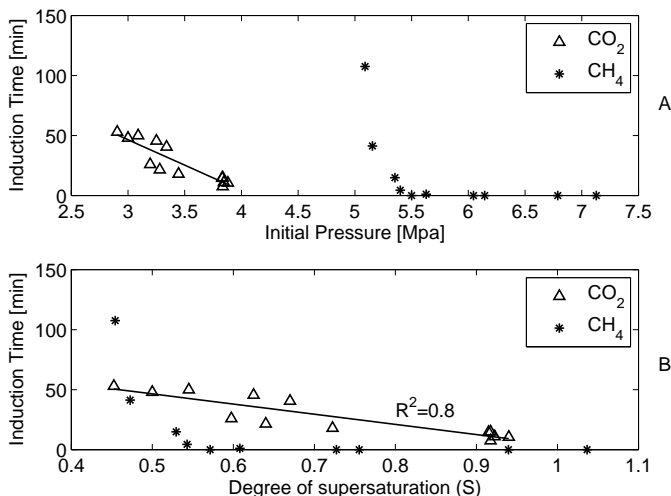


Figure 3.8: Induction time as function of the initial pressure (A) and as a function of the degree of supersaturation (B) for the systems $CO_2 + H_2O$ and $CH_4 + H_2O$. The line is a linear regression of the CO_2 data.

For the $CO_2 + H_2O$ system, the induction time decreases linearly with the degree of supersaturation. Despite the scatter in the data, a linear relation [109] with a regression coefficient of 0.8 fits the experimental data reasonably. For the $CH_4 + H_2O$ system, at a low degree of supersaturation, the induction time is rather high. With increasing degrees of supersaturation, the induction time drops steeply and stays almost at zero at a degree of supersaturation higher than 0.58. This indicates that the nucleation kinetics of the CO_2 and CH_4 systems are different, even though they form the same gas hydrate structure (structure I). For most of the experiments in this study, methane nucleation was found to be faster than the CO_2 nucleation. Only at a very low degree of supersaturation the induction time for the $CO_2 + H_2O$ system is shorter than for the $CH_4 + H_2O$ system. Both CO_2 and CH_4 can fit in either the medium cavities ($5^{12}6^2$) or the small cavities (5^{12}) present in structure I. However, CO_2 tends to occupy the larger ones, while the methane is more stable in the smaller cavity [90]. The affinity to different cavity structures may be the reason for the different nucleation behaviour. However, in order to prove this behaviour experiments on microscopic

scale are required.

In the induction period, formed gas hydrate nuclei either dissociate or keep growing. Only after nuclei has reached the critical size, the hydrate growth process starts and the nuclei grow further into a larger crystal. Therefore, it can be concluded that if the critical size is small, the induction time is shorter. According to Englezos the critical size of a nuclei depends on the interfacial tension between the aqueous phase and the gas hydrate σ and the change in Gibbs free energy for the nucleation Δg [33]:

$$R_{cr} = -\frac{2\sigma}{\Delta g} \quad (3.4)$$

The interfacial tension (σ) between the liquid water and the gas hydrate is considered to be constant for methane. The pressure dependent of Gibb's energy is described by (assuming ideal gas):

$$\frac{\Delta g}{n} = kT \ln\left(\frac{P_{eq}}{P_{ini}}\right) \quad (3.5)$$

where, n is the number of mole, k is the gas constant and T is temperature. Combining Equation 3.4 and 3.5, it can be concluded that the critical nuclei size decreases sharply with increasing initial pressure P_{ini} assuming a constant interfacial tension (see Equation. 3.6).

$$R_{cr} = -\frac{2\sigma}{nkT \ln\left(\frac{P_{eq}}{P_{ini}}\right)} \quad (3.6)$$

Thus the induction time decreases with increasing degrees of supersaturation (which can be seen Figure 3.8). However, the induction time for the carbon dioxide system is longer than for the methane system at the same degree of supersaturation and decreases linearly with supersaturation. This suggests that the interfacial tension between water and gas hydrate in the $CO_2 + H_2O$ system changes with the degree of supersaturation because of the dissolution of CO_2 in the aqueous phase.

The absolute half-decay time ($t_{1/2}$) is determined at the half-decay pressure. Thus it is very sensitive to the initial and final pressure ³ (P_{end}) of the experiments. For example, if the equilibrium pressure is the same but the initial pressure varies, the determined half-decay pressure also varies. Since the initial pressure and equilibrium pressure for CO_2 and CH_4 are different, the determined absolute half-decay time cannot be compared. The normalised half-decay time is introduced

³Note here that P_{end} does not necessarily equal to P_{eq}

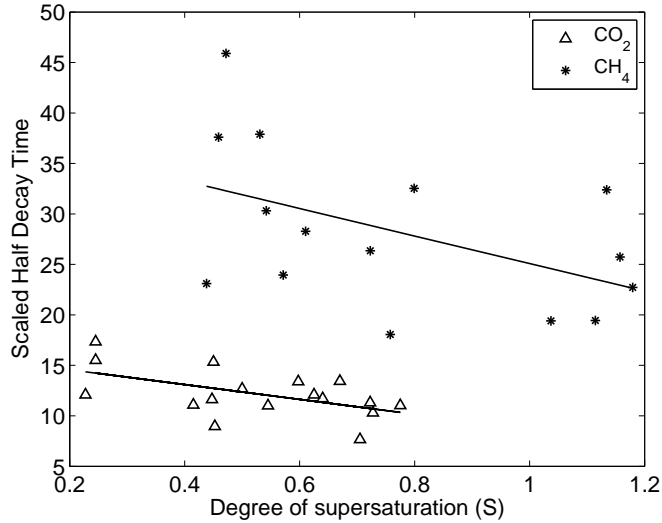


Figure 3.9: Normalised half-decay time as a function of degree of super saturation for the system $CO_2 + H_2O$ and $CH_4 + H_2O$. Lines are drawn to guide the eye.

to allow interpretation and comparison of the data from the various experimental runs. The scaled half-decay time ($t_{s,1/2}$) is determined by:

$$t_{s,1/2} = t_{1/2} \left(\frac{P_{end}}{P_{ini} - P_{end}} \right) \quad (3.7)$$

where, P_{end} is the final pressure, $t_{1/2}$ is half-decay time.

Figure 3.9 gives the scaled half-decay time ($t_{s,1/2}$) as a function of the degree of supersaturation for the experiments with CO_2 or CH_4 . It can be observed that the scaled half-decay time for the CO_2 system is smaller than for the CH_4 system in same range of the degree of supersaturation. This indicates that CO_2 gas hydrate crystals grow faster than CH_4 gas hydrates at the same degree of supersaturation.

The data for the system containing CH_4 show more scatter due to the less accurate determination of the induction time which then also influences the accuracy of the determination of the half-decay time. For CH_4 , it is more difficult to distinguish between the nucleation and the crystal growth process than for CO_2 (see Figure 3.10). The change in the pressure decline is not as clear as for the CO_2 system. This is probably due to the low solubility of CH_4 in water.

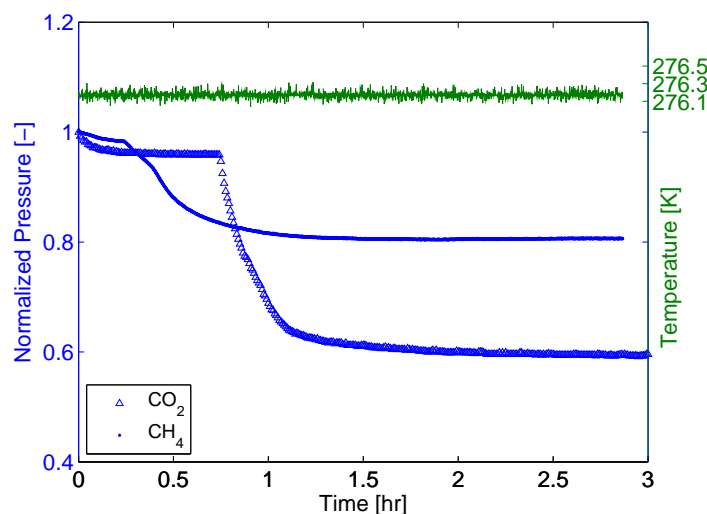


Figure 3.10: Pressure (left y-axes) and temperature (right y-axes) as a function of time during methane (dots) and carbon dioxide (open triangles) hydrate formation at a temperature of 276.15 K.

3.4.4 Effect of Stirring

The stirring rate influences the mixing of gas and liquid phase. Agitation enhances the dispersion of gas bubbles into the liquid phase and dissolution of gas in water. Therefore, the effect of stirring on the kinetics of hydrate formation was studied at an initial pressure of 3.5 MPa while keeping the overall amount of water and gas constant. The stirring speed is varied from 0 to 1400 RPM. For all the previous experiments, the stirring rate was kept constant at 700 RPM.

The effect of stirring on the induction time is displayed in Figure 3.11 for the CO_2 and the CH_4 system. For both systems the induction time decreased with increasing stirring speed. The data of the CH_4 hydrates are scattered. This again might be due to the fact that it is difficult to distinguish between nucleation process and crystal growth process (as see Section 3.4.3). For the carbon dioxide, the induction time decreases linearly with increased stirring speed. The induction time in the CO_2 system becomes almost zero at a stirring rate of 900 RPM. Above this value, the induction time is completely eliminated. For CH_4 the maximum stirring rate at which the induction time becomes zero is 1400 RPM. This means that above a maximum stirring rate nucleation is no longer limiting the gas hydrate formation. As mentioned earlier (see Section 3.3.2), a special stirrer is used allowing not only to agitate the system but also to bubble gas through the

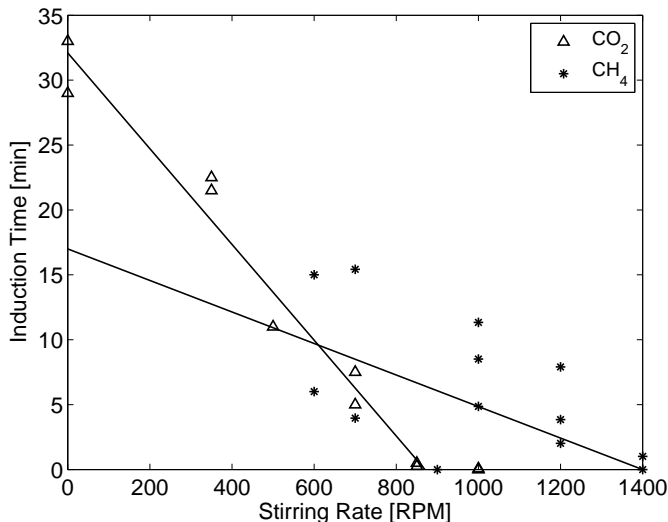


Figure 3.11: Induction time as a function of the stirring rate during CO_2 and CH_4 gas hydrate formation. Experiments were performed at a constant initial pressure of 3.5 MPa for CO_2 and 5.0 MPa for CH_4 . Lines are added to guide the eye.

aqueous liquid phase. As a consequence, the gas-water interface is continuously renewed. During the experiment small ‘snow-ball’ crystals of gas hydrates were observed. After some time the hydrate crystals agglomerate when more gas was dispersed and dissolved in the water and finally forms ‘ice-like’ crystals. The onset of agglomeration did not remarkably change the pressure decay curve (see Figure. 3.10) indicating that there is no mass transfer hindrance due to the formed gas hydrate agglomerates.

The gradient of the induction time of CO_2 system is larger than that for CH_4 system. This suggests that stirring enhances the formation of CO_2 hydrate nuclei more than that of CH_4 hydrate nuclei.

Figure 3.12 shows the half-decay time ($t_{1/2}$) as a function of the stirring rate for the formation of CO_2 and CH_4 hydrates. Similarly to the induction time, the half-decay time decreases with increasing stirring rate. Interestingly the half decay times for both systems react similarly on changes of the stirring rate. This means that the actual growth of the gas hydrates for both systems behave similarly. This supports that due to the continuously renewed contact area between the (liquid) aqueous phase and the gas phase, the gas hydrate formation is enhanced due to accelerated mass transfer of the gas into the liquid phase. The stirring also accelerates the particle movement; therefore, it could enhance the

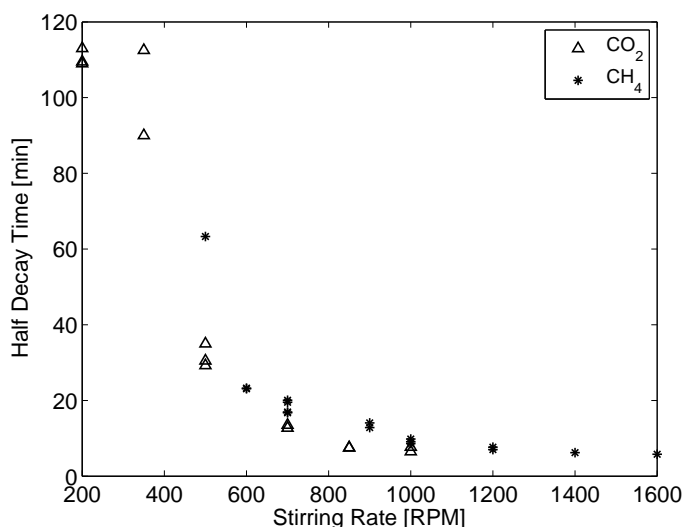


Figure 3.12: Half-decay time as a function of the stirring rate during CO_2 and CH_4 gas hydrate formation at constant temperature of 276.15 K. Experiments were performed at a constant initial pressure of 3.5 MPa for CO_2 and 5.0 MPa for CH_4 .

agglomeration of small crystals.

3.5 Conclusions

The formation kinetics of CO_2 and CH_4 hydrates in a bulk phase was studied in detail. The macroscopic hydrate kinetics behaviour was studied in terms of induction time and (scaled) half-decay time.

Two stages of the hydrate formation process were identified, namely the nucleation and the crystal growth. These different stages were analysed separately. The influence of the water quality, the stirring rates and the kind of gas (CO_2 , CH_4) on the kinetics of the gas hydrate formation were studied.

Experiments indicate that the gas hydrate growth process, namely the growth of the single nuclei to larger crystals, is not improved by either increasing supersaturation or the presence of residual hydrogen-bonded water structures in the aqueous phase. Since, the induction time can be completely eliminate, the rate limiting factor for gas hydrate growth is thus not the formation of the single nucleus, but the crystal growth of small nuclei into larger crystals.

It was found that within the same degree of supersaturation, the crystal growth

CHAPTER 3. SINGLE GAS HYDRATE

of carbon dioxide hydrates is faster than that of methane hydrates. This shows that the exchange of CH_4 hydrates by CO_2 gas hydrates is not only favourable from a thermodynamic point of view but also from formation rate aspects. The nucleation process is accelerated by increasing the degrees of supersaturation for both carbon dioxide and methane system. However, the degree of supersaturation has hardly any effect on the crystal growth process.

For both the CO_2 and the CH_4 system the induction time (t_{ind}) diminishes as the degree of supersaturation increases. The induction time of the system with CO_2 decreases almost linearly, while for CH_4 the induction time only decreases strongly for low supersaturation. For a high degree of supersaturation (> 0.6) the induction time approaches zero.

The nucleation time for hydrates formed with 'used' water is significantly lower than for 'fresh' water. This can be explained by the residue water structure from dissociated gas hydrates and the abundance of hydrogen bonds in the aqueous liquid phase at low temperatures. However, the different water quality does not enhance the crystal growth. The half decay times of both systems are similar.

It was found that stirring promotes the gas hydrates formation, nucleation and growth, for both gases because the interface between the gas and the aqueous liquid phase is continuously renewed.

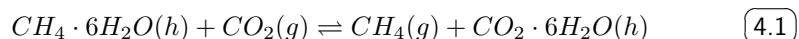
4

Hydrate Formation and Exchange in Ternary Systems

In this chapter two aspects of gas hydrate behaviour will be discussed: the first is the formation kinetics of gas hydrates in the ternary system ($CO_2 + CH_4 + H_2O$) and the second is the feasibility to exchange methane by CO_2 as guest molecule in the already formed methane hydrates without dissociation.

4.1 Introduction

Simultaneous production of CH_4 hydrate and sequestration of CO_2 has attracted attention in recent years. The greatest advantage of this process is that it combines production of natural gas and reduction of CO_2 from the atmosphere.



The success of the proposed process depends on whether CO_2 hydrate formation is more favourable than CH_4 and how well the methane can be replaced by CO_2 in the gas hydrates.

Ohgaki et al. [97] presented the phase equilibrium data of the $CH_4 + CO_2 + H_2O$ system under isothermal conditions of 280K. Seo et al. [107, 108] determined phase equilibrium line ($H - L_w - V$) for the same system at pressure range between 1.5 and 5.0 MPa and temperature range from 273.5 to 283.5K. Nakano et al. [90] determined the relative cage occupancy for small (I) and medium (II) cavities in mixed CO_2 and CH_4 hydrates by Raman spectroscopy under 46 MPa. So far, research on the gas hydrate formation from a mixed gas systems have mainly focused on equilibrium conditions. The kinetics of hydrate formation from mixed gas systems have not yet been well studied.

CHAPTER 4. HYDRATE FORMATION AND EXCHANGE IN TERNARY SYSTEMS

In Chapter 3, we discussed the gas hydrate formation from a single-component (CO_2 or CH_4) gas phase in bulk condition. The results suggest that not only from a thermodynamic point of view but also from the kinetics of gas hydrate, the formation of CO_2 hydrates is more favourable than CH_4 hydrate formation. However, it is unclear whether the presence of another component in the gas phase affects the gas hydrate formation. This makes the experiments in the ternary system ($CO_2 + CH_4 + H_2O$) necessary.

The first part of this chapter reports a detailed experimental study on the competitive formation of CO_2 and CH_4 hydrate in the ternary system of $CO_2 + CH_4 + H_2O$. Gas hydrates were formed and dissociated while the gas phase composition was being monitored. The experiments were done at isothermal conditions (275.65 K) while the initial pressure varied from 2.5 to 6.0 MPa.

In the second part of this chapter, an experimental investigation on the efficiency of methane exchange by CO_2 in the gas hydrates in the bulk system will be discussed. Experiments were carried out at conditions above the $H-L_w-V$ phase equilibrium line of $CH_4 + H_2O$ system. Therefore the dissociation of methane hydrates during the CO_2 exchange process can be avoided. The exchange rate of methane by CO_2 as guest molecules in the gas hydrates was deduced from the changes in the composition of the gas phase. The subsequent dissociation of the CO_2 hydrate was done to identify how much CH_4 has been replaced by CO_2 within the gas hydrates during the exchange process.

4.2 Phase Behaviour

4.2.1 Binary System

Figure 4.1 shows the $H-L_w-V$ equilibrium line for the $CO_2 + H_2O$ and the $CH_4 + H_2O$ system. For the $CO_2 + H_2O$ system, at temperatures above 283K, the equilibrium line describes the coexistence of an aqueous liquid phase (L_w), a liquid phase rich in CO_2 (L_g) and the hydrate phase (H). For temperatures below 283K, the $H-L_w-V$ curve of the $CH_4 + H_2O$ system was found at higher pressures than for the $CO_2 + H_2O$ system. Typically, natural gas hydrate reservoirs were found in the temperature range between 274K and 283K. Therefore, in this study, the experiments were performed at low temperatures. In this way, only the $H-L_w-V$ equilibrium line needs to be considered and the pressures necessary to form gas hydrates are not too high to handle with the given experimental set-up.

From the phase diagram (Figure 4.1) it is evident that CO_2 hydrates are stable at lower pressures than CH_4 hydrates at the same temperature (for $T < 283K$). This indicates again that CO_2 hydrates are energetically more favourable than CH_4 . It was also found in a previous study that CO_2 hydrates grow faster than CH_4 hydrates [50]. This suggests that the exchange of methane by CO_2 within

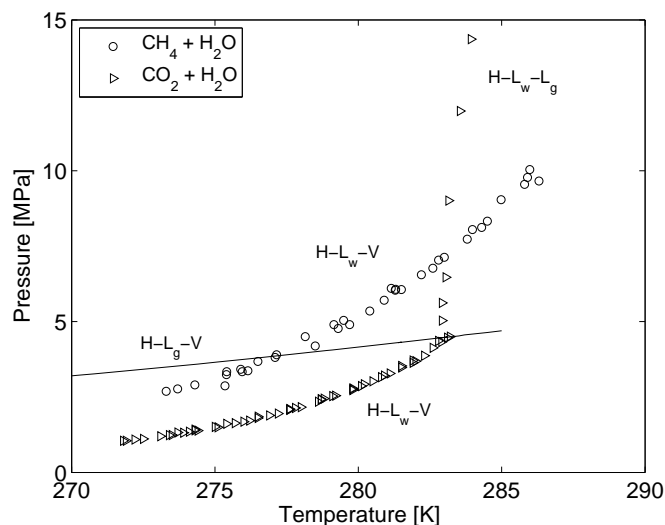


Figure 4.1: Phase diagram of the binary systems $CO_2 + H_2O$ and $CH_4 + H_2O$ respectively. In the diagram, only the equilibrium lines with a hydrate phase coexisting are depicted. L_w describe aqueous phase, V describes vapour phase, H describes hydrate phase and L_g describes the liquid phase rich in CO_2 . Data are taken from literature [27, 103, 122, 148, 71, 92]

gas hydrates is possible from the kinetic point of view.

4.2.2 Ternary System $CO_2 + CH_4 + H_2O$

In the ternary system, depending on the composition of the vapour phase, the $H - L_w - V$ curve shifts between the phase equilibrium lines of the respective binary systems [107, 108]. For high methane concentrations the $H - L_w - V$ of the ternary system is closer to the $H - L_w - V$ curve of the $CH_4 + H_2O$ system. For high CO_2 concentrations, the phase line is closer to the $H - L_w - V$ curve of the $CO_2 + H_2O$ system.

Figure 4.2 depicts the phase equilibria curves ($H - L_w - V$) of the $CO_2 + CH_4 + H_2O$ ternary system. The phase equilibrium data for 20 mol% and 60 mol% of CO_2 in the gas phase were taken from Seo et al. [107, 108]. The $H - L_w - V$ line for the 50 mol% CO_2 gas phase composition was obtained by interpolating these data. Points A to E depict the initial pressures used in this experimental study.

Point A and B are above $H - L_w - V$ lines for the $CO_2 + H_2O$ and $CH_4 + H_2O$ system, meaning that methane and carbon dioxide hydrates are stable at these

CHAPTER 4. HYDRATE FORMATION AND EXCHANGE IN TERNARY SYSTEMS

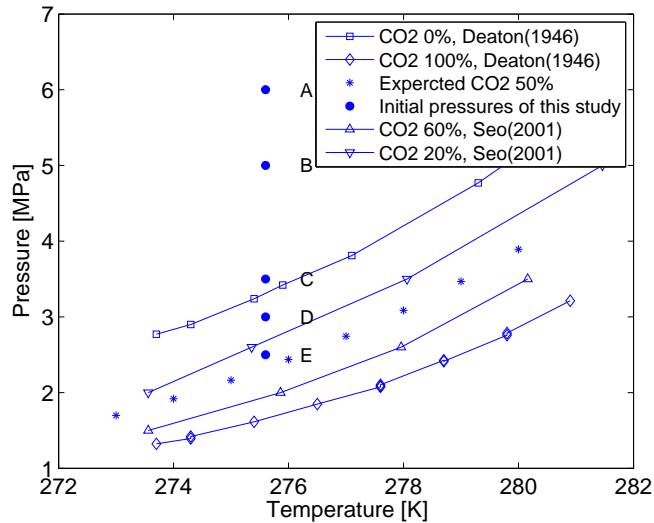


Figure 4.2: The phase equilibrium line of the ternary system with carbon dioxide, methane and water [27]. The curves shift with changing gas phase composition. The 50/50 mol% equilibrium line is interpolated from literature data. Point A, B, C, D and E indicate the initial pressure conditions for this work.

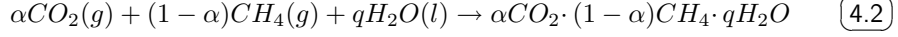
pressures. Point C is slightly above the $H-L_w-V$ line of the $CH_4 + H_2O$ binary system and point D is slightly lower than this line. Point E is approximately on the $H-L_w-V$ curve for the ternary system ($CO_2 + CH_4 + H_2O$) with a 50/50 gas phase composition.

Experiments were focused on the competitive formation of CO_2 and CH_4 hydrates from a mixed gas phase. It is important to know the concentration of CO_2 and CH_4 hydrates in the already formed gas hydrates. For example, point C is above the ternary phase equilibrium, which means mixed hydrates could form. However, from the given equilibrium data, it cannot be deduced how much of methane (or CO_2) contributed to the hydrate formation process. Therefore, we used a parameter to evaluate the contribution of each gas to form hydrates. This is called the contribution factor and it is calculated from the composition changes in the gas phase.

4.2.2.1 Contribution Factors

The van der Waals diameter of CO_2 (0.47 nm) is slightly larger than that of CH_4 (0.41 nm) [146], yet, they form the same types of hydrate structure (I) [58]. In

the ternary system, the gas hydrate formation can be stated as¹:



where α is the mole fraction of CO_2 hydrates in the hydrate phase. q is the hydration number of gas hydrate in the ternary system; in the ideal case, $q = 6$ [58].

The contribution factor is defined as the number of moles of a specific gas incorporated into the gas hydrates over the total number of moles of gas, thus it varies between 0 and 1. For CH_4 and CO_2 the contribution factor is expressed by Equation 4.3 and 4.4 respectively:

$$\alpha_{CH_4} = \frac{n_{CH_4}^H}{n_{tot}^H} = \frac{n_{CH_4}^H}{n_{CH_4}^H + n_{CO_2}^H} \quad (4.3)$$

$$\alpha_{CO_2} = \frac{n_{CO_2}^H}{n_{tot}^H} = \frac{n_{CO_2}^H}{n_{CH_4}^H + n_{CO_2}^H} \quad (4.4)$$

where n_{tot}^H is the total number of moles of gas captured in gas hydrates at the end of the experiment. The moles of gas hydrates equals the moles of gas that ‘disappear’ from the vapour phase. Therefore, n_{tot}^H can be calculated by the amount of gas components consumed in the gas phase (see Equation 4.5).

$$n_{tot}^H = n_{tot,ini}^V - n_{tot,end}^V - n_{tot,loss}^V \quad (4.5)$$

where $n_{tot,ini}^V$ is the number of moles of gas initially present in the gas phase, $n_{tot,loss}^V$ is the number of moles of gas ‘lost’ due to sampling, and $n_{tot,end}^V$ is the number of moles of gas at the end of the experiment. The calculation of the number of moles was done by applying the Peng-Robinson equation of state [102]. Similarly, $n_{CH_4}^H$ and $n_{CO_2}^H$ are the number of moles of methane or CO_2 in the hydrate phase.

$$n_{CH_4}^H = n_{CH_4,ini}^V - n_{CH_4,end}^V - n_{CH_4,loss}^V \quad (4.6)$$

$$n_{CO_2}^H = n_{CO_2,ini}^V - n_{CO_2,end}^V - n_{CO_2,loss}^V \quad (4.7)$$

¹Here, it was assumed that in the ternary system mixed gas hydrates are formed and all CH_4 , CO_2 and H_2O are consumed to form gas hydrates

CHAPTER 4. HYDRATE FORMATION AND EXCHANGE IN TERNARY SYSTEMS

The contribution factor is calculated for the ternary experiment to characterise the mole fractions of CH_4 and CO_2 in the hydrate phase. This value also indicates the competition of CH_4 and CO_2 molecules in occupying the hydrate cavities. The calculation of contribution factor and number of moles in the gas phase are issued in detail in Appendix A.

4.3 Experiments

4.3.1 Materials

For the ternary experiments a pre-mixed gas consisting of 50 mol% carbon dioxide and 50 mol% methane was used (Linde Company). For exchange experiment, CH_4 with a purity of 99.5 mol% and CO_2 with a purity of 99.7 mol% was used. Double distilled water was injected initially into the autoclave and repetitively used for all experiments.

4.3.2 Experimental Set-up

The set-up used to carry out the experiments is shown in Figure 4.3. It consists of a gas supply system (1), a high pressure stainless steel autoclave(2) with two sapphire windows for visual observation (3) and an in-house data acquisition system (not included in the figure). This set-up differs from the set-up used in Chapter 3. The difference is in the gas supply system and in the agitation in the autoclave.

The autoclave was designed as a double-walled stainless steel cell. Through the outer chamber, cooling liquid was circulated to establish the desired temperature. The inner volume of the autoclave is 67 ml and can withstand pressures up to 10 MPa. The maximum operating pressure was set to 8 MPa by means of a safety valve. A LAUDA RE 220 thermostat was used to control the temperature within ± 0.2 K.

A magnetic stirrer was used to agitate the liquid. This enhances the mass transfer and the dispersion of the gas into the liquid phase before and during gas hydrate formation. The autoclave has three inlet lines (L1, L2 and L3 as indicated in Figure 4.3). One reaches 5 mm above the bottom of the autoclave (L1). This was done to assure that from this line the injected gas was bubbled through the aqueous liquid phase, increasing the gas-liquid contact area. The rest line ends at the cap of the autoclave and is used for flushing CO_2 (L2) and sampling the gas phase (L3) without contamination by liquid.

The pressure in the cell was monitored by a Druck PTX 600 pressure transducer with an accuracy of 0.08 % over the full determined pressure range. The pressure

4.3. EXPERIMENTS

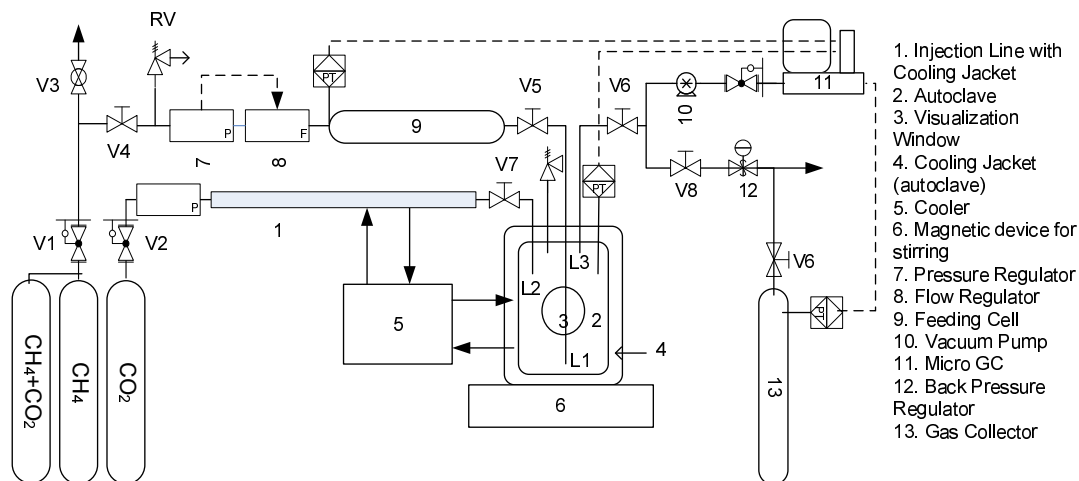


Figure 4.3: Schematic of the experimental set-up

transducer can withstand a maximum pressure of 15 MPa. The temperature within the cell was determined using a THERMOCOAX thermocouple (with an accuracy of ± 0.3 K, including the error for the data acquisition system). The temperature and pressure data were collected every 10 seconds using an in-house data acquisition software.

A stainless steel tube of known volume (0.7 mL) was connected to the outlet of the cell for sampling the gas phase. The pressure decrease due to sampling of this volume was less than 0.02 MPa, so that it can be assumed that it does not influence the results. The gas samples were analysed by means of an Agilent 3000 Micro Gas Chromatograph (GC) with a plot U column².

4.3.3 GC Analysis

The retrieved gas sample are analysed by a GC. Helium was used as carrier gas. The temperature of the GC was set to 373 K and kept constant. The error of the analysis was determined to be less than 0.42%. The chromatograms of pure CO_2 , CH_4 and 50/50 mol% mixture of CO_2 and CH_4 are shown in Figure 4.4.

Prior to the analysis, the GC needs to be calibrated. For this purpose a standard calibration gas mixture of know composition was used (Mixture of Helium, Hydrogen, Oxygen, Nitrogen, Methane, Ethane, Carbon Dioxide, Carbon Monoxide, etc. Sample No. 080801A, manufactured by Agilent). Afterwards, calibrations were also performed with pure methane, pure carbon dioxide and 50/50 mixture

²A column is the capillary tube for composition analyse in the GC. Plot U column is suitable for detecting hydrocarbons (C1-C7) and CO_2

CHAPTER 4. HYDRATE FORMATION AND EXCHANGE IN TERNARY SYSTEMS

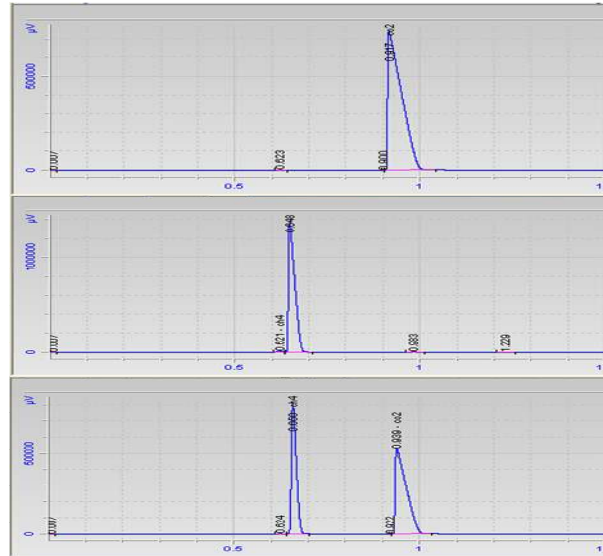


Figure 4.4: Chromatograms of pure carbon dioxide (top), pure methane (middle) and 50/50 mol% gas mixture of methane and carbon dioxide.

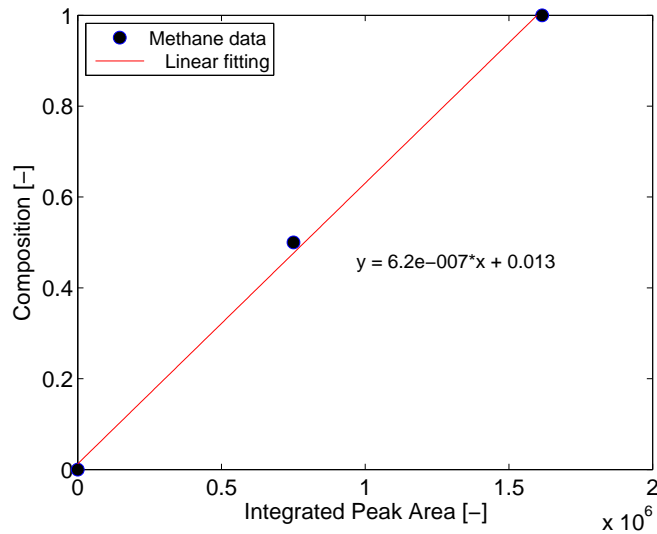


Figure 4.5: The calibration curve for methane given in terms of mole fractions as a function of the peak area. The symbols represent determined methane concentration. The line gives the linear fit of the data.

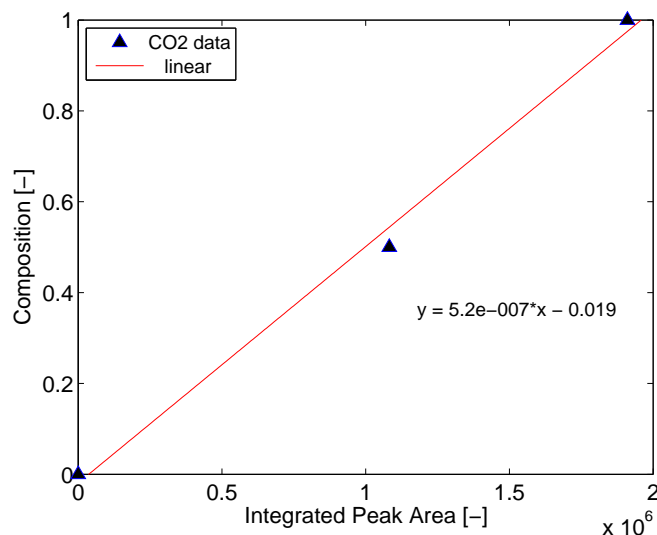


Figure 4.6: The calibration curve for carbon dioxide given in terms of mole fractions as a function of the peak area. The symbols represent determined CO_2 concentration. The line gives the linear fit of the data.

of CO_2 and CH_4 . Figure 4.5 and 4.6 shows the calibration curve for CO_2 and CH_4 . The correlation between the integrated peak area and gas phase composition was depicted.

4.3.4 Experimental Procedure

4.3.4.1 Gas Hydrate Formation with CH_4 and CO_2 Mixtures

First, 30 ml of double distilled water was charged into the autoclave. After the addition of water, the cell was sealed and gradually cooled. Air was removed from the gas phase by flushing gas mixtures at 1.0 MPa through the cell. After the temperature stabilised at the desired value, gas was injected into the autoclave up to the desired pressure. Then all valves were closed and the experiment started.

Temperatures and pressures in the cell were monitored and samples of the gas phase were taken at different time intervals and analysed with the GC. The experiments were carried out with the following initial pressures: 6.0, 5.0, 3.5, 3.0 and 2.5 MPa at a constant temperature of 275.65 K. At this temperature, the equilibrium pressure for the ternary system of given composition was 2.5 MPa³.

³This value was determined by experiments in this study.

CHAPTER 4. HYDRATE FORMATION AND EXCHANGE IN TERNARY SYSTEMS

The gas hydrate formation is regarded as finished when the pressure in the gas phase changes is less than 5 kPa per hour. Then the subsequent dissociation started. Gas hydrate dissociation was carried out by decreasing pressure in steps of 0.5 MPa while allowing the system to stabilise at each step. New experiments were started after the hydrates had completely disappeared from the cell.

4.3.4.2 Exchange of CH_4 with CO_2 in Methane Hydrates

The preparation and water injection were done in the same way as for the mixed gas hydrate formation experiments. However, the following procedures are different:

First, the cell was pressurised to 7.0 MPa while keeping the temperature constant at 276.15 K to promote CH_4 hydrate formation. After 24 hours the pressure became stable and it was observed that the autoclave was filled with ‘ice-like’ solid hydrates.

Then, CH_4 was removed from the gas phase by flushing the cell with CO_2 . In order to avoid methane hydrate dissociation during the flushing, the CO_2 was pre-cooled and injected at a pressure of 0.3-0.5 MPa higher than the stabilised pressure after methane hydrate formation. The flushing process took 15-20 minutes. When CO_2 mole fraction of >90 mol% in the gas phase was reached, the flushing was stopped and the actual exchange process was started. The composition of the gas phase was monitored by regularly taking samples and analysed by means of GC.

The experiment was stopped when no obvious decrease in the composition of the gas phase could be observed. The subsequent gas hydrate dissociation was started by decreasing pressure in steps 0.5 MPa. At each step pressure in the cell was allowed to stabilise. Three samples of the gas phase were taken and analysed for each pressure release.

4.4 Results and Discussion

4.4.1 Gas Hydrate Formation Kinetics in Ternary System

The gas hydrate formation from a gas mixture of CO_2 and CH_4 was investigated at constant temperature of 275.65 K with various initial pressures of 6.0, 5.0, 3.5, 3.0 and 2.5 MPa (see Figure 4.2). These pressures represent different states of the ternary system as it was described in section 4.2.2 Figure 4.2. It was observed that at an initial pressure of 2.5 MPa, liquid water was still present in the cell after gas hydrate formation. While with higher initial pressures, solid hydrates filled up the cell at end of the experiment. No liquid water was observed. So,

with higher initial pressures, the dissolution effect of CO_2 can be ignored, while for an initial of 2.5 MPa, the dissolution of CO_2 needed to be taken into account.

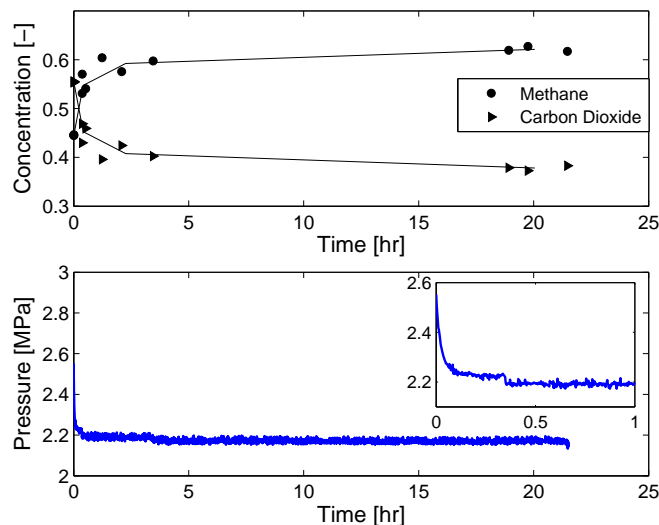


Figure 4.7: Mixed gas hydrate formation at an initial pressure of 2.5 MPa, $T = 275.65$ K. The top figure shows the composition of gas phase as a function of time, initial gas phase composition in the cell is $x_{CH_4} = 0.45$; $x_{CO_2} = 0.55$. Lines are drawn to guide the eye. The bottom figure shows pressure decline during gas hydrate formation.

Figure 4.7 to 4.11 show the results of gas hydrate formation experiments for different initial pressures. In these figures the gas phase composition and the pressure as a function of time are given. The pressure decline indicates the gas hydrate formation. At high initial pressures, the time for the ternary system to reach equilibrium state is long.

From these figures, it can be seen that the composition as a function of time follows a similar trend for all initial pressures: CO_2 mole fractions decreases while CH_4 mole fractions increases. It can be observed that the gas phase composition change is dramatic in the first 5 hours. Afterwards, the gas phase composition gradually stabilises. This separation effect of the CO_2 and CH_4 mole fraction indicates that the amount of hydrates formed with CO_2 and CH_4 are different. Otherwise, the gas phase composition at the initial state and the equilibrium state would be equal (neglecting the CO_2 dissolution into the liquid). This suggests that in the ternary system, more CO_2 hydrates were formed compared to CH_4 hydrates. This proves that it is more favourable to form CO_2 hydrates than CH_4 hydrates.

In Figure 4.12 the change of the CO_2 mole fraction over the initial CO_2 mole fraction as a function of the initial pressure is given. To allow direct comparison between the different experiments at different initial pressures, we used a scaled

CHAPTER 4. HYDRATE FORMATION AND EXCHANGE IN TERNARY SYSTEMS

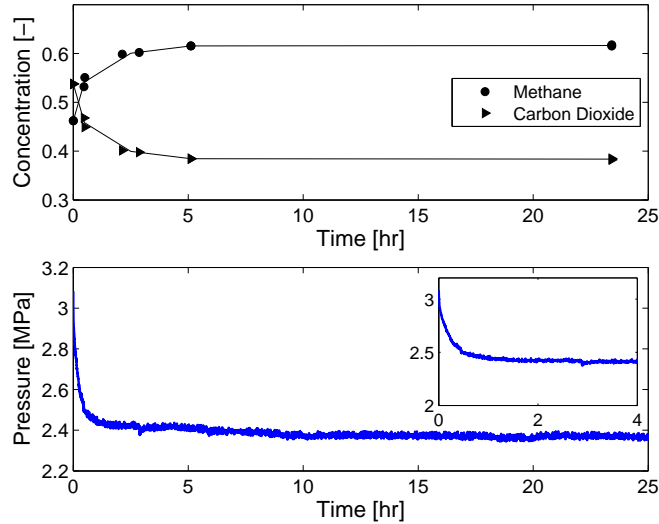


Figure 4.8: Mixed gas hydrate formation at an initial pressure of 3.0 MPa, $T = 275.65$ K. The top figure shows composition of gas phase as a function of time, initial gas phase composition in the cell is $x_{CH_4} = 0.46$; $x_{CO_2} = 0.54$. Lines are drawn to guide the eye. The bottom figure shows pressure decline during hydrate formation.

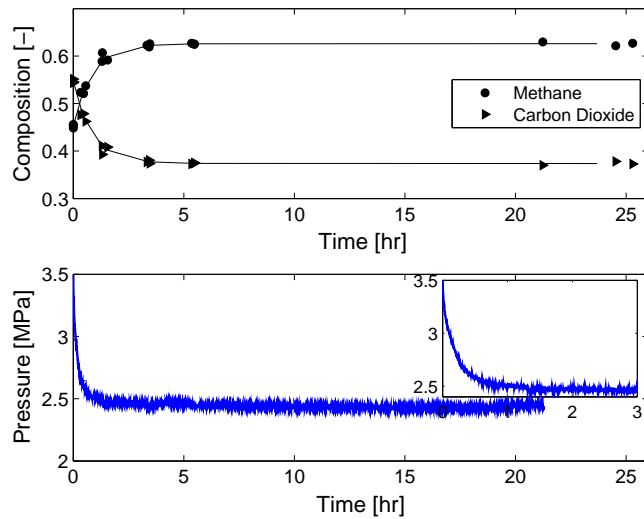


Figure 4.9: Mixed gas hydrate formation at an initial pressure of 3.5 MPa, $T = 275.65$ K. The top figure shows composition of gas phase as a function of time, initial gas phase composition in the cell is $x_{CH_4} = 0.45$; $x_{CO_2} = 0.55$. Lines are drawn to guide the eye. The bottom figure shows pressure decline during hydrate formation.

4.4. RESULTS AND DISCUSSION

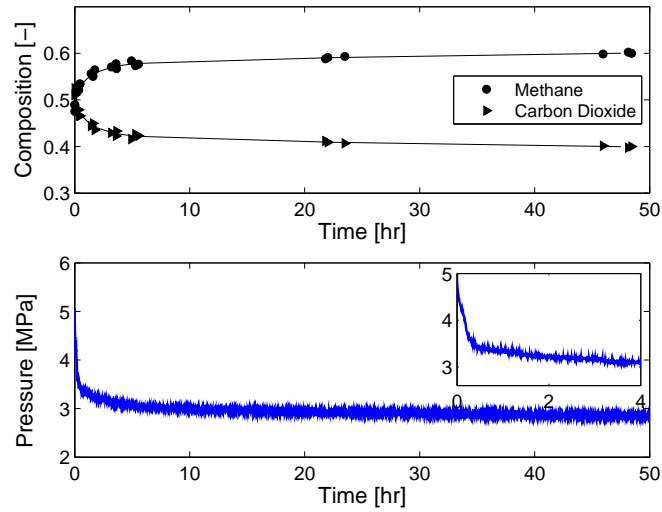


Figure 4.10: Mixed gas hydrate formation at an initial pressure of 5.0 MPa, $T = 275.65$ K. The top figure shows composition of gas phase as a function of time, initial gas phase composition in the cell is $x_{CH_4} = 0.48$; $x_{CO_2} = 0.52$. Lines are drawn to guide the eye. The bottom figure shows pressure decline during hydrate formation.

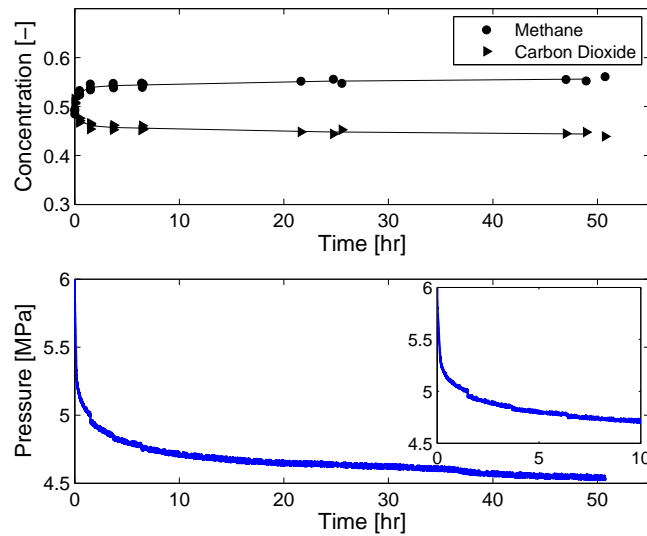


Figure 4.11: Mixed gas hydrate formation at an initial pressure of 6.0 MPa, $T = 275.65$ k. The top figure shows composition of gas phase as a function of time, initial gas phase composition in the cell is $x_{CH_4} = 0.49$; $x_{CO_2} = 0.51$. Lines are drawn to guide the eye. The bottom figure shows pressure decline during hydrate formation.

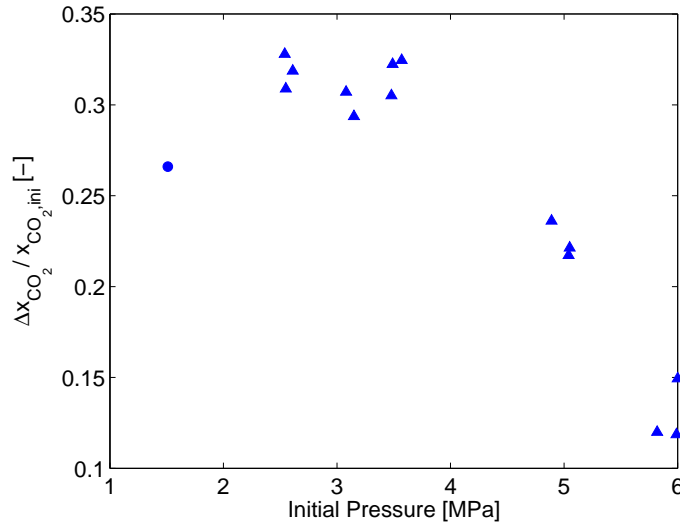


Figure 4.12: Separation effect during gas hydrate formation. The separation is indicated by the change in CO_2 mole fractions over the initial mole fractions ($\Delta x_{CO_2}^V / x_{CO_2,ini}^V$). The round dot shows the separation effect only by CO_2 dissolution into the liquid aqueous phase at 1.5 MPa at a temperature of 275.65 K.

mole fraction which is described as follow:

$$\Delta x_{CO_2}^V = x_{CO_2,ini}^V - x_{CO_2,eq}^V \quad (4.8)$$

$$\Delta x_{CO_2,s} = \frac{\Delta x_{CO_2}^V}{x_{CO_2,ini}^V} \quad (4.9)$$

The scaled composition difference ($\Delta x_{CO_2} / x_{CO_2,ini}$) tells how much CO_2 was removed from the vapour phase and it represents the separation effect by gas hydrate formation. $\Delta x_{CO_2} / x_{CO_2,ini} = 1$ is the maximum value which indicate the complete removal of CO_2 in the gas phase. The round dot is a benchmark experiment for the separation of the $CO_2 + CH_4$ mixture by only dissolving CO_2 into the liquid aqueous phase. This was carried out at the same temperature as the gas hydrate experiments but at a lower pressure (below the $H - L_w - V$ equilibrium curve of CO_2) to avoid gas hydrate formation. $\Delta x_{CO_2,s}$ decreases with increased initial pressures. It can be seen that for experiments with initial pressure of 2.5, 3.0 and 3.5 MPa, $\Delta x_{CO_2,s}$ does not differ much with respect to the pressure and the plateau value is around 0.3. At high initial pressures the separation of CO_2 and CH_4 in the gas phase becomes less obvious. At initial pressure of 6.0 MPa, the composition difference ($\Delta x_{CO_2,s}$) is only 0.12, meaning

4.4. RESULTS AND DISCUSSION

that only 12% of the initially present CO_2 was removed from the gas phase after the gas hydrate formation. Results show that the separation effect is more pronounced for lower initial pressures within the gas hydrate stability zone. CO_2 has a high solubility in the aqueous liquid phase which already gives a reasonable separation effect. Therefore, a combined process of gas hydrate formation with CO_2 dissolution could probably achieve a better separation.

For calculation of the contribution factor, it was assumed that the volume of the gas phase at the end of experiment is 10% less than initial volume of the gas phase. This decrease of vapour phase volume is due to the expansion of hydrate solids after gas hydrate formation. Table 4.1 shows the calculated contribution factors for methane and carbon dioxide at various initial pressures. For the experiment at an initial pressure of 2.5 MPa, liquid water was present at the end of experiments, thus, Equation 4.10 does not hold anymore. Thus the number of moles of gas hydrates should be calculated by:

$$n_{tot}^H = n_{tot,ini}^V - n_{tot,end}^V - n_{tot,loss}^V - n_{di} \quad (4.10)$$

where, n_{di} is the number of moles of gas dissolved in the liquid aqueous phase. However, the solubility within the hydrate region is difficult to determine. Therefore, at 2.5 MPa, when aqueous liquid phase was present at the end of experiment, the effect of the CO_2 dissolution cannot be ignored. Therefore, the contribution factor cannot be accurately calculated.

P_{ini} [MPa]	T [K]	$x_{M,ini}^V$	$x_{C,ini}^V$	Std. DIV.	α_M	α_C
6.00	275.61	0.494	0.506	2.04E-3	0.34	0.66
5.99	275.65	0.484	0.516	1.86E-3	0.28	0.72
5.82	275.59	0.491	0.509	9.64E-4	0.36	0.64
5.05	275.61	0.490	0.510	2.02E-3	0.37	0.63
5.04	275.65	0.489	0.511	1.49E-3	0.36	0.64
4.89	275.81	0.475	0.525	1.69E-3	0.31	0.69
3.57	275.58	0.448	0.552	2.37E-3	0.11	0.89
3.49	275.60	0.454	0.546	1.73E-3	0.12	0.88
3.48	275.54	0.456	0.544	2.13E-3	0.14	0.86
3.15	275.75	0.462	0.538	2.39E-3	0.09	0.91
3.08	275.54	0.463	0.537	2.09E-3	0.06	0.94

Table 4.1: Computed gas hydrate contribution of CH_4 and CO_2 under various initial pressures. 3 repetitive GC tests were performed for each sample. Standard deviation was calculated from the 3 GC results.

The data in Table 4.1 show that the CH_4 contribution factor decreases with increasing initial pressures. At an initial pressure of 6.0 and 5.0 MPa on average 35% of the gas captured in gas hydrates is methane. At these high initial pressures, both CO_2 and CH_4 hydrates are stable. The gas hydrates in the cell are a

CHAPTER 4. HYDRATE FORMATION AND EXCHANGE IN TERNARY SYSTEMS

mixture of CO_2 and CH_4 hydrates but they contains more CO_2 than methane. This indicates that at a condition where both CO_2 and CH_4 hydrate are able to form, the CO_2 are still more favourable to form hydrates than CH_4 .

In the binary $CH_4 + H_2O$ system, the phase equilibrium pressure is 3.43 MPa at 275.65 K (See Figure 4.1). However, in our experiments, no methane hydrate formation was noticed for initial pressure of 3.5 MPa in the binary system. In the ternary system ($CO_2 + CH_4 + H_2O$), methane hydrates were identified at the initial pressure of 3.5 MPa and 12% of the formed gas hydrates were captured by methane. At lower pressures (at 3.0 MPa) 7% of the gas hydrates contain methane. This implies that even at conditions under which no CH_4 hydrates can be formed in the binary system ($CH_4 + H_2O$), methane can still be captured by water cavities due to the presence of CO_2 (or CO_2 hydrates). When CO_2 hydrates start to form, the water molecules organise around the CO_2 molecules forming hydrogen bonds. It would probably help to attract methane molecules and forms hydrates. However, more work on molecular simulation is needed to identify the microscopic mechanism.

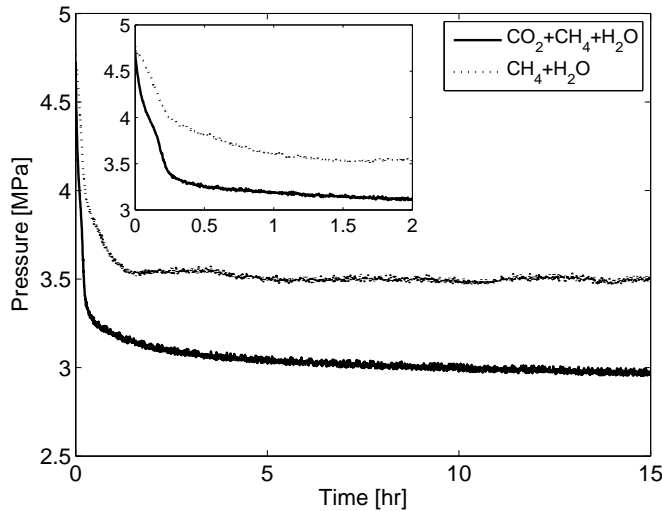


Figure 4.13: Pressure profile during gas hydrate formation in the ternary ($CO_2 + CH_4 + H_2O$) and binary ($CH_4 + H_2O$) system. Both experiments were operated at an initial pressure of 5.0 MPa and a constant temperature of 275.65 K.

To further illustrate the difference between gas hydrate formation from a mixed gas phase and pure gas phase, the pressure decline curves were compared. The hydrate formation experiment of the two binary systems of $CO_2 + H_2O$ and $CH_4 + H_2O$ cannot be operated at the same initial pressure. At high initial pressures, CO_2 condenses and at low initial pressures CH_4 cannot form gas hydrates.

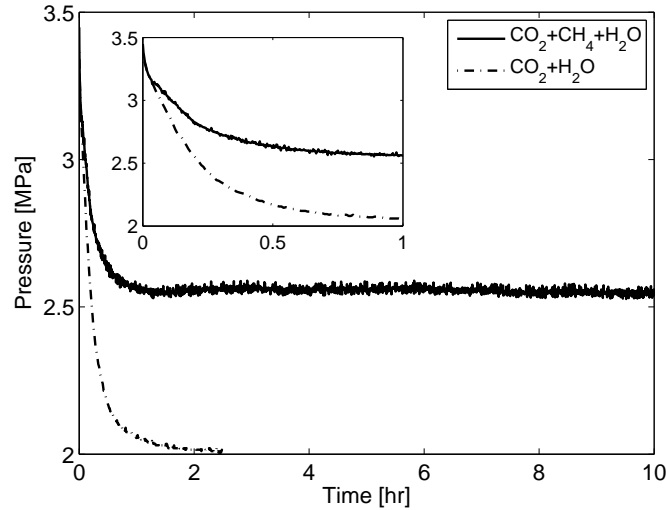


Figure 4.14: Pressure profile during gas hydrate formation in the ternary ($CO_2 + CH_4 + H_2O$) and binary ($CO_2 + H_2O$) system. Both experiments were operated at an initial pressure of 3.5 MPa and a constant temperature of 275.65 K.

Therefore, the pressure curves during CH_4 hydrate formation and the mixed gas hydrate formation were shown in Figure 4.13 with an initial pressure of 5.0 MPa. The pressure decline of $CO_2 + H_2O$ binary and $CO_2 + CH_4 + H_2O$ ternary system were depicted in Figure 4.14 with an initial pressure of 3.5 MPa.

It can be seen that the pressure depletion for the ternary system was faster than for the CH_4 binary system but slower than the CO_2 binary system. This implies that mixed gas hydrate formation is faster than CH_4 hydrate formation.

As already explained in Section 4.2, the $H - L_w - V$ curve of the ternary system lies in between the $H - L_w - V$ curve of the $CO_2 + H_2O$ and $CH_4 + H_2O$ binary systems. The results of our experiments indicate that a similar behaviour holds also for the kinetic hydrate formation. When gas hydrates are formed from a gas mixture consisting A and B, assuming gas A forms gas hydrates faster than gas B in their respective binary system ($R_A > R_B^4$). Then the overall hydrate formation rate of the ternary system is between the formation rates of the two binary systems ($R_A > R_{AB} > R_B$).

⁴ R_A indicating the gas hydrate formation rate of A. R_{AB} indicating the formation rate of the mixed hydrates by A+B gas mixtures.

CHAPTER 4. HYDRATE FORMATION AND EXCHANGE IN TERNARY SYSTEMS

4.4.2 Exchange of CH_4 by CO_2 in Methane Hydrates

The experiment of exchange methane by CO_2 within already formed gas hydrates without dissociation was performed in 3 separate steps: 1) formation of methane hydrates and 2) replacing CH_4 with CO_2 in gas hydrates; 3) dissociation of the gas hydrates. The results of each process will be discussed below separately.

4.4.2.1 Methane Hydrates Formation

Figure 4.15 shows the pressure decline during methane hydrate formation at a constant temperature of 276.15 K. The initial pressure was set to 7.0 MPa but varied slightly for each experiment within the methane hydrate stability zone (see Figure 4.15). The initial amount of water and CH_4 were chosen as such that after gas hydrate formation no liquid water was present. This was to avoid CO_2 dissolution in the liquid aqueous phase which would make the interpretation of the data inconclusive.

According to the phase diagram of the $CH_4 + H_2O$ system (Figure 4.1), the $H - L_w - V$ equilibrium pressure at 276.15K is 3.5 MPa [27]. However, from the pressure decline curve in Figure 4.15, it can be seen that the pressure stabilises at a higher pressure than the equilibrium pressure. This means that the water initially present in the cell has been consumed completely leaving excess CH_4 in the cell.

Three experiments were performed. The pressure decline curves for experiment 1 and 2 almost overlap which shows a good reproducibility. During the CH_4 hydrate formation, the pressure in experiment 1 and 2 dropped from 6.95 and 6.85 MPa to 4.58 and 4.64 MPa. For experiment 3, the pressure dropped from 7.15 MPa to 4.80 MPa. The stabilised pressure of experiment 3 is slightly higher than experiment 1 and 2. This is due to the accidental water loss when dissociating the previously formed gas hydrates. Therefore, experiment 3 has less water in the cell than for experiment 1 and 2.

4.4.2.2 $CH_4 - CO_2$ Exchange Process

After CH_4 hydrate formation, CH_4 in the vapour phase was removed by flushing pre-cooled CO_2 through the cell. The flushing pressure was raised 0.3 to 0.5 MPa higher than the stabilised pressure to avoid dissociation of methane hydrates. For experiment 3, the pressure stabilised at a higher pressure, thus the flushing pressure is also higher (see Figure 4.16).

After flushing the gas phase with CO_2 , the valves were closed. Initially the pressure dropped steeply for about 10 hours (see Figure 4.16). Accordingly, the mole fractions of CH_4 in the gas phase decreased from 0.09 (initial value) to 0.05

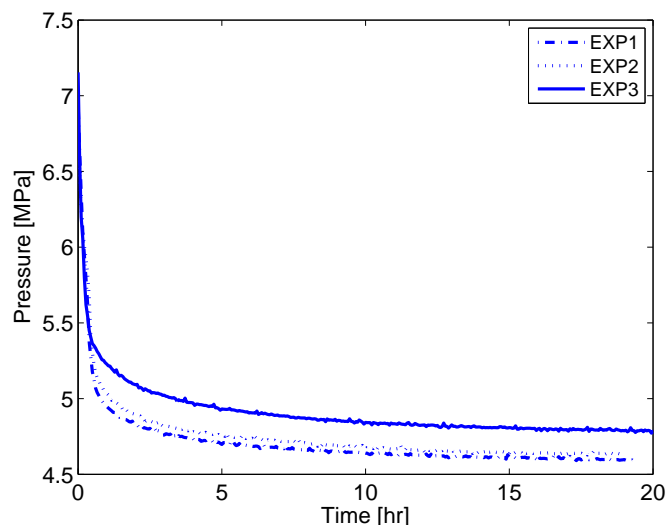


Figure 4.15: Methane hydrate formation at $T = 276.15K$. The initial pressure for experiment 1, 2 and 3 are 6.95 MPa, 6.85 MPa and 7.15 MPa respectively. The final pressures are 4.58 MPa, 4.64 MPa and 4.8 MPa. Experiment 1 is the initial experiment, experiment 2 is the repeated experiment immediately after experiment 1. Experiment 3 has a higher stabilised pressure due to accidental water loss during previous dissociation of gas hydrates.

in this period (see Figure 4.17). It can also be seen in Figure 4.18 that the amount of methane in the gas phase decreased from 4.67×10^{-3} to 3.04×10^{-3} mole from time 0 to 25 hours. This pressure decline accompanied by CH_4 mole fraction decrease in the gas phase indicates methane hydrate formation. The flushing pressure which is higher than the stabilised pressure, provides extra driving force to the system. Therefore, the secondary methane hydrate formation could be initiated by occupying the water cavities which have not been completely filled by the initial methane hydrate formation.

After pressure stabilisation, the methane content in the gas phase gradually increased with time as shown in Figure 4.17, indicating the actual replacement of CH_4 by CO_2 in the gas hydrate. The error between experiment 1 and 2 with respect to the gas phase composition is ± 1.5 mol%. The exchange process in experiment 3 is slower than for the first two experiments due to the higher flushing pressure. At end of the exchange process 4.75×10^{-3} moles of CH_4 were replaced by CO_2 (see Figure 4.18).

After 300 hours, the pressure and the gas phase mole fractions hardly change (see Figure 4.16). At the end of the exchange process, the CO_2 composition in

CHAPTER 4. HYDRATE FORMATION AND EXCHANGE IN TERNARY SYSTEMS

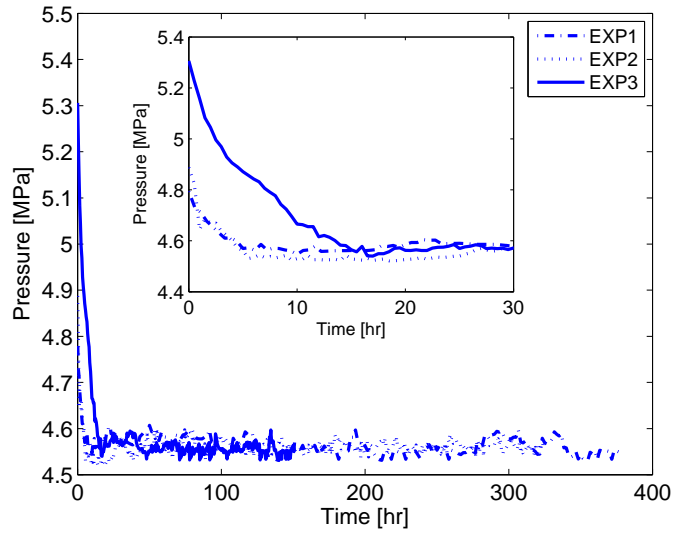


Figure 4.16: Pressure as a function of time during the $CH_4 - CO_2$ exchange. After CO_2 flushing, the starting pressure for experiment 1, 2 and 3 is 4.79 MPa, 4.88 MPa and 5.3 MPa respectively. $T=276.15$ K.

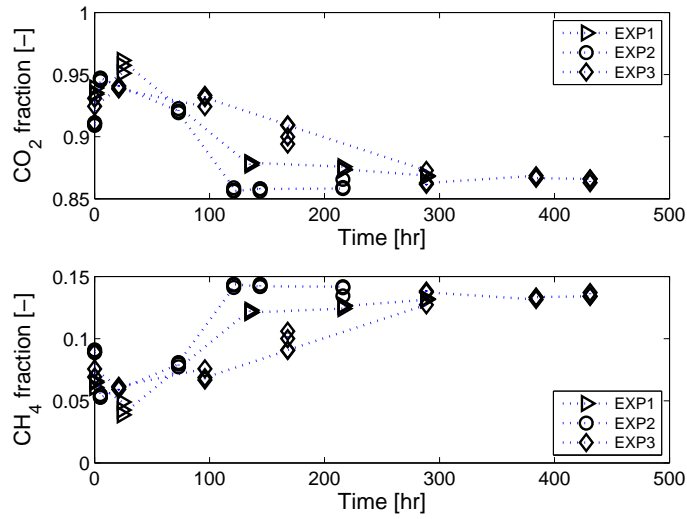


Figure 4.17: $CH_4 - CO_2$ exchange in the gas hydrates. CO_2 and CH_4 composition changes in the gas phase. Temperature is constant at 276.15 K.

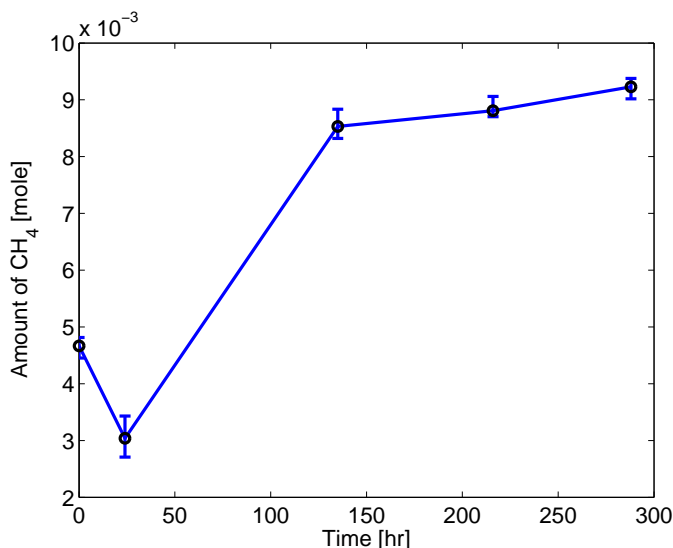


Figure 4.18: Average number of moles of CH_4 exchanged by CO_2 in the hydrate phase ($\Delta n_{CH_4}^H$). Error bars are determined from 3 experiments.

the gas phase is 85%. This suggests that not all CH_4 is replaced by the CO_2 in the gas hydrates. Most likely, the exchange process only takes place near the interface between the solid hydrate phase and the gas phase. After CH_4 is replaced by CO_2 in the top hydrate layers, there is no direct contact between methane hydrates and CO_2 . Further exchange is limited by the diffusion of CO_2 through the already formed CO_2 hydrate layer into the CH_4 hydrates and by CH_4 diffusion through the hydrate layer towards the gas phase.

The results indicate that the replacement of CH_4 by CO_2 as guest molecule in CH_4 hydrate cavities is feasible even at conditions where the CH_4 hydrates are expected to be stable. However, this process is rather slow. The exchange of CH_4 with CO_2 at solid surfaces is time consuming because the mechanics of this process are probably related to the reorganisation of the water cavities. The exchange only takes place in the gas hydrates close to the solid-gas interface. Thus the area of interface is another factor controlling the efficiency of the exchange process.

4.4.2.3 Gas Hydrate Dissociation

The dissociation experiment was started once the composition of the gas phase did not considerably change anymore. The pressure in the cell was released in steps of 0.5 MPa using a back pressure regulator. The gas released by dissociation

CHAPTER 4. HYDRATE FORMATION AND EXCHANGE IN TERNARY SYSTEMS

after each pressure step was analysed. The results are shown in Figure 4.19. The upper graph shows the mole fractions of CO_2 and the lower graph shows the mole fractions of methane. The solid lines in the graphs correspond to the stepwise pressure release. The graph shows that the CO_2 mole fractions in the gas phase first increase, then CO_2 and CH_4 mole fractions remain approximately constant before the CH_4 mole fractions increase further with decreasing pressure. When atmospheric pressure has been reached, the CO_2 content in the gas phase increases abruptly again.

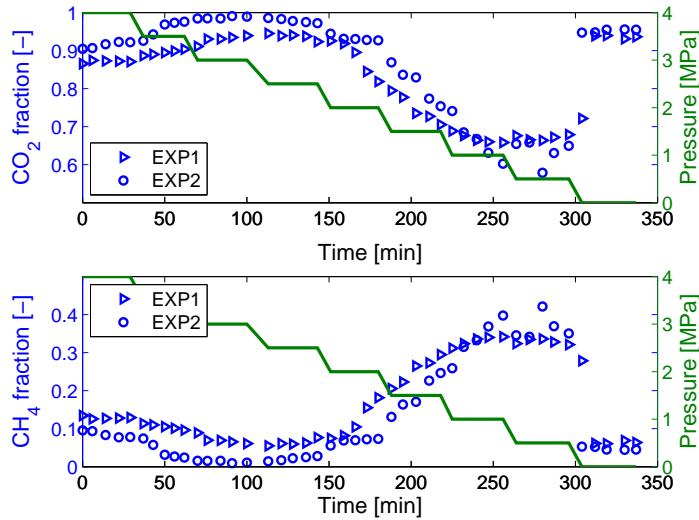


Figure 4.19: Composition change in the gas phase during stepwise gas hydrate dissociation. The top one shows the mole fractions of CO_2 and the bottom one shows the one for CH_4 . The solid line indicates the stepwise decrease of pressure in the cell.

This behaviour can be explained as follows: when the pressure decreases, the top layer of the gas hydrate phase is dissociated first. The amount of CO_2 captured in this layer is higher than the amount of CH_4 and consequently the CO_2 amount in the gas phase increases. When this first layer has been dissociated at a pressure lower than 2.0 MPa, gas hydrates containing CH_4 start to dissociate. At this stage, the CH_4 content in the gas phase increases substantially. Finally the lower layers of methane hydrates are completely dissociated. The amount of dissociated methane hydrates confirms that the exchange of CH_4 by CO_2 did not reach the deeper hydrate layers. This also explains why the pressures at the end of the exchange experiment for all runs are the same even though less CH_4 hydrates have been formed for experiment 3. The strong increase of CO_2 content in the gas phase when atmospheric pressure is reached, is due to CO_2 released from the aqueous liquid phase.

It is interesting to note that the pressure at which the methane mole fraction increases (indicating the dissociation of methane hydrate) is much lower than the $H - L_w - V$ equilibrium pressure of the binary $CH_4 + H_2O$ system. This could be explained by the fact that CH_4 hydrates are protected by the CO_2 hydrate layer at the interface. Only after the complete dissociation of this layer, the methane hydrates start to dissociate. The presence of CO_2 hydrates in the interface inhibits, or in other words, delays the dissociation of methane hydrates.

4.5 Conclusions

4.5.1 Formation Kinetics of Ternary System

A series of experiments was carried out to study the kinetics of gas hydrate formation from a mixed gas phase consisting CO_2 and CH_4 . With this study, the feasibility of using gas hydrates for gas separation was investigated. This is also of importance for the combined CH_4 production by CO_2 injection into gas hydrate bearing layers.

In the ternary $CO_2 + CH_4 + H_2O$ system, the mole fraction of methane in the gas phase increases during gas hydrate formation, while the CO_2 mole fraction decreases. It indicates that CO_2 hydrate formation is more favourable than methane hydrate formation in all pressure ranges tested in this study. At low initial pressures less CH_4 is consumed to form hydrates. When initial pressure increases, more methane is incorporated in gas hydrates. However, the formed gas hydrates still contains mainly CO_2 (65% of the total gas hydrates are CO_2 hydrates) even for experiment with an initial pressure of 6.0 MPa which is far into the gas hydrate stable zone of the binary $CH_4 + H_2O$ system.

Methane hydrate formation at low initial pressures where no CH_4 hydrates would form in the binary $CH_4 + H_2O$ system, is confirmed in the ternary system of $CH_4 + CO_2 + H_2O$.

It was found that the (mixed) gas hydrate formation rate in the ternary system is faster than CH_4 hydrate formation rate for the binary system ($CH_4 + H_2O$). The presence of a component, such as CO_2 , which forms gas hydrates faster and at lower pressures, promotes methane hydrate formation and stabilises these gas hydrates at lower pressures than for pure methane.

Gas separation by means of gas hydrate formation is challenging for CO_2 and CH_4 gas mixtures. The most successful separation of CO_2 and CH_4 was established at low initial pressures (when pressures are lower than 3.5 MPa). These pressures are lower than the $H - L_w - V$ equilibrium pressure of the binary $CH_4 + H_2O$ system. At these conditions, the CO_2 content in the gas mixtures could be reduced from 55 mol% to 37 mol% . A better separation might be achieved by optimising the

CHAPTER 4. HYDRATE FORMATION AND EXCHANGE IN TERNARY SYSTEMS

design of the reaction cells, e.g. using a multi-stage or water spray systems. The gas hydrates formed at these conditions are still a mixture of CO_2 and CH_4 . This means that multiple stages (secondary, ternary etc.) separation are required to improve the separation. The gas hydrate formation time is long, thus, efforts to improve the efficiency of the separation should also focus on reducing the formation time.

4.5.2 Exchange of Methane by CO_2 within gas hydrates

The exchange of CH_4 by CO_2 in formed CH_4 hydrates without hydrate dissociation was confirmed. The exchange mainly takes place at the interface between the solid hydrate and the gas phase. Exchange of the guest molecules in the gas hydrates in the deeper hydrate layers is controlled by diffusion of CH_4 and CO_2 through the solid gas hydrate phase.

The CO_2 hydrate layer at the interface between the gas and solid hydrate phase shields the deeper methane hydrates in the hydrate bulk. Therefore, dissociation of methane hydrates is observed at lower pressures than the $H - L_w - V$ equilibrium pressure of the binary $CH_4 + H_2O$ system.

The rate of exchange of CH_4 by CO_2 in gas hydrates is slow and the amount of exchanged guest molecules is limited by the size of interfacial area between the gas and solid hydrate phase. These are the two main limiting factors for the efficiency of the exchange process. It is suggested to apply this exchange experiment in a porous media. The interface between gas and hydrate is larger in porous media than in bulk conditions, thus even though the injection of CO_2 is more complicated, a better exchange of the guest molecules would be expected.

5

Gas Hydrate Formation in Porous Media

In the previous chapters, gas hydrate formation in the bulk phase was investigated. However, for the combined natural gas production and CO_2 sequestration in gas hydrate bearing reservoirs, knowledge about gas hydrate formation in porous media is crucial. Therefore, this chapter is devoted to the gas hydrate formation kinetics in porous media.

5.1 Introduction

The study of the formation and dissociation of gas hydrates in porous media can provide knowledge and data on kinetics behaviour of gas hydrates e.g. reaction rate and influence of physical parameters on gas hydrate formation in reservoir conditions. This knowledge has extraordinary significance for gas production from natural gas hydrate reservoirs combined with carbon dioxide storage.

As already discussed in Chapter 2, the phase behaviour and the gas hydrate formation of binary systems are different in porous media than in the bulk phase. The $H - L_w - V$ equilibrium curve in porous media shifts to lower temperatures or higher pressures compared to the conditions in the bulk phase [48, 128, 25, 129, 2, 3]. Handa and Stupin [48] characterised this behaviour as inhibition effect of the porous media.

However, it was proven that for pore sizes larger than $0.06 \mu m$ this inhibition is negligible [124, 126, 3]. In general, most sub-sea hydrate bearing sediments have pore sizes much larger than this value (e.g. typical pore size for medium grain sized sandstone reservoir is around $10 \mu m$ [145]). Thus it can be assumed that the phase behaviour is not affected in porous media, if pores are sufficiently large.

It was found by several research groups [58, 111] and also in this study, that the gas hydrates grow at the water-gas, ice-gas and hydrate-gas interfaces. Typically

sandstone reservoirs¹ are water-wet, so the grain surface is covered by a thin water film. Consequently, the interface between the aqueous and the gas phase in porous media is much larger than the interface in the bulk at the same conditions. In bulk experiments, gas hydrate formation could be enhanced by dispersion of gas bubbles in the aqueous liquid phase by means of agitation. But in porous media the gas-liquid interface cannot be easily increased by agitation (except acoustically). Even though initially the interface between gas and liquid phase is larger than in bulk, the contact area between gas and water decreases during hydrate formation. Therefore, it is expected that the kinetics of gas hydrate formation in porous media will differ from that found during bulk experiments.

A number of studies have been published on gas hydrate formation in porous media. These publications mainly focus on the impact of the porous medium on the thermodynamic behaviour. Only a few groups investigated the actual gas hydrate formation in porous medium [15, 115, 44, 37]. Many published studies were done in unconsolidated porous media, e.g. Holland et al. [55], Waite et al. [143, 144], Spangenberg et al. [115]. Graue et al. [44] published NMR studies of hydrate formation and exchange in consolidated porous media. While studies reported in the literature provide good description of gas hydrate formation and dissociation. The corresponding kinetics aspects are not completely understood. The focus of this study is investigation the kinetics of gas hydrate formation in consolidated porous media. Our experiments were performed using a glued glass beads core with an average pore size large enough to assume that there is no inhibition effect on the phase behaviour. The gas hydrate formation rate in porous media and the influence of pressure, temperature, and gas injection rate on the gas hydrate formation were studied in detail. The results of this study give insight on gas hydrate reservoir behaviour and the possibility to sequester CO_2 in the form of gas hydrates. X-ray images of the gas hydrates in the porous media were obtained to analyse the distribution of the formed gas hydrates in the core.

5.2 Experiments

5.2.1 Material

For gas hydrate formation in porous media, only CO_2 with a purity of 99.7 mol% (Linde Company) was used to conduct the experiments². The water used was double-distilled water. The porous core sample was made of uniformly sized glass beads. The average size of the glass beads (manufactured by SCHOTT AR-Glas) is 1.8 mm with a variation of ± 0.1 mm.

¹Most gas hydrate bearing layers are sandstone or sand-beds, other geology sediments e.g. clay can also be a proper hydrate bearing layer, but it is out of the scope of this study.

²The CH_4 experiment in porous media takes too long to be feasible in this study.

5.2.2 Experimental Set-up

The porous media was made by uniform sized glass beads glued together using a resin. The glue coats the beads and hold them in position. The detailed preparation of the porous media core can be found in Appendix B. The properties of the synthetic glass beads core are given in Table 5.1.

Table 5.1: Properties of the glass-beads core

Parameter		
Mass of tube	0.46	<i>kg</i>
Tube inside diameter (D_{in})	0.06	<i>m</i>
Cross-sectional area (A)	2.83×10^{-3}	m^2
Mass of glass beads	1.39	<i>kg</i>
Length of core	0.31	<i>m</i>
Pore volume (V_p)	2.86×10^{-4}	m^3
Porosity (ϕ)	0.32	–
Permeability (k)	2.60×10^{-10}	m^2
Water saturation	0.58	–

The set-up used to perform the experiments is shown in Figure 5.1. It consists of a high grade aluminium core holder designed to withstand pressures up to 13.0 MPa. The length of the core holder is 0.32 *m* and the diameter is 0.10 *m*. At the inlet of the core there are three ports: two for injection of water and gas respectively and the third houses a thermocouple for temperature monitoring. At the core outlet, one port was used for the out-flow of the gas, the other port was used for temperature monitoring. The temperature in the core was kept constant by circulating water through the cooling chamber which is mounted to the outside of the core holder. A certain amount of ethanol is added to the cooling water to achieve a lower cooling temperature without freezing the water. Pressure sensors were connected to the inlet and outlet to determine the pressure drop over the whole core. A mass flow regulator (SIERRA. digital) was attached to the injection line. The maximum operating pressure for this flow controller is 3.0 MPa for CO_2 gas, and it regulates the flow rate between 0-900 *ml/min*. For extra control, the flow rate can additionally be set manually with a needle valve.

A thermostat of the type LAUDA RE 220 was used to regulate temperature in a range between 253 and 423 K and allowed to maintain a constant temperature within ± 0.20 K. The temperatures at the beginning and at the end of the core were determined using THERMOCOAX thermal sensors. Pressures were determined using Druck PTX 600 pressure transducers. These pressure transducers can withstand a maximum pressure of 15.0 MPa with an accuracy of 0.08 % over its measurement range. The temperature, pressure and flow rate data were collected on a PC using an in-house data acquisition system and software.

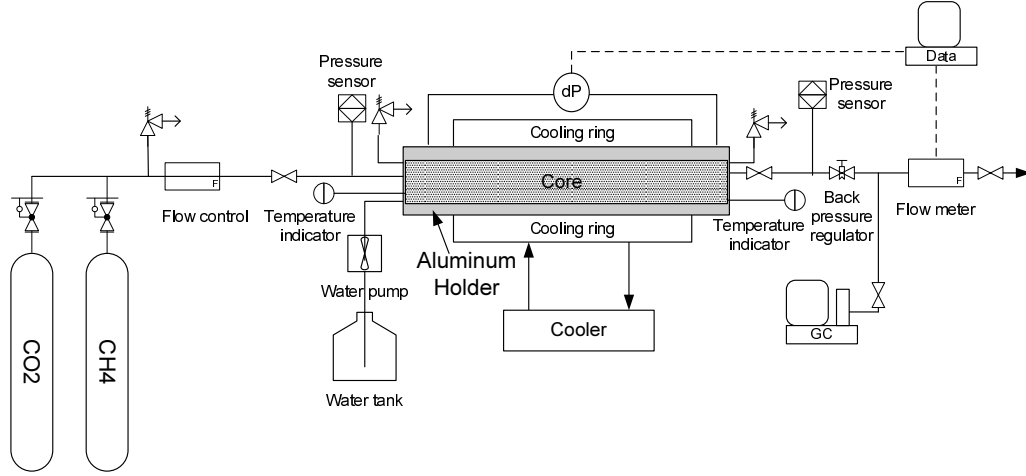


Figure 5.1: Schematic of the experimental set up for investigation of the gas hydrate formation in porous media

5.2.3 Determination of Porosity and Permeability

The porosity of the glass bead core can be usually estimated by Equation 5.1 and 5.2. By Equation 5.1 it is difficult to estimate the influence of the glue, therefore, Equation 5.2 is used to determine the porosity.

$$\phi = \frac{V_p}{V_{tot}} = \frac{V_{tot} - m_{glassbeads}/\rho_{glassbeads}}{V_{tot}} \quad (5.1)$$

$$\phi = V_{w,i} - V_{w,o} \quad (5.2)$$

It is done by determining the water volume injected into the core. The core was previously flushed with CO_2 . Then double distilled and degassed water was injected from the bottom of the core at a pressure of 1.5 MPa. A slow flow rate of 30 ml/h was applied to ensure a better displacement of CO_2 . When no bubbles was released from the liquid flowing out of the core, the injection was continued for another 24 hours to make sure no CO_2 was left in the core. The total volume of water injected ($V_{w,i}$) and volume of produced water ($V_{w,o}$) was determined. The pore volume of the core was determined by subtraction $V_{w,o}$ from $V_{w,i}$.

The permeability of the sample was determined by the standard technique. After fully saturating the core with water, the core was placed horizontally and water was injected through the core using a piston pump at five different flow rates ranging from 100 and 500 ml/h. The accuracy of the pump is within 2 ml/h. During the water injection, the pressure drop over the core was determined by

a pressure difference gauge with an operating range from 0 to 1000 Pa (gauge pressure). Due to the horizontal position, the gravity effects could be neglected, the permeability was estimated using Darcy's Equation 5.3:

$$Q = \frac{kA \Delta P}{\mu L} \quad (5.3)$$

where k is the permeability, Q is flow rate, μ is the water viscosity ($1.002\text{E-}3 \text{ Pa} \cdot \text{s}$) and $\Delta P = P_i - P_o$ is the pressure difference between inlet (P_i) and outlet (P_o). A is the cross-sectional area of the core sample and L is the length of the core. (see Table 5.1). The pressure drop over the core as a function of the flow rate and the computed permeability are shown in Figure 5.2.

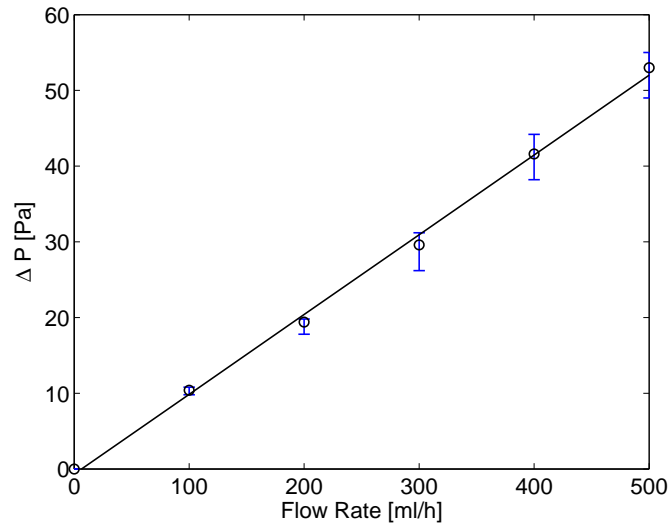


Figure 5.2: Pressure drop and determined permeability of the glass-bead core at various flow rates

5.2.4 X-ray CT Imaging

X-ray Computed Tomography (CT) enables the visualisation through an optically opaque objects by reconstructing the X-ray attenuation coefficients from multi-directional X-ray transmission data [150].

The attenuation coefficient is described by the Beer-Lambert law [10] as follow:

$$I = I_0 e^{-\alpha x} \quad (5.4)$$

CHAPTER 5. GAS HYDRATE FORMATION IN POROUS MEDIA

where, α is the attenuation coefficient, I_0 and I are the emitted and the measured X-ray intensities respectively, x is the path crossed by the X-ray beam through the examined object.

The attenuation coefficient is proportional to the density of a substance, it is given by:

$$\alpha = \rho \left[\sigma(E) + b \frac{Z^{3.8}}{E^{3.2}} \right] \quad (5.5)$$

where ρ is the bulk density, $\sigma(E)$ is the Klein-Nishina coefficient, b is a constant ($b = 9.8 \times 10^{24}$), Z is the atomic number of the substance and E is the X-ray photon energy (in keV) [150].

The medical CT scanner used for the experiments gives the X-ray attenuation data which is given in international standard Hounsfield Units, representing the attenuation of a sample relative to the attenuation of pure water (Equation 5.6). The Hounsfield Unit gives values in a range -1000 to 3000HU, where for vacuum $HU = -1000$ and for water $HU = 0$.

$$HU(x, y, z, t) = 1000 \left[\frac{\alpha(x, y, z, t)}{\alpha_w} - 1 \right] \quad (5.6)$$

The visualisation of the gas hydrate formation and dissociation by means of CT-scanning add extra requirements to the experimental set-up. The choice of using high-grade aluminium as a core holder is because not only can it withstand high pressures but it also has a low X-ray attenuation. The high thermal conductivity also makes it efficient to conduct heat/cold.

5.2.5 Experimental Procedure: Without CT-Scan

All gas hydrate formation experiments in porous media were done according to the procedures described below. Additionally, a summary of the essential steps can be found in Table 5.2.

First, the pore porosity and permeability of the core sample were determined by the method discussed above (see Section 5.2.3). When the core was fully saturated with water, the set up was ready to start an experiment.

The desired water saturation in the core is established by injecting CO_2 at a controlled low flow rate of 20 *ml/min* at a pressure of 0.5 MPa. The amount of water produced due to the injection of the CO_2 was determined and used to compute the water saturation in the core:

$$S_w = \frac{(m_{w,i} - m_{w,o})/\rho_w}{V_p} \quad (5.7)$$

where, $m_{w,i}$ is the mass of water initially in the core, $m_{w,o}$ is the mass of water produced, V_p is the pore volume determined previously and ρ_w is the density of the water.

After desired water saturation was reached, the cooling of the core was started. The cooling was started at low a pressure to avoid CO_2 hydrate formation before the actual experiment started. When the temperatures determined at both ends of the core were equal and stable, CO_2 was further injected until the desired initial pressure was reached. Then, the inlet valve was closed. When gas was injected with a flow rate of 450 ml/min , it took around 30 minutes to reach the desired initial pressure of 3.0 MPa .

The pressure gauges in the inlet and outlet lines were connected with the core and the pressure was monitored. The experiment terminated when the pressure stabilised. Next, the core was prepared for the subsequent experiment. Gas hydrates were dissociated by slowly releasing pressure to atmospheric pressure. The gas hydrate dissociation was done with very small steps to make sure that no water was flowing out of the core³. In this way, it can be assumed that the subsequent experiment has the same level of water saturation as the first experiment and allowing comparison of the sets of data. After the system reached atmospheric pressure, a new experiment was started with injection of gas into the core again.

Table 5.2: Summary of the important steps for in porous media experiments

Step	Description	Determined Parameters
step 1	Flush the core with CO_2	-
step 2	Flush the core with Water	V_p
step 3	Inject gas to replace water	S_w
step 4	Cool down the system	$T(t)$
step 5	Inject gas to reach desired pressure	P_{ini}
step 6	Close valves, gas hydrates formation	$P(t)$, $T(t)$, P_{eq}
step 7	Release pressure, gas hydrate dissociation	-

³This means avoiding water being flushed out from the core. However, the amount of water in the core might decrease slightly due to evaporation during gas hydrate dissociation. This water loss is small with respect to the total amount of pore water in the core, thus it can be neglected.

5.2.6 Experimental Procedure: With CT-scan

The experiments for which X-ray CT scans were performed to visualise the gas hydrate formation require a slightly different procedure. The previously mentioned steps before reach the desired water saturation of the core are the same. After that CO_2 was immediately injected to reach a desired initial pressure at room temperature (298.15 K). Then, the cell was mounted horizontally on the CT-table concentrically with the ring shaped gantry where X-ray tube and detectors are mounted. The gantry rotates and images were taken. It is necessary to maintain the set-up at exactly same position throughout the complete experiment to minimise the noise of the reconstructed images.

The first cross sectional scan⁴ was taken along the core at a condition where no hydrates were present. Then, the cooler was switched on and the temperature started to decrease. CO_2 hydrate formation initiated when the temperature was sufficiently low to reach the $H - L_w - V$ equilibrium line.

The second scan was taken after one week when the temperature and pressure had stabilised. Duplicated scans at exact same condition were made to analysis the system error.

5.3 Results and Discussion

5.3.1 Gas Hydrate Formation in Porous Media

CO_2 hydrates was formed in the synthetic core which was initially partially saturated with water. Figure 5.3 shows a typical pressure decay during the CO_2 hydrate formation in the glass-bead core with an water saturation of 0.58. The initial pressure of 3.0 MPa was achieved by injecting CO_2 with a flow rate of 450 ml/min . The temperature in the system was kept constant at 275.15 K. This experiment is used as the reference case to explain the general behaviour and as the basis for comparison of the different experiments. The pressure decline indicates that CO_2 is consumed from the gas phase during the gas hydrate formation. The pressure then stabilised at the equilibrium pressure expected for the given temperature. The initial fast decrease of pressure indicates that the mass transfer of CO_2 into the aqueous phase and the gas hydrate formation process is rapid. Based on the pressure data the total rate (R_t) is determined as the time derivative of pressure:

$$R_t = -\frac{dP}{dt} \quad (5.8)$$

⁴The scan is cross sectional with a slice thickness of 1 mm . Altogether, 160 cross-sectional images of the core were obtained from one single scan.

This parameter was further used to analyse the kinetics of gas hydrate formation in porous media. The formation rate (R_t) is a time-dependent parameter; it decreases with time, and finally approaches zero.

In order to prove that the pressure decay in the core was mainly due to hydrate formation, some experiments have been conducted to study the pressure decay in the case of only CO_2 dissolution in the aqueous phase without CO_2 hydrate formation. This is done with a low initial pressure below the $H - L_w - V$ equilibrium pressure of CO_2 hydrates.

Before the experiments could be done, the phase behaviour available in literature was analysed. From this, it could be concluded that the increase in the solubility of CO_2 in the aqueous phase with increasing pressure is negligible when hydrates coexist (Hashemi et al. [49], Mooijer, [134]). Therefore, in this study it was assumed that the solubility of CO_2 at any pressure (e.g. 3.0 MPa) higher than the equilibrium pressure of $H - L_w - V$ curve (1.5 MPa in this study) is equal to the solubility at the equilibrium pressure. Accordingly it can be assumed without introducing a major error, that the solubility of CO_2 in the aqueous phase at a slightly lower pressure than the $H - L_w - V$ equilibrium pressure is the same as the solubility at the $H - L_w - V$ equilibrium pressure. Based on this assumption, experiments at a temperature of 275.15 K and an initial pressure of 1.4 MPa, which is 0.1 MPa lower than the $H - L_w - V$ equilibrium pressure, were conducted. At this pressure (1.4 MPa), no gas hydrate formation was observed; the pressure decay curve is only due to dissolution of CO_2 in the aqueous phase. The obtained pressure decline curve is also valid for all the other experiments conducted in the porous medium.

In Figure 5.3 the normalised pressure (P/P_{ini}) decline curve for the experiment with only CO_2 dissolution at an initial pressure of 1.4 MPa and for the experiment with CO_2 hydrate formation at an initial pressure of 3.0 MPa are compared. It can be seen that dissolution of CO_2 in the aqueous phase is only responsible for about 10% of the total pressure decrease. The main contribution of pressure decay is due to the formation of gas hydrates.

Assuming that the dissolution of CO_2 in the aqueous phase and the CO_2 hydrate formation are two independent processes, the gas formation rate (R_H) can be calculated by:

$$R_H = R_t - R_{di} = \frac{dP_{tot}}{dt} - \frac{dP_{di}}{dt} \quad (5.9)$$

where, R_t is the total rate, R_{di} is the rate of dissolution. In Figure 5.4 the total rate (R_t) and the hydrate formation rate (R_H) are plotted as a function of time.

It can be seen that the gas hydrate formation rate at the beginning of the experiment has decreased from the total rate $6 \times 10^2 \text{ kPa/hr}$ to 10^2 kPa/hr . This suggests that initially, dissolution of CO_2 into the aqueous liquid phase has a

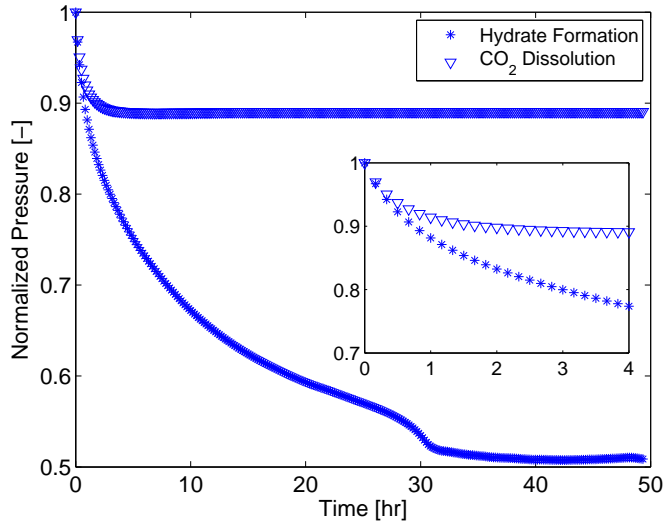


Figure 5.3: Normalised pressure (P/P_{ini}) as a function of time during CO_2 dissolution ($P_{ini} = 1.4$ MPa) and CO_2 hydrate formation experiment ($P_{ini} = 3.0$ MPa) in glass bead core at a constant temperature of 275.15 K.

strong influence on the total pressure decay. However, the data show also that CO_2 hydrate formation and CO_2 dissolution occur simultaneously. After about 3 hours, the further pressure decline can solely be attributed to CO_2 hydrate formation.

In theory, gas hydrates can form in two ways: in the first, which is more commonly accepted, gas hydrates are formed at the gas-water interface [58]; the second is gas hydrates formed by dissolving gas in the water [123, 66]. In a binary system these two mechanisms of gas hydrate formation are difficult to distinguish. Especially in our experiments, the water was initially saturated with CO_2 . The gas dissolution and gas hydrate formation cannot be distinguished as an independent process. Therefore, in the following sections, the gas dissolution was not discussed separately but taken account into the total formation rate.

In Figure 5.5 the total rate (R_t) as a function of time is given. From the decreasing trend of the total rate, different regimes can be distinguished. The first regime describes the dissolution of CO_2 into the aqueous phase and the initial gas hydrate formation at the gas-liquid interface. It was named the ‘reaction limited’ process.

The second regime is characterised by a slow logarithmic decay of formation rate with time (shown linearly in Figure 5.5). In this regime, there is hardly any dissolution of CO_2 in the aqueous liquid phase. At the gas-liquid interface CO_2 hydrates have already been formed, so that further CO_2 transfer from the gas

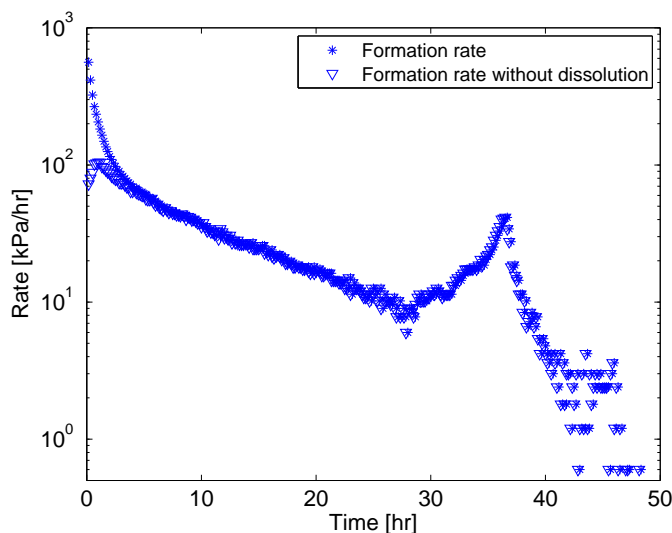


Figure 5.4: Rates determined from the pressure decay with time during CO_2 hydrate formation with and without the effect of CO_2 dissolving into the aqueous liquid phase.

phase into the gas hydrate phase is limited by diffusion of CO_2 through this first layer of gas hydrates. Therefore, it is denoted as ‘reaction limited’ regime.

Before pressure stabilised, the formation rate suddenly increased sharply and finally dropped again to almost zero when pressure approached its equilibrium value (see Figure 5.5). In this study, this regime is denoted as the ‘pre-equilibrium’ regime because it starts when the pressure is about 0.2 to 0.3 MPa higher than the equilibrium pressure. This sudden increase in the rate before equilibrium has been reached seems not to be an artifact because it was observed for all experiments. However, for the gas hydrate formation experiments in the bulk phase this behaviour was not found. By comparing the rates obtained from the experiments in the bulk phase and the porous medium, one might speculate that this increase is caused by a limited gas-liquid contact in the porous media. During the bulk phase experiments, the system was continuously agitated so that the interface between the gas and the water was constantly renewed. The formation of gas hydrate was uniform (macroscopically). Consequently, only one gas hydrate formation process was observed before equilibrium was reached (see Figure 5.6). The hydrate formation rate in the bulk also decreased in a logarithmic manner, but it is 10 times higher than the formation rate in the porous media.

The kinetics before a system reaches equilibrium is not fully understood for both bulk and porous media systems. In bulk, Englezos’s [34, 35] kinetics model can

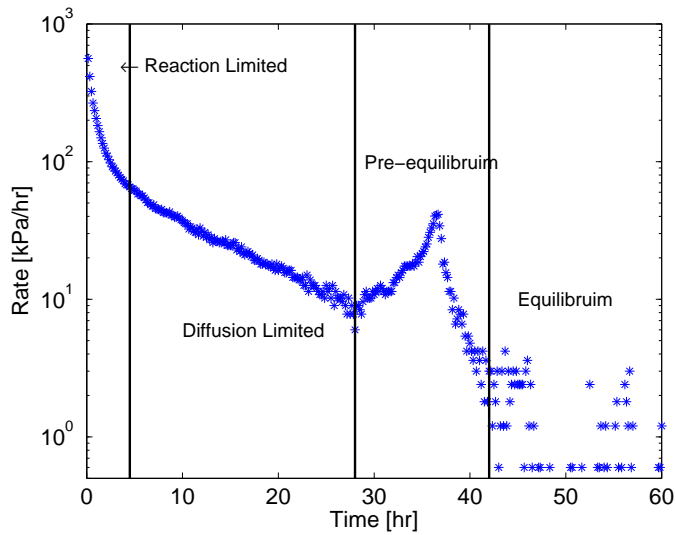


Figure 5.5: Total rate during gas hydrate formation experiment and the regimes as defined in this work describing the gas hydrate formation process in porous media.

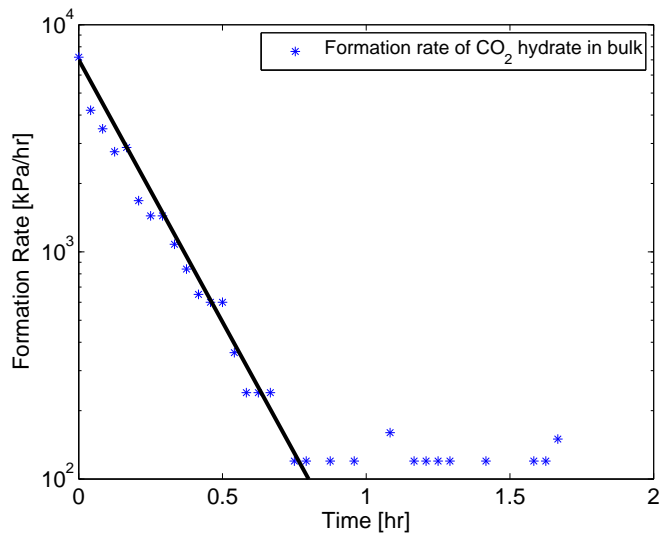


Figure 5.6: CO_2 hydrate formation rate calculated from bulk experiments in Chapter 3. Here the rate declines smoothly before equilibrium pressure is reached.

only predict the formation rate when it is constant. The model by Kawamura et al. [62] also failed to predict the slowdown of the formation rate before reaching equilibrium. Studies which focusing on the pre-equilibrium process in porous media are scarce. Unfortunately, the experimental data at hand do not provide sufficient information to clarify the responsible mechanism for this behaviour. Experiments on microscopic level might reveal the cause for it. But these are out of the scope of this study. Therefore, the ‘pre-equilibrium’ process will not be discussed any further below.

5.3.2 Influence of gas injection rate

The first set of experiments was done by injecting gas directly from the gas vessel with a high flow rate controlled solely by the pressure in the gas vessel (3.5 MPa) and was manually adjusted with a needle valve. Consequently, the injection rate was not the same for the different experiments and the injection time to reach the desired initial pressure of 3.0 MPa varied between 20 to 40 seconds. In a bulk system, the injection rate was found to have no influence on the formation of gas hydrates. However, in porous media the injection rate is a sensitive parameter.

In Figure 5.7 the pressure decline curves of four experiments performed at the same initial pressure of 3.0 MPa and temperature of 275.15 K are shown. These experiments only differ in the time which was needed to reach the initial pressure (25, 30, 40 seconds respectively). In Figure 5.8 the total rate (dP/dt) during gas hydrate formation is shown.

The reproducibility of the pressure decay curves is low. Even for the same injection time of 40 seconds, the pressure decay curve is different. From these experiments two types of pressure curves can be found. For some experiments (e.g. $t_{inj} = 30s$ in Figure 5.7), the pressure declined smoothly with time, for others (e.g. $t_{inj} = 25s$ in Figure 5.7) the pressure decay slows down for some time before it suddenly increases again at an early stage of gas hydrate formation (Figure 5.7 at $t = 3hr$). It can be seen more clearly in Figure 5.8 that the formation rate suddenly increases about 10 times. Interestingly, the peak value of the formation rate increase for all experiments is almost the same at $3000 kPa/hr$; even though the time at which these peak values occur were random. In Table 5.3 the absolute value of formation rates for the different experiments is listed. It was found that the increase in the formation rate has no clear relationship to the gas injection rate.

Possible explanations for this sudden formation increase might be: (1) due to the gas compression during the gas injection a local temperature variance could occur (Joule Thompson effect). (2) due to the unsteady injection rate the gas is irregularly distributed in the porous space of the core. Consequently diffusion barriers or even blocking zones could have been formed.

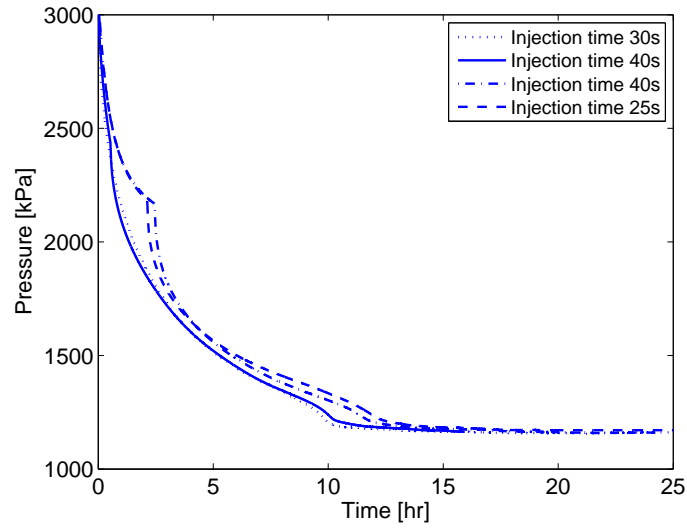


Figure 5.7: Pressure decay curve for CO_2 gas hydrate formation experiments in glass bead core. Initial pressure is 3.0 MPa and the temperature is constant at 275.15 K. The injection time varies from 20 to 40s.

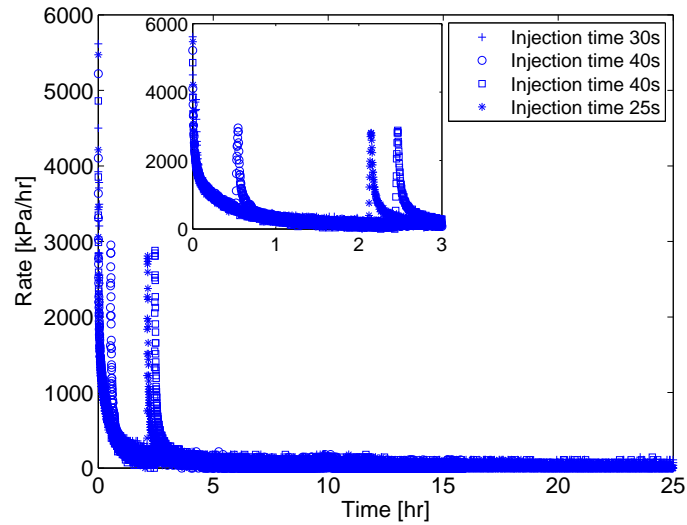


Figure 5.8: Rates during CO_2 gas hydrate formation experiments in glass bead core. Initial pressure is 3.0 MPa and the temperature is constant at 275.15 K. The injection time varies from 20 to 40s.

5.3. RESULTS AND DISCUSSION

Table 5.3: Data of CO_2 gas hydrate formation experiments in glass-beads core. P_{ini} is the initial pressure of experiments, T_1 is the time at which increase of formation rate occurs, R_{t1} is the formation rate before the increase, R_{t2} is formation rate after the increase, ΔR_t is the absolute rate increase.

P_{ini} [kPa]	T_1 [h]	R_{t1} [kPa/h]	R_{t2} [kPa/h]	ΔR_t [kPa/h]
3000	0.52	576	2952	2376
3000	2.43	100	2880	2780
3000	2.11	144	2808	2664
2500	0.16	1000	2952	1952
2500	0.64	288	2304	2016
2500	0.79	256	2252	1996

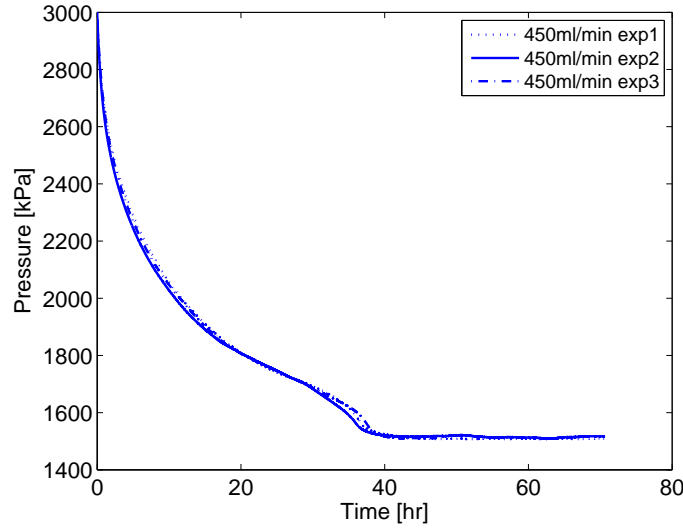


Figure 5.9: Pressure decay curve for CO_2 gas hydrate formation experiments in glass bead core. Initial pressure is 3.0 MPa and the temperature is constant at 275.15 K. The injection rate is 450 ml/min .

In the subsequent experiments the injection rate of CO_2 to reach the desired initial pressure was controlled to 450 ml/min . With this injection rate, the initial pressure of 3.0 MPa was reached after 27 minutes, while in the previous experiments it took less than 1 minute. In Figure 5.9 and 5.10 the pressure and rates as a function of time are given. The pressure decreases from the initial 3.0 MPa to the equilibrium pressure of 1.53 MPa in 38 hours. It can be seen from Figure 5.9 and 5.10 that the pressure and formation rate data overlap for three

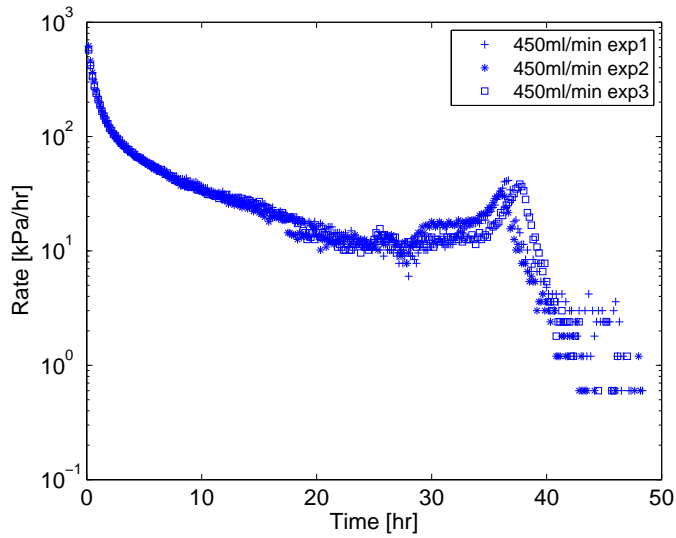


Figure 5.10: Gas hydrate formation rate curve for CO_2 gas hydrate formation experiments in glass bead core. Initial pressure is 3.0 MPa and the temperature is constant at 275.15 K. The injection rate is 450 ml/min .

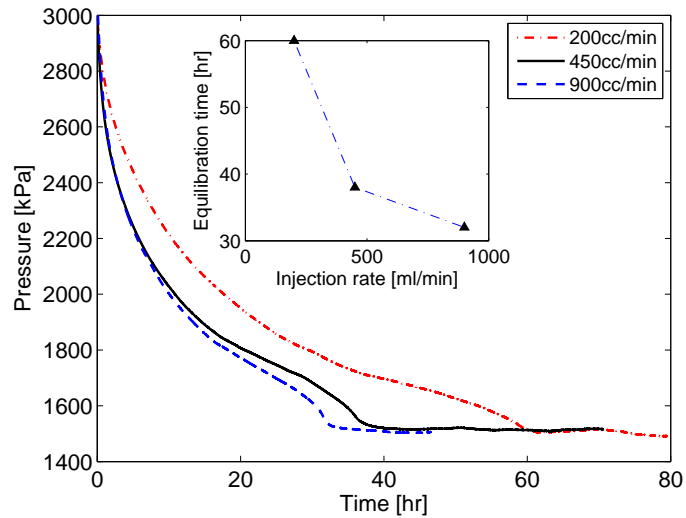


Figure 5.11: Pressure decay curve for CO_2 gas hydrate formation experiments in glass bead core. Initial pressure is 3.0 MPa and the temperature is constant at 275.15 K. Injection rate varies from 200 to 900 ml/min

experiments which show an excellent reproducibility. Controlling the injection rate improves the reproducibility and the pressure drop is smooth.

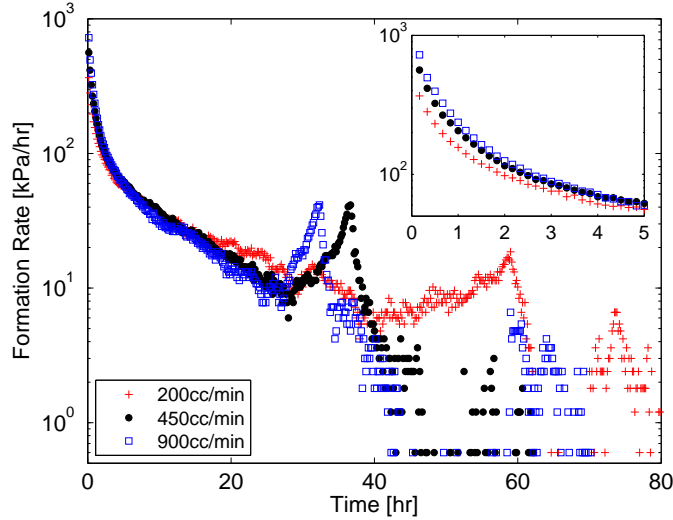


Figure 5.12: Gas hydrate formation rate curve for CO_2 gas hydrate formation experiments in glass-beads core. Initial pressure is 3.0 MPa and the temperature is constant at 275.15 K. Injection rate varies from 200 to 900 ml/min

In this study, experiments were performed at least twice under the same conditions to check their reproducibility. It was found that the reproducibility is as good as shown in Figures 5.9 and 5.10. Therefore, in the following discussions, only one experimental result from each series of experiments will be shown.

The sensitivity study of the gas injection rate to gas hydrate formation was to investigate the feasible injection rate of CO_2 into the reservoir for sequestration. Figure 5.11 shows the pressure decay and Figure 5.12 shows the rate during CO_2 hydrate formation with different gas injection rates of 200, 450 and 900 ml/min . The temperature and initial pressures for these experiments were identical.

The pressure profiles reveal that the equilibration time⁵ is shortened when the gas injection rate increases. The equilibration time was decreased by 23 hours when gas injection rate was increased from 200 to 450 ml/min , while the difference in equilibration time between 450 and 900 ml/min was only 5 hours. But the equilibration time did not linearly decrease with increasing the injection rate. In the range between 450 and 900 ml/min , the influence on equilibration time was less significant as in the range from 200 to 450 ml/min (as seen in the subplot of Figure 5.11).

Figure 5.12 shows that for the reaction limited regime ($t \lesssim 5$ hr), the gas hydrate formation rate for experiment with an injection rate of 200 ml/min is the slowest. When entering the diffusion limited regime, the formation rates are almost the

⁵The equilibrium time is defined at the point when dP/dt smaller than $1kPa/hr$.

CHAPTER 5. GAS HYDRATE FORMATION IN POROUS MEDIA

same for all injection rates at a time range of $5 \lesssim t \lesssim 15$ hr. Afterwards, the gas hydrate formation rate of 200 ml/min increased slightly. Nevertheless seen from the overall process, the slope of formation rate for 900 ml/min is most steep, meaning that gas hydrate formation is fastest. The high injection rate might create more turbulence to the flow, thus resulting in a larger interfacial area. This could be a possible explanation to the higher formation rate for experiment with an high injection rate.

It can be concluded that in the diffusion limited process, the formation rate is not very sensitive to the injection rate, especially in the range between 450 ml/min and 900 ml/min . Small changes of the gas injection rate within these ranges cannot effect the hydrate growth in the porous media.

5.3.3 Influence of Initial Pressure

From gas hydrate formation experiments in the bulk (Chapter 3), it was concluded that the initial pressure has a strong influence on the gas hydrate formation. In the following, the impact of the initial pressure on the gas hydrate formation in porous medium is discussed based on the results of experiments with an initial pressure of either 3.0 MPa or 2.5 MPa. Both experiments have been conducted at a constant temperature of 275.15 K and CO_2 was injected at a rate of 450 ml/min .

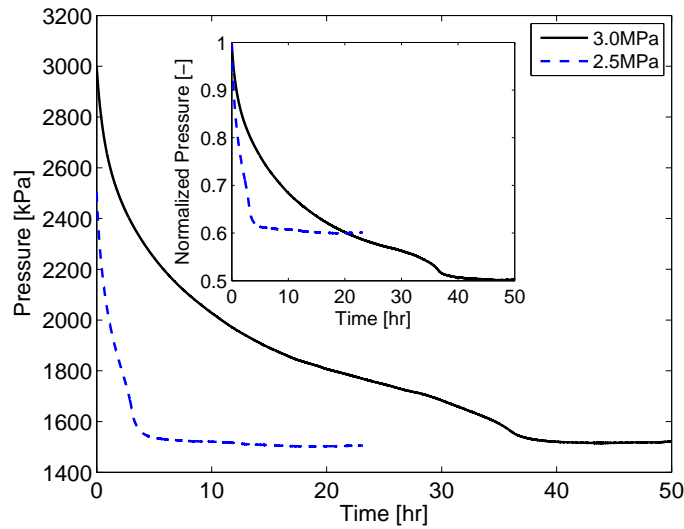


Figure 5.13: Pressure decay curve during gas hydrate formation in glass bead core. Injection rate is 450 ml/min , temperature is 275.15 K. Initial pressure is either 3.0 MPa or 2.5 MPa.

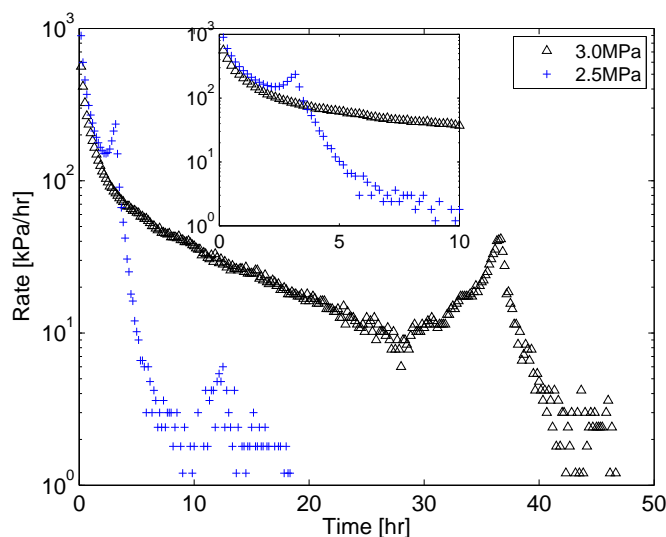


Figure 5.14: Rates during CO_2 hydrate formation in glass-beads core. Injection rate is 450 ml/min , temperature is 275.15 K . Initial pressure is either 3.0 MPa or 2.5 MPa .

Figure 5.13 shows the pressure decay for the two experiments. For both experiments, the same equilibrium pressure of 1.51 MPa was reached. The time for the pressure to stabilise is about 5 hours for the experiments at initial pressure of 2.5 MPa , while for experiment with an initial pressure of 3.0 MPa the equilibration time is 38 hours. To allow for better comparison a normalised pressure (P/P_{ini}) decay was also displayed as a subplot in Figure 5.13. The normalised pressure plot clearly shows that the pressure drops faster for an initial pressure of 2.5 MPa .

Figure 5.14 depicts the gas hydrate total rate as a function of time at an initial pressure of 2.5 and 3.0 MPa . In the first 4 hours, the formation rate at a low initial pressure was slightly higher than the formation rate with an initial pressure of 3.0 MPa . Afterwards, the formation rate for initial pressure of 2.5 MPa decreased dramatically because the system entered the equilibrium state.

It can be seen from Figure 5.13 and Figure 5.14 that after 4 hours the system almost reached equilibrium for the experiment with an initial pressure of 2.5 MPa . This indicates that the gas consumed in the reaction limited process brought the system near the equilibrium already. The driving forces was released, therefore, further diffusion-limited process was not necessary (see Figure 5.14). The pre-equilibrium process initiated immediately after the reaction limited regime in stead of the diffusion-limited regime and bring the system finally into a state of equilibrium.

5.3.4 Influence of Relaxation Time

In this study, the dissociation of the gas hydrates was done by releasing pressure at a slow flow rate to make sure that no water was been flushed out. This process took around 15-20 hours to complete. The relaxation time is the time between complete dissociation of the hydrates and starting of a new formation experiment. It was concluded from bulk experiments that the memory effect of water could reduce the nucleation time significantly (see Chapter 3). In the porous media experiment the nucleation time is already greatly reduced due to use the water with ‘memory’ effect, and possibly the silica surface of the glass beads acts as seed for hydrate formation. Therefore, in the following, the influence of relaxation time on the gas hydrate formation in the porous media will be discussed.

Two set of experiments were conducted and compared: 1) experiments with almost no relaxation time; 2) experiments with 15 hours of relaxation time at atmospheric conditions. In both cases, the temperature was kept constant at 275.15 K and initial pressure was 3.0 MPa.

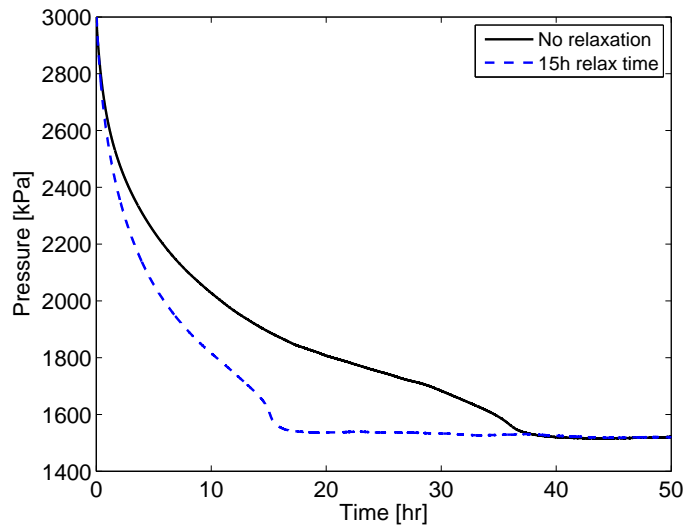


Figure 5.15: Pressure decay curve for CO_2 gas hydrate formation experiments in glass bead core. Injection rate is 450 ml/min , temperature is 275.15 K, and the initial pressure is 3.0 MPa. Experiments are done directly after preceding experiment (without relaxation) and after 15 hours (with relaxation).

Figure 5.15 shows the pressure decay curves for the experiments with and without relaxation time. As expected, the equilibrium pressure for both experiments was the same (at 1.5 MPa). It showed clearly that the time to reach the equilibrium is 25 hours shorter for the experiment with relaxation. Figure 5.16 shows that in the reaction-limited regime ($t \lesssim 5 \text{ hr}$) the gas hydrate formation rate is higher for experiment with relaxation. However, in the reaction-limited regime, the

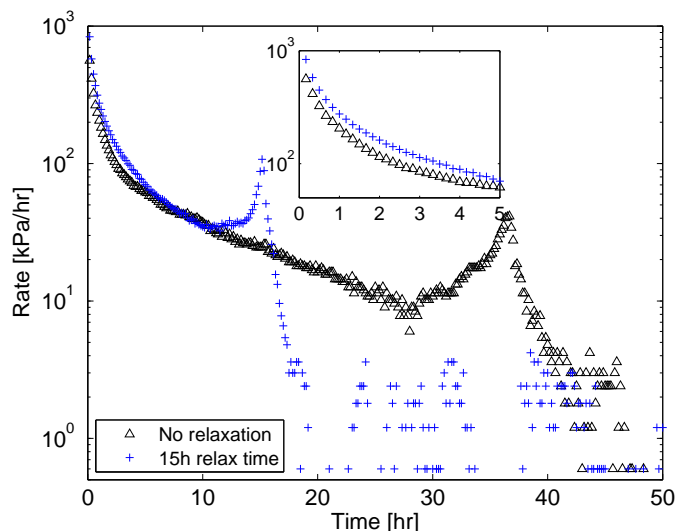


Figure 5.16: Rates during CO_2 gas hydrate formation experiments in glass bead core. Injection rate is 450 ml/min , temperature is 275.15 K , and the initial pressure is 3.0 MPa . Experiments are done directly after preceding experiment (without relaxation) and after 15 hours (with relaxation).

formation rate is similar for both experiments.

The memory effect of water, which can be interpreted as the structuring of the water, gradually fades with relaxation time. Water has the strongest memory effect when new experiment started immediately after the previously formed hydrates were dissociated. With 15 hours relaxation time, the memory effect is weaker. Results suggest that with a stronger memory effect, the formation of gas hydrate is slower. This is in agreement with results in the bulk (see Figure 3.7 in Chapter 3). In bulk, the half decay time is longer for water with memory effect, meaning the hydrate formation is slower for water with memory effect.

Vysniauskas and Bishnoi [141, 142] found that memory effect only shortens the nucleation time but it has no apparent influence on the kinetics of hydrate formation after the hydrate nuclei have been found. However, we found that the memory of water actually has a negative effect on the gas hydrate growth. The presence of residue structure probably hinders the agglomeration of crystals.

5.3.5 Gas Hydrate Visualisation by X-Ray CT

The formation and distribution of gas hydrates in the pore media were visualised and analysed by the assist of X-Ray CT technology. From the reconstructed images, the minimum size of pixel that can be detected and distinguished was

CHAPTER 5. GAS HYDRATE FORMATION IN POROUS MEDIA

estimated to be $300 \mu\text{m}$. The porous media has an average grain diameter of 1.8 mm . Thus the resolution is relatively low to obtain a precise image of the pore space. However, the CT images provide qualitative information on hydrate formation in porous media.

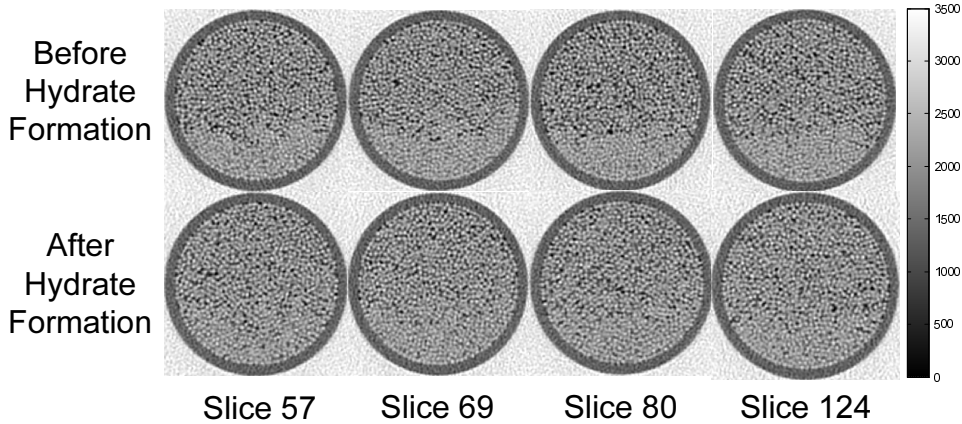


Figure 5.17: CT-scan images of cross-sectional slices at four different locations along the core. The upper four images show the scans before gas hydrate formation; the lower four images show the same cross-sectional images after gas hydrate formation. For this experiment, the initial pressure was 3.0 MPa and the final temperature was 275.15 K

Figure 5.17 shows the reconstructed CT images of the cross-sections of the core at four different positions. The upper four images demonstrate the core sample before gas hydrate formation. The images show a clear separation of the liquid and gas phase due to gravity segregation: the aqueous phase occupies the lower part of the core while the CO_2 occupies the upper part (with connate water). The four images at the bottom show the same cross-sections after gas hydrate formation. The formation of hydrates was identified by the pressure decay. The CT images show that after gas hydrate formation, the difference between the lower part and the upper part of the core could not be clearly distinguished. Comparing the images at same location before and after hydrate formation, it can be seen that the top part of the core was gradually filled up with gas hydrates, while no obvious changes in the lower part was found.

In Figure 5.18 and Figure 5.19 the averaged intensities over the core at various positions along the core are shown. From duplicated scans, the error of these intensity values could be estimated and is given as error bars in the figure. It was calculated that the offset between two duplicated scans is $\pm 10 \text{ HU}$. A deviation of $\pm 17 \text{ HU}$ was found when correct the intensity with a reference material ⁶ before and after the gas hydrate formation. See for more details Appendix B.

⁶The reference material is the Perspex tube used to hold the glass bead core.

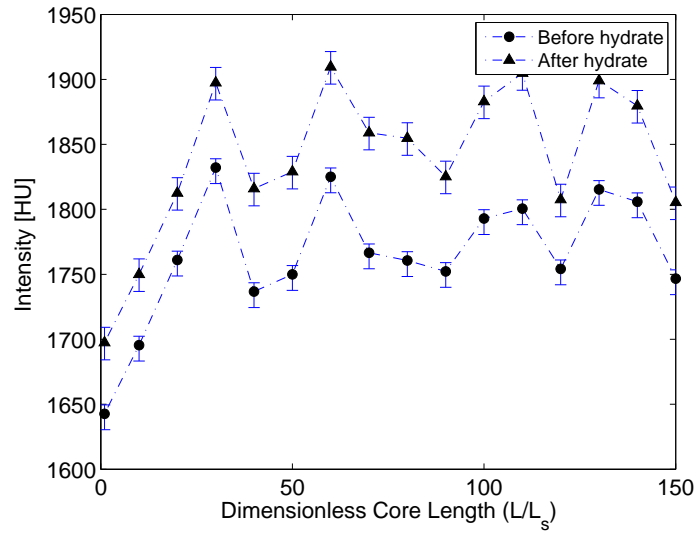


Figure 5.18: The intensity determined in the upper part of the core from CT images along the core sample before and after gas hydrate formation. L is the length along the core, L_s is the thickness of slice for scanning.

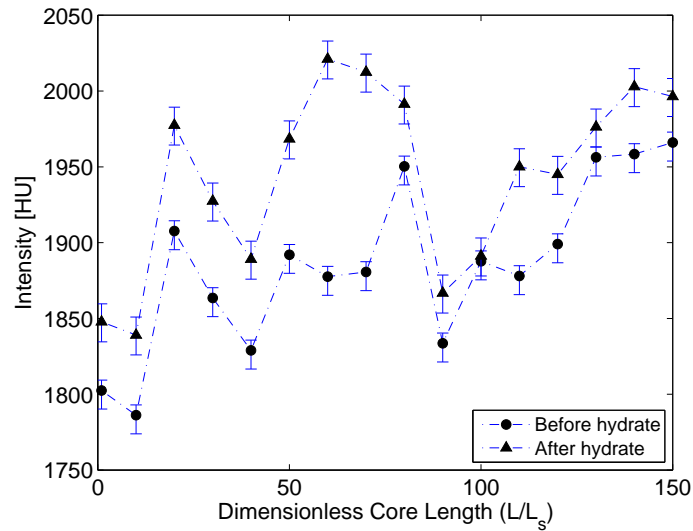


Figure 5.19: The intensity determined in the lower part of the core from CT images along the core sample before and after gas hydrate formation. L is the length along the core, L_s is the thickness of slice for scanning.

Figure 5.18 shows the intensity variation in the upper part of the core which is filled mainly with CO_2 before and after gas hydrate formation along the core length. The density of CO_2 hydrates is 1.11 g/cm^3 [5], denser than the pure water. Therefore, the intensity shifted to higher values indicating the formation of gas hydrates. In the upper part, the changes were quite uniformly distributed along the core length. This suggests that gas hydrates were formed around the grains with connate water. Therefore, a relatively homogeneous distribution of hydrates in the upper part was achieved. This also explains the filling-up in the upper part of the core in Figure 5.17 after hydrates were formed. While in the lower part which mainly saturated with water, the distribution of hydrates was quite local as shown in Figure 5.19. At some locations of the core, a significant change (150 HU) of the intensity was observed, while at other locations, the difference is barely noticeable. This local difference could be due to the irregular water distribution along the core.

5.4 Conclusions

The formation of carbon dioxide hydrates in a porous media was studied. The influence of initial pressure, temperature, gas injection rate and time between experimental runs was investigated.

The gas hydrate formation in porous media can be characterised into 3 regimes, namely: the reaction-limited, the diffusion-limited and the pre-equilibrium regime. This is different than for the gas hydrate formation in the bulk phase. In principle, the gas hydrate formation mechanism in the molecular level seems to be the same in porous media and in the bulk phase. However, the macroscopic hydrate behaviour differs. This is mainly influenced by capillary effects, area of gas-liquid interfaces and mass transfer etc. The porous structure creates a larger gas-liquid interface for hydrates to grow on, but the contact area between gas and water decreases during hydrate formation. Once the gas-water contact surface disappears, gas hydrate formation is limited by diffusion of CO_2 through the gas hydrate layer. Consequently, the gas hydrates formation rate is much slower in porous media than in the bulk phase where agitation is possible.

The reaction-limited regime ($t \lesssim 5 \text{ hr}$) is responsible for about 50% of the total pressure decay. In this regime, the highest formation rates were observed for the experiments with a low initial pressure and for the experiments with relaxation time. The lowest formation rates were found at a 200 ml/min injection rate.

The diffusion limited regime starts when the accessible gas-water interface disappears. It is a much slower process, which is not very sensitive to the injection rate and relaxation time. The diffusion limited gas hydrate formation rate is found to be slightly lower as temperature increased. Unfortunately, the pre-equilibrium regime cannot be explained in detail. Detailed work on thermodynamic and

molecular modelling is needed to clarify its mechanism.

It is known that with a changing gas injection rate, the water displacement in the core sample varies, resulting in a local heterogeneous distribution of water and gas. Therefore, the overall gas hydrate formation was also influenced by the gas injection rate. It was found that the equilibration time decreased with increasing injection rate. However, the influence of the injection rate to the CO_2 hydrate formation revealed a non-linear behaviour. A low gas injection rates resulted in a relatively low formation rate and long time for the system to reach equilibrium. Therefore, to achieve a faster CO_2 sequestration process in the reservoirs, faster injection rates are suggested.

CO_2 hydrate formation in porous media could be visually detected with the aid of X-ray computer tomography. Gas hydrates in the upper part of the core is formed with CO_2 and connate water mainly during the reaction limited regime. Therefore, the distribution of gas hydrates in the upper part of the core is more homogeneous. In the lower part of the core, the available gas-water surface is small compared to the area in the upper part and the distribution of water is localised; these results in a regional clusters of gas hydrates in the porous medium. Unfortunately the resolution of applied CT scanner does not allow quantification of the gas hydrates. Therefore, it is suggested to use a micro CT-scan with higher resolution. In order to reduce the noise, it is better to have a core holder with thinner wall.

6

Enhanced Gas Hydrate Production

In the previous chapters we reported experimental results on the formation of CH_4 and CO_2 hydrates at various conditions by using laboratory-scale setups. For real applications, the results from the lab-scale need to be up-scaled to the reservoir scale. In this chapter, modelling and numerical simulations were performed to evaluate methods to enhance gas production in hydrate reservoirs. The gas production by a combination of thermal stimulation or CO_2 injection will be compared.

6.1 Introduction

It is generally believed that natural gas hydrate accumulations are formed by seeping gas entering the hydrate stability zone [73]. A wide varieties of natural gas hydrate accumulations exist in the permafrost and in the sub sea. For a systematic study these accumulations are usually subdivided into four main classes [111]: Class 1 hydrate reservoirs occur together with a conventional gas reservoir above the free gas zone. Class 2 gas hydrate reservoirs overlay water bearing formations eventually containing dissolved methane. Class 3 gas hydrate accumulations are those occupying the entire permeable zone. Finally, Class 4 gas hydrate accumulations consist of dispersed patches of hydrates. The hydrate saturation¹ is relatively low and no confining overburden and under burden can be defined. Class 2 gas hydrate reservoirs are encountered in both permafrost and deep sea sediments [86]. Therefore, in this work, a Class 2 gas hydrate accumulation was modelled for simulating the gas production strategies.

Modelling and numerical simulations on the reservoir scale have laid a foundation and are an important tool for evaluating the potential of methane extraction process from natural gas hydrates. Many studies have been devoted to gas hydrate production by simulations as already mentioned in Chapter 2.

¹The gas saturation is volume of gas hydrates over the total pore volume of the reservoir.

From a few test wells that have been drilled for gas production from hydrate bearing reservoirs it was observed that gas production rates were not high enough to be economically feasible at the current gas price [84]. The endothermic behaviour of gas hydrate dissociation cause the decrease of reservoir temperature. Consequently, secondary hydrate formation² or ice formation are likely to occur which hinder further dissociation of hydrates and gas transport in the reservoir. Therefore, the main challenge of gas production from hydrate reservoir is either the large amount of heat or the sufficient low pressure required to support the hydrate dissociation.

Typical production methods from gas hydrate bearing layer are depressurisation, thermal stimulation and injection of a chemical inhibitor. The thermal stimulation is ineffective as the main dissociation strategy due to the low energy efficiency [87]. The injection of hydrate inhibitors is also not recommend due to high costs and the dilution of inhibitor by water originated from dissolving the gas hydrates [86]. Recently, a new method was proposed by Ohgaki et al. [97] who suggests that the exploitation of CH_4 from gas hydrate reservoirs could be achieved by injecting CO_2 . The combined CH_4 hydrate production and CO_2 sequestration by gas hydrates have three benefits: it can increase CH_4 production, achieve storage of CO_2 and maintain mechanical stability of the geological strata.

From a thermodynamic point of view, the CH_4 hydrates could be replaced by CO_2 hydrates because the $H - L_w - V$ equilibrium line of $CO_2 + H_2O$ system lies below the $H - L_w - V$ of $CH_4 + H_2O$ system when temperatures are lower than 283 K (see Figure 4.1). In the previous chapters, we compared the kinetics of CH_4 and CO_2 hydrate formation (Chapter 3). We also investigated the possibility to exchange CH_4 by CO_2 in already formed methane hydrates (Chapter 4). In this Chapter, modelling and simulations of gas production from hydrate reservoirs by depressurisation, hot water injection (thermal stimulation) and CO_2 injection are compared.

6.2 Model

The commercial program STARS 2008.12 from CMG was used to perform numerical reservoir simulations. STARS is a thermal simulator which is designed to process and simulate enhanced oil recovery processes such as steam flooding, in-situ combustion, water flooding, chemical injection, polymer injection and other processes. The module for simulating gas production from gas hydrate reservoirs was modified from a chemical reaction module which is often used to simulate in-situ combustion.

²During gas hydrate dissociation, the system temperature will decrease, when the temperature drop to below the $H - L_w - V$ equilibrium temperature, gas hydrate will start to form again. This behaviour is often referred as secondary hydrate formation.

6.2.1 Hydrate Reservoir Model

The simulated reservoir is described by Cartesian coordinates. The number of the grid blocks in the reservoir is $20 \times 20 \times 20$ in the X, Y and Z direction (see Figure 6.1). The size of each grid block is $30 \times 30 \times 5m$ ($L \times W \times D$). The depth of the sea is 300 meters. The top layer of the reservoir is located at a depth of 400 m below the seafloor. The upper 10 layers (from 400 m to 450 m depth) contain CH_4 hydrates, mobile water and CH_4 . The lower 10 layers (from 450 m to 500 m depth) are fully saturated with water. The total volume of the reservoir is 36 million m^3 with $5.57 \times 10^8 m^3$ CH_4 (at standard conditions) originally present in the reservoir of which $8.15 \times 10^7 m^3$ exist as free gas and $4.75 \times 10^8 m^3$ are in the form of solid gas hydrates.

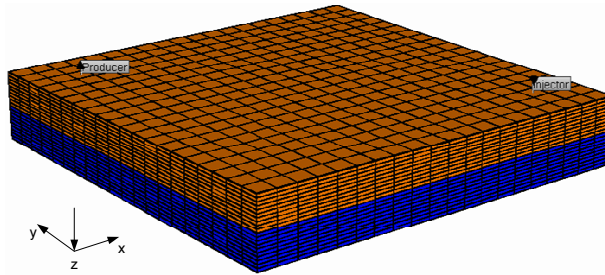


Figure 6.1: Reservoir geometry used for the CH_4 production simulations. The producer is located on the left corner and injector well located on the right. The brown layers indicate the CH_4 hydrate bearing layers, the blue layers are aquifer. A Class 2 hydrate reservoir was used.

Table 6.1: Reservoir properties

Parameters	Hydrate Zone	Water Zone
Horizontal Permeability k_h (mD)	200	200
Vertical Permeability k_v (mD)	20	20
Porosity ϕ	0.25	0.25
Water Saturation S_w	0.2	1.0
Gas Saturation S_g	0.2	0.0
Hydrate Saturation S_h	0.6	0.0
Heat Capacity ($J/m^3.K$)		
Rock	2.120×10^6	2.120×10^6
Hydrates	1.600×10^3	1.600×10^3
Thermal Conductivity ($J/m.day.K$)		
Rock	1.296×10^5	1.296×10^5
Hydrate	3.395×10^4	3.395×10^4
Water	5.183×10^5	5.183×10^5
Gas	5.183×10^5	5.183×10^5

For the simulation two vertical wells, one producer and one injector were placed

at two opposite corner of the reservoir (see Figure 6.1). The production well was completed from top layer to layer 8 of the hydrate bearing zone, with a total depth of 40 m (from 400 m to 440 m). The injector was completed only in the lower part of the reservoir, the aquifer (from 450 m to 500 m).

A constant bottom hole pressure (BHP) of 3.0 MPa is assumed for the production well. At this value the equilibrium temperature of the CH_4 hydrates is 274.50 K, higher than the freezing point of water. Thus, ice formation during hydrate dissociation is unlikely. The injection pressure is set to 5.0 MPa which means injection is only initiated when pressure around the injector is lower than 5.0 MPa.

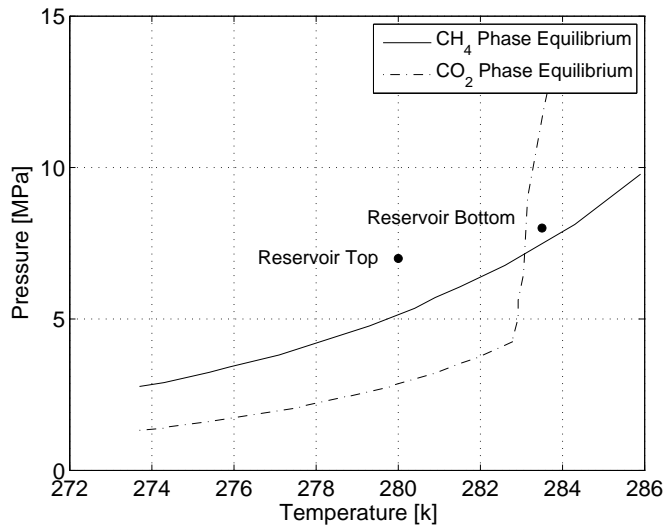


Figure 6.2: Schematic presentation of the $H - L_w - V$ equilibrium curves of the $CH_4 + H_2O$ and $CO_2 + H_2O$ system. The dots represent the reservoir conditions.

The temperature at the top of the reservoir is 280.15 K and the (hydrostatic) pressure is 7.0 MPa. Figure 6.2 shows the top and bottom reservoir condition in the phase diagram of $CH_4 + H_2O$ and $CO_2 + H_2O$.

6.2.2 Components and Phases

For the simulations, CH_4 and CO_2 hydrates were regarded as specific solid components rather than a combination of CH_4 or CO_2 and water. Thus five components were considered: water, CH_4 , CO_2 , CH_4 hydrates and CO_2 hydrates. Because of the low solubility of CH_4 in water (only 0.2 mol%), it was assumed that no methane was present in the aqueous phase.

Table 6.2: Components and their possible existence in the corresponding phases as assumed for the simulations

	Gas	Aqueous	Oil	Solid
Water	✓	✓		✓
CO_2	✓	✓	✓	
CH_4	✓			
CO_2 hydrate				✓
CH_4 hydrate				✓

CO_2 is present as liquid, gas or dissolved in the aqueous phase while CH_4 is only present in the gas phase.

In STARS, hydrates are regarded as part of the solid phase occupying part of the pore space of the reservoir matrix. Therefore, gas hydrate saturation cannot be computed directly but needs to be derived from the solid phase density. Consequently, the sum of gas, liquid and water saturation is equal to one (Equation 6.1). The volume of void space is the volume of the initial pore space minus the volume occupied by gas hydrates. Therefore, it is possible that the sum of the hydrates, gas, water and liquid saturation exceeds one (see also Equation 6.2).

$$S_w + S_l + S_g = 1 \quad (6.1)$$

$$S_h + S_w + S_l + S_g \geq 1 \quad (6.2)$$

where S_h , S_w , S_l and S_g is the saturation of hydrate phase, aqueous liquid phase, CO_2 rich liquid phase and vapour phase.

6.2.3 Hydrate Saturation and Permeability

Gas hydrate dissociation and formation during gas production and CO_2 injection lead to changes in the effective porosity and permeability. Equation. 6.3 gives the relationship between the porosity (ϕ), effective (fluid) porosity (ϕ_e) and the hydrate saturation (S_h).

$$1 - S_h = \frac{V_f}{V_p} = \frac{V_w + V_g}{V_h + V_w + V_g} = \frac{\phi_e}{\phi_v} \quad (6.3)$$

where, V_p is the total pore volume, V_f is the pore volume occupied by fluid, V_h , V_w and V_g is the volume of hydrate phase, aqueous liquid phase and vapour phase.

CHAPTER 6. ENHANCED GAS HYDRATE PRODUCTION

The effective porosity decrease with increasing gas hydrate saturation. Consequently, the permeability also decreases. In porous media gas hydrates are formed either at the pore neck or along the small film of water persisting on the grain surfaces [123]. Several models exist to describe the change of permeability and/or porosity as a function of the hydrate saturation (e.g. Carman-Kozeny model [16], Masuda et al. model [78], etc). When hydrates form at the pore neck, the major flow path will be intercepted resulting in a severe blockage. When hydrates only form around the grains but does not completely block the pore neck, the permeability reduction will be smaller.

In Figure 6.3, the permeability ratio (permeability with the presence of gas hydrates over permeability without gas hydrates) as a function of the hydrate saturation for different correlations is plotted.

Uddin et al. used the Carman-Kozeny relation (Equation 6.4) with $n = 10$. It gives an extreme permeability reduction. The permeability drops to 1% of the initial permeability (k_0) at $S_h = 0.37$ (see Figure 6.3).

$$\frac{k(S_h)}{k_0} = (1 - S_h)^n \left(\frac{1 - \phi_v}{1 - \phi_e} \right)^2 \quad (6.4)$$

If it is assumed that the gas hydrates grow on the grain surface, as in the Kozeny Grain Coating model, the hydrate saturation has much less impact on permeability. The permeability approaches 1% of the initial permeability (k_0) at $S_h = 0.83$ (see Figure 6.3).

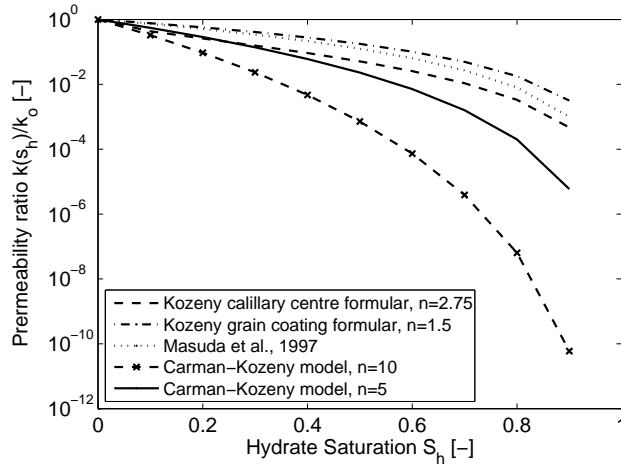


Figure 6.3: Permeability ratio as a function of gas hydrate saturation according to the various correlations.

In this study, we assumed that gas hydrates can form randomly in porous spaces and therefore the Carman-Kozeny model with $n = 5$ was used. The permeability reduction due to hydrate formation is less severe than the assumption by Uddin et al. but higher than Kozeny Grain Coating model. The permeability reduces to 1% of the initial permeability (k_0) at $S_h = 0.58$ (see Figure 6.3). The relative permeability of each phases were given in correlations shown in Appendix C.

6.2.4 Reaction Kinetics

Hydrate dissociation can be described by a two-step processes consisting of the destruction of the clathrate lattice and the desorption of the guest molecules [63].

According to Englezos et al. [34] the rate of dissociation is a function of the area of the gas hydrate surface exposed to the liquid phase. The driving force is described by the difference in pressure of the guest component in the hydrate phase and in the gas phase. Assuming a two liquid film approach (see Chapter 2 Figure 2.3) the rate of hydrate dissociation can be expressed by:

$$\frac{dc_h}{dt} = k_d A_s (P_e - P_g) \quad (6.5)$$

where, dc_h/dt is the rate of dissociation, k_d is dissociation rate constant, A_s is the surface area, P_e is the $H - L_w - V$ equilibrium pressure and P_g is the gas pressure in gas phase.

According to Kim et al. [63] and Uddin et al. [132], Equation 6.5 can generally be used for the description of the dissociation or, in a similar form, for the formation of gas hydrates. The size of the hydrate surface exposed to the liquid phase is crucial for the description of the formation and dissociation. Equation 6.6 describes the hydrate surface for dissociation, while Equation 6.7 was used to describe the surface for the formation of hydrates. This equation contains two terms, the first one describes the initial surface necessary to form a nucleus. The second term describes the surface of the already formed hydrates. The hydrates fill up the pore space and the gas-liquid contact becomes smaller. Thus, the available surface for gas hydrate formation decreases with the hydrate saturation.

$$A_s = \phi_e^2 S_h S_w A_{si} \quad (6.6)$$

$$A_s = \phi_e S_w A_{si} + \phi_e^2 S_h S_w A_{si} \quad (6.7)$$

where, A_{si} is the specific surface area per unit volume of hydrates, S_w and S_h is the saturation for water and gas hydrates respectively, ϕ_e is effective porosity.

CHAPTER 6. ENHANCED GAS HYDRATE PRODUCTION

The accessible hydrate surface for dissociation is much smaller than for formation because the pore space is occupied by gas hydrates. During dissociation, the water saturation (S_w) increases due to the water release from gas hydrates, while the gas hydrate saturation (S_h) decreases. Therefore, the dissociation area first increases with hydrate saturation but after reaching a maximum value, the surface decreases.

Substituting Equation 6.6 into Equation 6.5 gives the kinetics equation of hydrate dissociation.

$$\frac{dc_h}{dt} = r_{rk1} e^{-\frac{E}{RT}} (\phi_e S_w \rho_w) (y_i p_g) \left(1 - \frac{1}{K}\right) \quad (6.8)$$

Similarly, substituting Equation 6.7 into Equation 6.5 gives:

$$\frac{dc_h}{dt} = r_{rk2} e^{-\frac{E}{RT}} (\phi_e \rho_w S_w) (y_i p_g) \left(\frac{1}{K} - 1\right) + r_{rk3} e^{-\frac{E}{RT}} (\phi_e \rho_h S_h) (\phi_e \rho_w S_w) (y_i p_g) \left(\frac{1}{K} - 1\right) \quad (6.9)$$

where, E is activation energy, R is the gas constant, x_i and y_i is the mole fraction of component i in gas phase and liquid phase respectively and K is equilibrium constant. r_{rk1} , r_{rk2} and r_{rk3} are defined as kinetics rate constants (shown in Equation 6.10, 6.11, 6.12). r_{rk1} is rate constant for gas hydrate dissociation, r_{rk2} and r_{rk3} are the rate constants for gas hydrate formation.

$$\frac{k_d^o A_{si}}{\rho_h \rho_w} = r_{rk1} \quad (6.10)$$

$$\frac{k_f^o A_{si}}{\rho_w} = r_{rk2} \quad (6.11)$$

$$\frac{k_f^o A_{si}}{\rho_w \rho_h} = r_{rk3} \quad (6.12)$$

where, k_d is intrinsic dissociation rate constant and k_f is intrinsic formation rate constant. They are functions of the components and the hydrates structures. The complete derivation of these equations can be found in Appendix C.

According to the data of Clark et al. [19, 20, 21] and Englezos et al. [34, 35], CO_2 hydrate formation is slower than CH_4 hydrate formation. However, recent experiments [42, 60, 75] and also this study (Chapter 3) show that the formation of CO_2 hydrates is much faster than the formation of CH_4 hydrates. Therefore in this study, it was assumed that CO_2 hydrate formation is much faster than CH_4 hydrate formation rate.

6.3. RESULTS AND DISCUSSION

The parameters for describing the reservoir and gas hydrates used in simulations are given in Table 6.3. The correlation of heat capacity, viscosity and relative permeability of components are issued in Appendix C.

Table 6.3: Properties of gas hydrates used in the simulation

	Unit	CH_4 hydrate	CO_2 hydrate
Molecular Weight ³	$kg/gmole$	0.124	0.175
Molar Density	kg/m^3	0.919×10^3	1.112×10^3
Volumetric Density	$gmole/m^3$	7.408×10^3	6.335×10^3
Dissociation Rate	$gmole/(day.kPa.m^2)$	3.11×10^{12}	6.05×10^{12}
Specific Area A_{si}	m^2/m^3	3.75×10^5	3.75×10^5
Activation Energy	$J/gmole$	8.108×10^4	8.108×10^4
Reaction Enthalpy (Gas)	$J/gmole$	5.186×10^4	5.99×10^4
Reaction Enthalpy (Liquid)	$J/gmole$	N/A	5.419×10^4
Hydration Number	-	6.0	7.3
Formation Rate	$gmole/(day.kPa.m^2)$	5.01×10^6	3.37×10^7
R_{rk1}	$m^3/(gmole.day.kPa)$	2.84×10^9	N/A
R_{rk2} (gaseous)	$1/(day.kPa)$	3.39×10^7	2.28×10^8
R_{rk3} (gaseous)	$m^3/(gmole.day.kPa)$	4.58×10^3	3.59×10^4
R_{rk2} (liquid)	$1/(day.kPa)$	N/A	2.28×10^6
R_{rk3} (liquid)	$m^3/(gmole.day.kPa)$	N/A	3.59×10^2

6.3 Results and Discussion

6.3.1 Base Case

The base case simulate the depressurisation production strategy and was used as reference case. The CH_4 production was achieved by only decreasing the bottom hole pressure (BHP) without injecting CO_2 . The minimum BHP was set to 3.0 MPa.

Figure 6.4 displays the distribution of CH_4 hydrate saturation in the reservoir at different simulation times. The initial hydrate saturation is 0.6. Figure 6.5 and Figure 6.6 show the pressure and temperature in the reservoir before and after gas production, respectively.

From these three figures, it can be concluded that as soon as the pressure reduced below the $H - L_w - V$ equilibrium pressure of the $CH_4 + H_2O$ system, CH_4 hydrates started to dissociate. Due to the endothermic nature of gas hydrate dissociation, the temperature in the reservoir decreases. From the simulation

³The molecular weight of gas hydrates was calculated based on the assumed chemical formula of gas hydrates. The chemical formula of CH_4 hydrate is $CH_46(H_2O)$ and of CO_2 hydrate is $CO_27.3(H_2O)$.

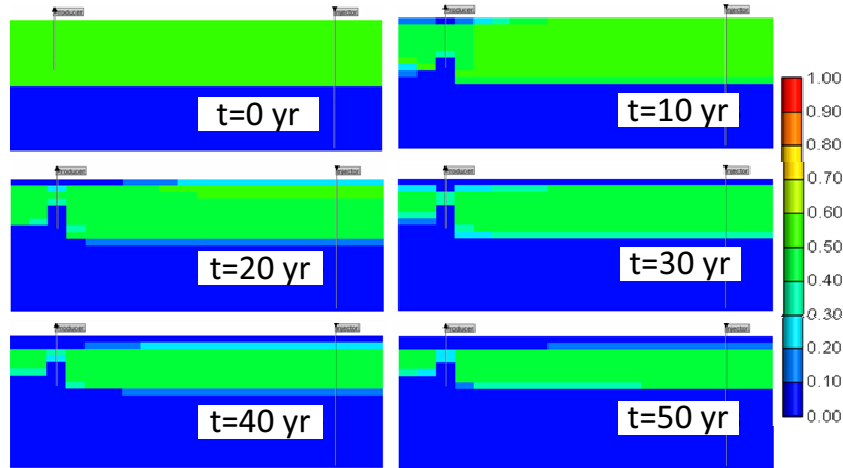


Figure 6.4: Base case without CO_2 injection. CH_4 hydrate saturation in the reservoir at different simulation times. Producer is at the left hand side of the reservoir. At the right hand side the colour bar gives the scale of hydrate saturation from zero (blue) to one (red).

results, it was calculated that after 28 years of production, 35% of the initially present CH_4 hydrates were dissociated and the pressure in the hydrate-bearing zone was reduced to almost 3.0 MPa. The temperature in the initially hydrate-bearing layers dropped to 274.50 K. These temperature and pressure coincide with the $H - L_w - V$ equilibrium line of $CH_4 + H_2O$ system (as shown in Figure 6.2).

After the equilibrium temperature was reached, further hydrate dissociation depended on the heat supply from the over- and under-burden layers. However, in the configuration used in this simulation the heat transfer is too slow to support dissociation of all gas hydrates initially present. Consequently, due to heat influx from the surrounding strata CH_4 hydrate dissociation was only observed in the top and bottom layers of the hydrate zone. As can be seen in Figure 6.4 after 50 years, the CH_4 hydrates in the middle of the hydrate layers were still present in the reservoir. Only the hydrates close to producer have been dissociated because the pressure was continuously kept at a low value of 3.0 MPa.

Figure 6.7 shows the CH_4 hydrate saturation and temperature change in layers 8 to 11 as a function of time. In layers 8 to 10 CH_4 hydrates were initially present, while layer 11 is the top layer of the aquifer. It can be seen that in layer 10 the hydrate saturation decreases fast. This is accompanied by a steady temperature drop in the hydrate bearing layers and the adjacent aquifer layer (layer 11). The dissociation in layer 10 is fastest because it has a direct heat supply from the underlying aquifer (layer 11-20). In Figure 6.7, it can be seen that, after 24

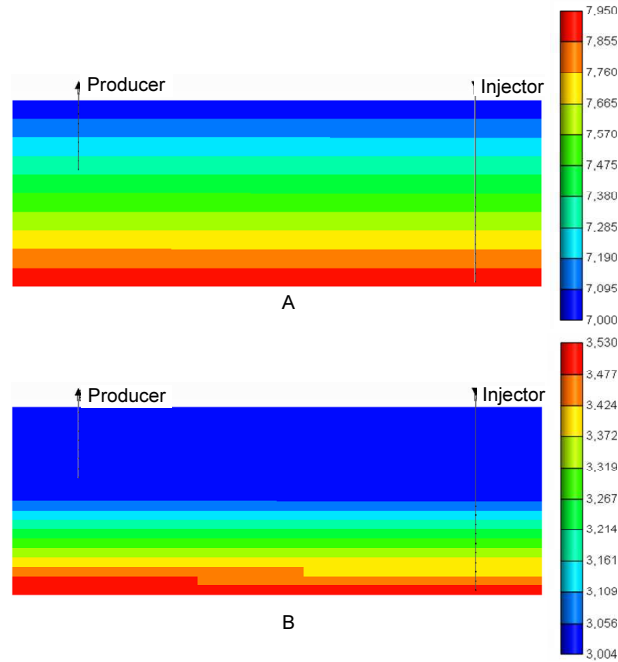


Figure 6.5: Pressure distribution in the reservoir at $t=0$ (A) and after 50 years (B) of production by pressure reduction. The producer is at left hand side and the injector is positioned at right hand side. The colour bar at the right hand side gives the pressure scale in MPa.

years, all hydrates in layer 10 were dissociated. The temperature in layer 10 increases due to the heat transferred from the aquifer and finally stabilises at the average temperature of layer 9 and 11. The heat from aquifer is conducted through layer 10 to layer 9. Thus, the dissociation of hydrates in layer 9 also commences as soon as the temperature becomes high enough to dissociate the gas hydrates. However, as long as there are still hydrates present in layer 10, the hydrate dissociation rate in layer 9 is lower than layer 10. The dissociation rate in layer 9 increases when all gas hydrates have been dissociated in layer 10. This is indicated by the dramatic saturation decrease of CH_4 hydrates in Figure 6.7. Comparable behaviour was observed for layer 8 and 9. After 46 years, when all CH_4 hydrates have dissociated in layer 9, the rate of dissociation in layer 8 increases. A similar process can also be observed for the top layers, where heat is supplied from the overburden layers.

It was assumed that the temperature in the over- and under-burden kept constant which suggests that the heat source is unlimited. However, the rate of heat transfer is slow compared to the dissociation rate of the CH_4 hydrates. Therefore, the gas production was limited by the inefficiency of the heat transfer from the adjacent layers within the simulation time of this study. When the equilibrium

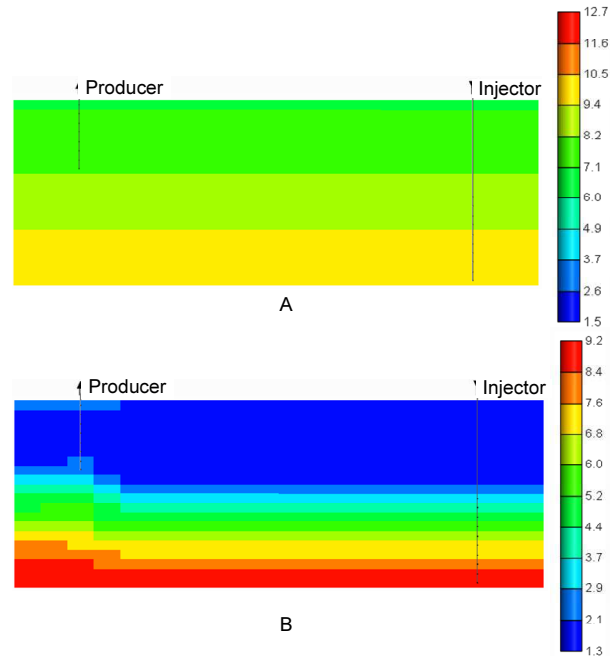


Figure 6.6: Temperature distribution in the reservoir at $t=0$ (A) and after 50 years (B) of production by pressure reduction. The producer is at left hand side and the injector is positioned at right hand side. The colour bar at the right hand side gives the temperature scale in Celsius.

pressure and temperature of the $H - L_w - V$ equilibrium curve was reached, the production dramatically decreased. It was found that the heat capacity initially in the hydrate-bearing layers itself was only enough to support 35% CH_4 hydrate dissociation. The subsequent production was supported by heat transfer from over and under-burden which is a rather slow process. In the base case where only depressurisation was applied, in total, 50% of initial gas in the reservoir (IGIP) was produced after 50 years.

6.3.2 Enhanced Gas Recovery

In order to enhance the gas production from hydrate reservoirs, the depressurisation strategy, combined with either thermal stimulation or CO_2 injection was modelled. In the following, the production increase achieved by these two combined production methods will be investigated.

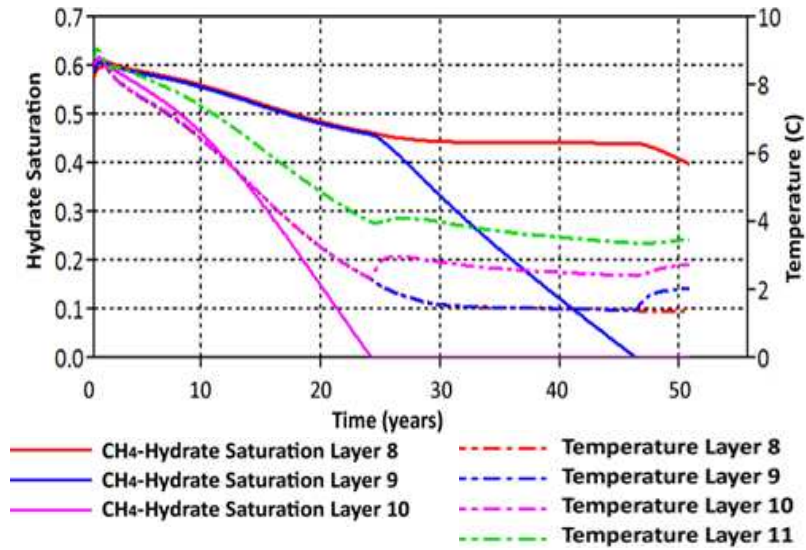


Figure 6.7: CH_4 hydrate saturation and temperature as function of time in different layers. Layer 1-10 is the gas hydrate bearing layer. Layer 11-20 is aquifer.

6.3.2.1 Thermal Stimulation Combined with Depressurisation

As discussed above, the gas production by only depressurisation are controlled by the rate of heat supply from surrounding geological strata. One option to solve this problem is injection of hot water to thermally stimulate the hydrate reservoir. In this study, hot water of various temperatures ranging from 286.15 to 303.15 K at an injection pressure of 5.0 MPa was studied. The rest of conditions are the same as used in the depressurisation production.

In Figure 6.8 the accumulative CH_4 production by means of combined depressurisation and warm water injection for different water temperatures is depicted. The cumulative gas production increases with increasing temperature of injected water. The lowest injection temperature 286.15 K to highest temperature 303.15 K, the CH_4 production only increased about 5% over 50 years. This is considerably a low efficiency with hot water injection.

It was observed that when water was injected at 303.15 K, after 50 years, the warm water reaches 200 m in horizontal and 70 m in vertical distance away from the injector (see Figure 6.9). This only enhanced CH_4 hydrate dissociation rate near the injection well. However, the warmed up area is relatively small compared to the size of whole reservoir, thus the additional heat from the injected water does not have a significant effect on CH_4 production.

Interestingly, the cumulative CH_4 production for all scenarios with hot water

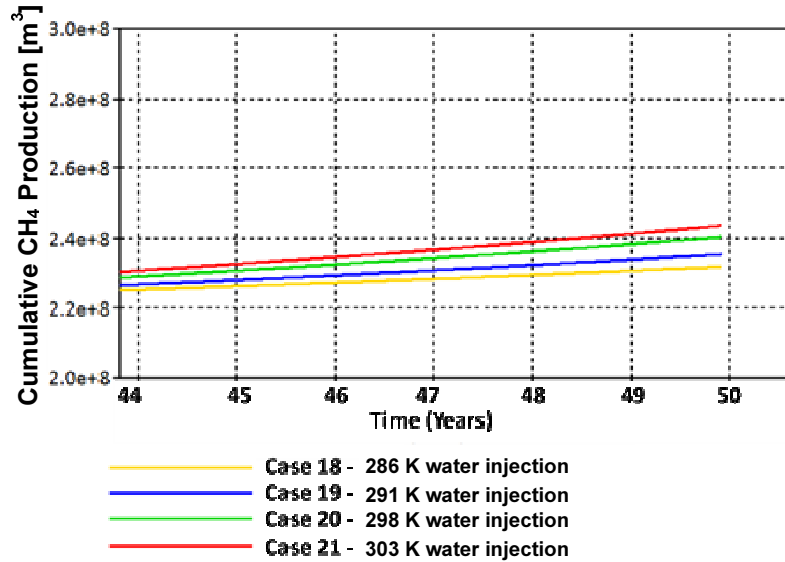


Figure 6.8: Accumulative CH_4 production as a function of time. Gas production achieved by depressurisation and combine hot water injection at different temperatures.

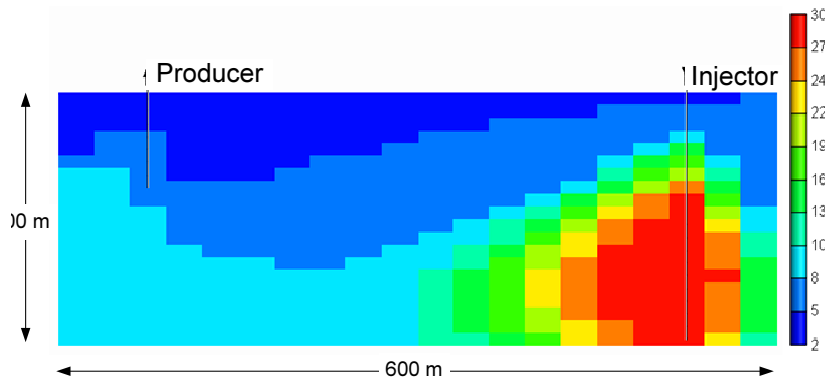


Figure 6.9: Temperature distribution in the reservoir after 50 years. Gas production achieved by depressurisation and combine hot water injection at a temperature of 303 K

injection is lower than the cumulative CH_4 production in the base case with only depressurisation (see Table 6.4). This can be explained by the fact that with hot water injection, the reservoir pressure is higher compared to the base case. The water injection was operated at 5.0 MPa while in the base case, the minimum pressure allowed is 3.0 MPa. When the reservoir maintains at a high pressure,

the dissociation of gas hydrates are hindered. In Table 6.4 the cumulative CH_4 production for the different temperature scenarios is listed. It can be concluded that thermal stimulation does not enhance the gas production significantly even when combined with depressurisation (see Table 6.4).

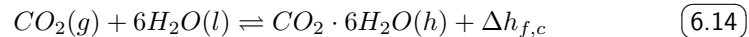
Table 6.4: Cumulative CH_4 production after 50 years by depressurisation combined with warm water injection at 5.0 MPa.

Case No.	Temperature [K]	BHP [MPa]	Cumulative CH_4 [SC m^3]
Base Case	-	3.0	2.78×10^8
18	286.15 (water)	5.0	2.32×10^8
19	291.15 (water)	5.0	2.35×10^8
20	298.15 (water)	5.0	2.40×10^8
21	303.15 (water)	5.0	2.43×10^8

6.3.2.2 CO_2 Injection Combined with Depressurisation

In this section, the gas production by depressurisation combined with CO_2 injection was investigated. Compared with the results from the water injection, the CO_2 is injected at a temperature of 286.15 K and the injection pressure is equal to the water injection pressure at 5.0 MPa. Therefore, CO_2 injection was started approximately 10 years after the production started, when pressure near the injector dropped to 5.0 MPa. Clearly, for the first 10 years, the cumulative CH_4 production was the same as for the base case. However, after CO_2 injection started, the CH_4 production increased steadily while for the base case (without CO_2 injection) the CH_4 production slowed down after 25 years (see Figure 6.10). Accordingly, the cumulative CH_4 production after 50 years with CO_2 injection was 58% higher than without CO_2 injection (see Figure 6.10).

After 20 years of CO_2 injection (30 years of production in total), a small amount of the injected CO_2 was produced. However, after 30 years of CO_2 injection (40 years of production in total), almost no CO_2 was produced anymore (see Figure 6.10). After 50 years, a total 1.8 million tonnes of CO_2 was sequestered in the reservoir of which 0.72 million tonnes were stored as gas hydrates. Only 2 mol% of the injected CO_2 was re-produced.



where, $\Delta h_{d,m}$ is the heat of dissociation for CH_4 and $\Delta h_{f,c}$ is the heat of formation for CO_2 .

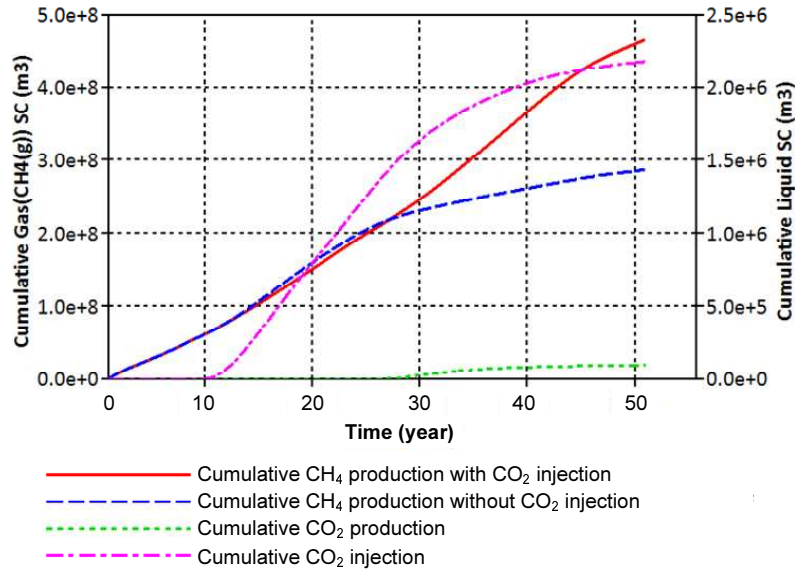


Figure 6.10: Comparison of the cumulative CH_4 production by depressurisation only and by combined depressurisation with CO_2 injection. Additionally the accumulative amount of injected and produced CO_2 are given.

The enhanced CH_4 production by CO_2 injection can be explained as follows. When CO_2 was injected, it travelled further through the reservoir and forms CO_2 hydrates when temperature and pressure conditions allow. The formation of CO_2 hydrates is an exothermic reaction (see Equation 6.14). The released heat induces the dissociation of CH_4 hydrates nearby. The latent heat⁴ of CO_2 hydrate is 500 kJ/kg [76] and for CH_4 is 415 kJ/kg [140]. Therefore, the heat generated by the formation of CO_2 is sufficient to support the dissociation of CH_4 hydrates.

Figure 6.11 depicts the temperature, pressure, CH_4 and CO_2 hydrate saturation in layer 8 (the third layer above the underlying aquifer). In the first 10 years, the temperature continuously decreases due to CH_4 hydrate dissociation. After CO_2 injection started at 10th year, the temperature stayed approximately constant with small scale fluctuations up till the 20th year. This suggests that the released heat from CO_2 hydrate formation compensates for the heat absorbed by CH_4 hydrate dissociation. After all CH_4 hydrates in layer 8 were dissociated (year 23) the temperature and the CO_2 hydrate saturation increased steeply. After 28 years, the temperature dropped again and the CO_2 hydrate formation rate became smaller. The temperature fluctuation in the layer can be explained by

⁴The heat released or absorbed during phase/state changes (e.g. from gas hydrates to gas and water) at constant temperature.

the interaction of layer 8 with adjacent layers.

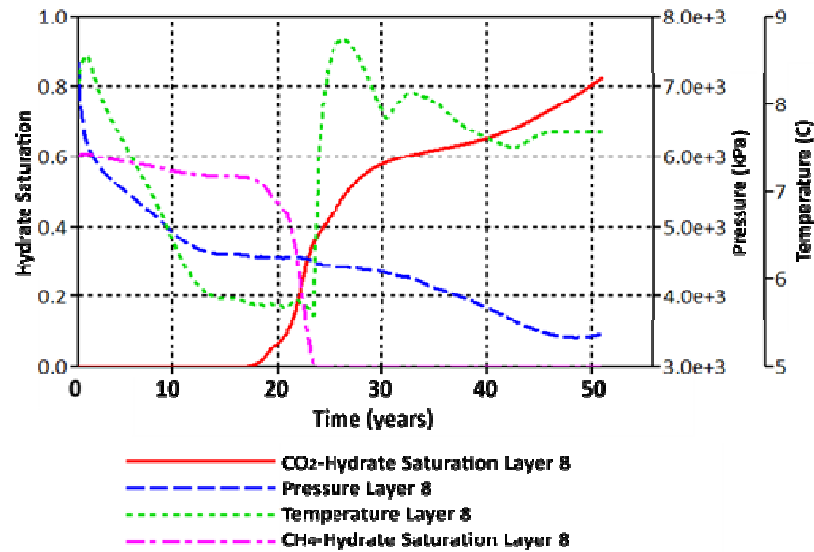


Figure 6.11: CO_2 and CH_4 hydrate saturation, pressure and temperature as a function of time in layer 8 (third layer above the underlying aquifer).

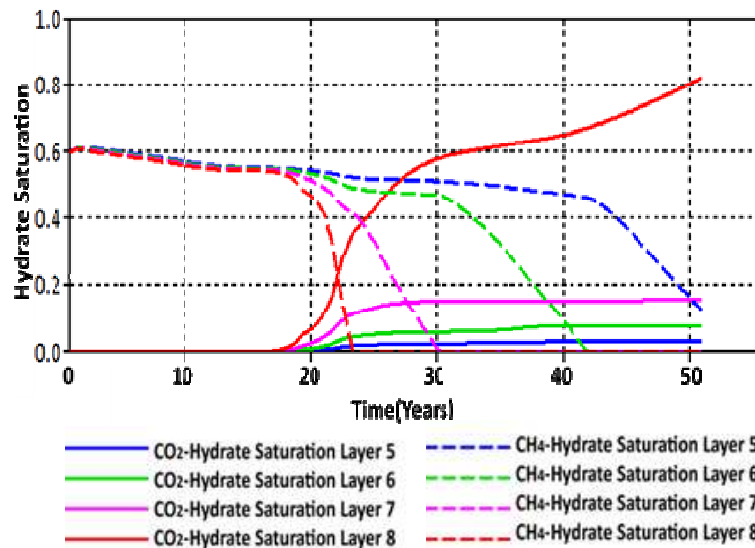


Figure 6.12: CO_2 and CH_4 hydrate saturation as a function of time in hydrate bearing layers 5 to 8.

In Figure 6.12 the CH_4 and CO_2 hydrate saturation in layers 5 to 8 are given. It

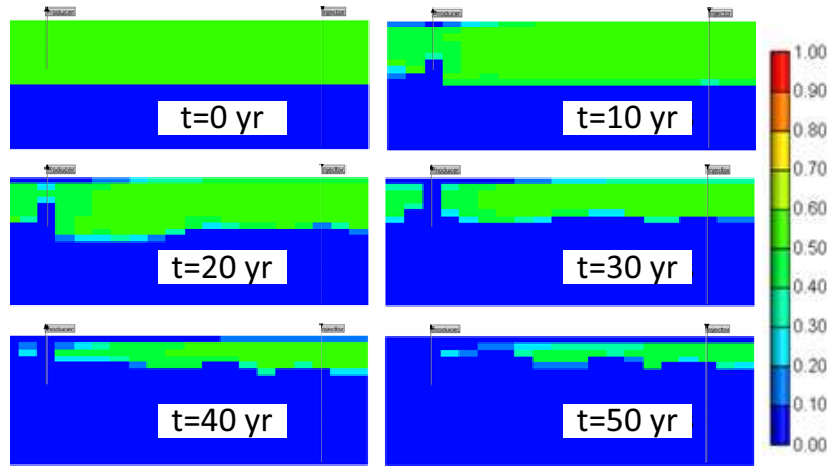


Figure 6.13: CH_4 hydrate saturation in the reservoir at different simulation times with combined CO_2 injection. Producer at the left hand side of the reservoir. At the right hand side the colour bar gives the scale of hydrate saturation from zero (blue) to one (red).

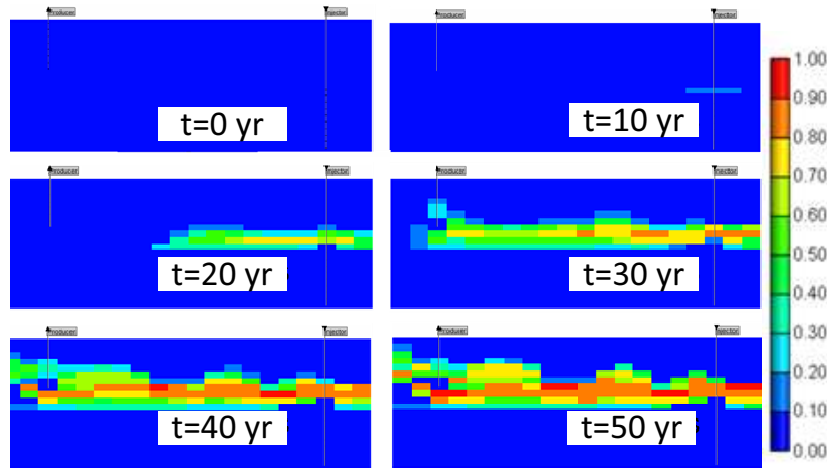


Figure 6.14: CO_2 hydrate saturation in the reservoir at different simulation times with combined CO_2 injection. Producer at the left hand side of the reservoir. At the right hand side the colour bar gives the scale of hydrate saturation from zero (blue) to one (red).

clearly shows that in each layer, after the formation of CO_2 hydrates, the CH_4 hydrate dissociation rate increases accordingly. This proves that the formation of CO_2 hydrates promotes gas production from hydrate-bearing reservoirs. It is

interesting to note that the amount of CO_2 hydrates in layer 8 is highest. After 50 years, the CO_2 hydrate saturation reaches 0.8 while in layers 5 to 7 it is less than 0.2.

It was noticed that more CO_2 hydrates are formed in the lower layers than in the upper layers (see Figure 6.14). This can be explained by the fact that the formed CO_2 hydrates reduce the effective permeability and block the upward flow of CO_2 . Although only a small amount of CO_2 hydrates are formed in the layers 5 to 7, the CH_4 hydrate saturation in the reservoir after 50 years is much lower than without CO_2 injection (compare Figure 6.13 with Figure 6.4).

Because the CO_2 hydrates form at lower pressures compared to CH_4 hydrates. CO_2 hydrates also form in the top layers in the aquifer as the CO_2 travels towards the production well. The injected CO_2 has a temperature of 286.15 K. The temperature in the aquifer varies from 281.75 K at the top to 283.50 K at the bottom. CO_2 hydrates do not form at temperatures above 283.20 K for all pressures at reservoir conditions. Consequently, the CO_2 hydrate saturation in the aquifer remains very low and does not exceed $S_h = 0.05$ (see Figure 6.14).

6.4 Summary and Conclusions

In this chapter three production strategies for the purpose of enhanced gas production from gas hydrate-bearing reservoirs have been studied by reservoir simulations and their results have been compared. The three methods are depressurisation, depressurisation combined with thermal stimulation and depressurisation combined with CO_2 injection.

Production of CH_4 by depressurisation causes a quite significant local temperature drop. This temperature drop results in a reduction of gas production rate. 50% of the initially presented gas hydrates were not yet dissociated after 50 years. A complete production of the gas hydrates would take a long time mainly because it is controlled by the rate of heat transfer from the over- and under-burden layers. Therefore, by only lowering the pressure in the reservoir, production cannot achieve complete extraction of the gas hydrates. This would be economically unfeasible due to very long production time.

The injection of warm water is not sufficient to overcome the heat loss due to the dissociation of gas hydrates. The increase in production as a result of hot water injection at 303.15 K is only 5% over 50 years. This is due to the fact that the temperature front does not reach the whole reservoir; but only a limited region around the injector is heated up after 50 years. Considering the size of the reservoir, this heated region is not sufficient to supply enough heat. This means that even if the thermal strategy is combined with depressurisation, the gas production is not efficiently increased.

CHAPTER 6. ENHANCED GAS HYDRATE PRODUCTION

The simulations reveal that gas recovery can be greatly enhanced by combining depressurisation with CO_2 injection. When CO_2 is injected at a pressure of 5.0 MPa, the cumulative gas production was improved by 60%. By this combined production strategy, the initially presented gas hydrates were almost dissociated completely. In the meantime, 98 mol% of CO_2 was efficiently stored in the reservoir, which gives a positive influence in terms of carbon sequestration.

These findings are based on the specific case study performed here. However, to achieve more reliable production results, real field data, e.g. porosity, permeability, hydrate saturation, thickness of gas hydrate bearing layer, temperature and pressure in the reservoir are essential. Results from larger scale production experiments in porous media would be valuable to validate the simulations.

7

Summary and Outlook

The research presented in this thesis was primarily aimed at investigating whether CO_2 could replace CH_4 in natural gas hydrates. For this purpose, the bulk kinetics of CO_2 and CH_4 hydrate formation was studied experimentally in an autoclave for $CH_4 + H_2O$, $CO_2 + H_2O$ binary system (Chapter 3) and $CH_4 + CO_2 + H_2O$ ternary system (Chapter 4). For the $CH_4 + H_2O$ and $CO_2 + H_2O$ binary gas hydrate forming systems, the influence of supersaturation, the stirring rate and the water quality on the kinetics of CO_2 and CH_4 hydrate formation were examined in detail. Then CO_2 hydrate formation in porous media was investigated (Chapter 5). The influence of initial pressure, temperature, gas injection rate and time between experimental runs was investigated. The extractive production of CH_4 from a commonly occurring type of gas hydrate reservoir combined with hot water or CO_2 injection was modelled and simulated (Chapter 6). Below, the most important findings of this research discussed in the previous chapters are summarised. Then an outlook on how future research can be directed is elaborated.

Gas hydrate formation is a crystallisation process. It consists of two stages, namely nucleation (formation of nuclei) and hydrate growth (growth of small nuclei into large hydrate crystals). In the binary system, these two processes are characterised by the nucleation time and the half decay time. It was found that the nucleation time decreases with increasing degree of supersaturation and stirring rate. Additionally, nucleation time decreases when experiments were performed with ‘used’ water due to the memory effect. This memory effect was reported by other authors [98, 149] and can be explained by the existence of hydrate (water) structures after dissociation of gas hydrates. The structuring of the water molecules is most likely ensured by the abundance of hydrogen bonds in the aqueous phase at low temperatures and the presence of dissolved guest molecules.

The second stage, the actual gas hydrate growth process was found to be insensitive to changes in supersaturation. The growth rate increases with increasing

CHAPTER 7. SUMMARY AND OUTLOOK

stirring rate. However, the memory effect of water has a slightly negative effect on the gas hydrate growth process. Therefore, the rate limiting step for gas hydrate formation is not nucleation, but the crystal growth. It was also found by binary experiments that at the same degree of supersaturation, the crystal growth of CO_2 hydrates is faster than CH_4 hydrates. This indicates that kinetically, the formation of CO_2 hydrates are more favourable than CH_4 hydrates. This is further supported by the findings in the ternary system.

In ternary system, CO_2 molecules are more easily entrapped into the cages formed by water molecules compared to CH_4 molecules at all tested initial pressures (Chapter 4). Even though the CH_4 concentration in the formed gas hydrates increases with the initial pressure, the formed mixed gas hydrates still contain more CO_2 than CH_4 . Methane hydrate formation at low pressure (below the equilibrium pressure of $H - L_w - V$ curve of $CH_4 + H_2O$ system) is confirmed. This means that the presence of an 'easier' gas hydrate former, such as CO_2 , can help to stabilise CH_4 hydrate cavities. Experiments of gas hydrate formation from 50/50 CH_4/CO_2 gas mixture revealed that the highest CH_4 and CO_2 separation efficiency was obtained at pressures lower than 3.5 MPa, for which a 18% of absolute CH_4 mole fraction change in the gas phase was observed.

Experiments under bulk conditions have provided tangible proof that CH_4 in the already formed methane hydrates can be exchanged by CO_2 without dissociation of the gas hydrates (Chapter 4). However, the replacement takes place at a very shallow depth near the interface between gas phase and gas hydrates. CO_2 rich hydrate layers thus act as a shield and hinder the penetration of CO_2 into deeper methane hydrate layers and counter current migration of CH_4 towards the gas phase. Due to this, the release of CH_4 from the lower layers of gas hydrates, requires the dissociation of the CO_2 hydrate layers first. Therefore, a lower pressures is needed for dissociating CH_4 hydrates.

CO_2 hydrates were formed in glass-bead packs where the beads were glued together using a resin (Chapter 5). Gas hydrate formation in the porous media was mainly observed in the upper part of the core which contained gas phase and connate water. In the lower part of the core which mainly contained CO_2 saturated liquid aqueous phase, the gas hydrate formation was found to be locally distributed, thus difficult to be observed with CT images. Three different regimes could be distinguished in the gas hydrate formation process: reaction-limited regime, diffusion-limited regime and the pre-equilibrium regime. Data showed that temperature and gas injection rate have little influence on gas hydrate formation.

Modelling and numerical simulations of simultaneous methane extraction and CO_2 injection in a Class II hydrate accumulation have shown that CO_2 injection increases the production of CH_4 compared to methane extraction by simple depressurisation (Chapter 6). In the best case, the accumulative production of CH_4 increased by 60% due to injecting CO_2 . At the same time, it was found

that CO_2 can be efficiently sequestered in the form of hydrates. Only 2 mol% of injected CO_2 was produced back with methane and water. CO_2 hydrates form directly below the CH_4 hydrates. The heat released due to formation of CO_2 hydrates enhanced further dissociation of CH_4 gas hydrates.

The research reported here has shed light into several aspects concerning the formation of mixed gas hydrates in bulk extending the existing knowledge about single gas hydrate systems. It also contributes to new insights about the formation of CO_2 hydrates in porous media for which few studies are available in the literature. However, a number of questions remain open, which provide an opportunity to look into possible future research, summarised in the following paragraphs.

A detailed thermodynamic study of gas hydrates was out of the scope of this study, mainly because the phase behaviour of binary systems is relatively well defined compared to the kinetics. However, thermodynamic data on ternary or multi-component gas hydrate forming systems are still lacking. The phase behaviour in complex porous media containing appreciable amounts of clay and silt is also far from being well understood. These aspects should be part of future studies.

This work mainly concerned macroscopic mechanism and many of the microscopic mechanisms have not been studied. A greater focus on microscopic or molecular gas hydrate behaviour is recommended for future studies. A possible approach to such studies could involve bulk or porous media hydrate experiments with binary and ternary systems aided by imaging techniques such as Nuclear Magnetic Resonance Imaging (NMRI) [44]. Use of this non-intrusive technique with high spatial and temporal resolution would help to further refine the kinetics of nucleation and crystal growth of gas hydrates. Through these studies knowledge about (relative) cage occupancy, formation rate, memory effect and hydrate exchange mechanism can be obtained.

Another future research direction is the molecular modelling of gas hydrates. It should be based on molecular, chemical and crystal reactions. This would allow modelling and simulation of the complete gas hydrate formation and dissociation process on the molecular level. The result of previously mentioned NMRI experiments can be used to validate the molecular model.

The present study focused mainly on the kinetics of gas hydrate formation. Further research could be extended to kinetics inhibition, the promotion of the dissociation of already formed gas hydrates etc. The knowledge about the kinetic inhibition and promotion can be used to control the formation and dissociation rate of gas hydrates. This will enable improvement of the application of gas hydrates in several fields, e.g. flow assurance, gas separation and gas transportation. Better understanding of the kinetics of gas hydrate formation and dissociation in porous media is critically needed and of significant importance in the exploration of natural gas hydrates. More research is also needed on the formation

CHAPTER 7. SUMMARY AND OUTLOOK

and dissociation of gas hydrates in porous media from multi-component systems containing more than one guest molecules. It is suggested to do new experiments using real reservoir rock or sand packs. Further more the influence of gas hydrate saturation on the permeability changes and the mechanic properties [96] are also important to validate reservoir models.

A

Appendix-Ternary System

The appendix is organised according the structure of the thesis. Appendix A gives the equations for calculation the number of moles and contribution factors in Chapter 4. Appendix B provides the supplementary information for studies in porous media (Chapter 5) and in Appendix C, the equations and correlations for numerical modelling and simulation (Chapter 6) are given. Finally, Appendix D displays the results of image analysis during gas hydrate formation and dissociation in small channels with the help of microscope.

A.1 Contribution Factor

The contribution factor is the number of moles of a specific gas incorporated into the gas hydrates over the total number of moles of gas, thus it varies between 0 and 1. For methane and CO_2 the contribution factor is expressed by Equation A.1 and A.2 respectively:

$$\alpha_{CH_4} = \frac{n_{CH_4}^H}{n_{tot}^H} \quad (A.1)$$

$$\alpha_{CO_2} = \frac{n_{CO_2}^H}{n_{tot}^H} \quad (A.2)$$

In which n_{tot}^H is the total number of moles of gas captured in gas hydrates at the end of the experiments. It is calculated by:

$$n_{tot}^H = n_{tot,ini}^V - n_{tot,end}^V - n_{tot,loss}^V \quad (A.3)$$

Where $n_{tot,ini}^V$ is the moles of gas initially present in the gas phase, $n_{tot,loss}^V$ is the

APPENDIX A. APPENDIX-TERNARY SYSTEM

moles of gas 'lost' due to sampling. Similarly, $n_{CH_4}^H$ and $n_{CO_2}^H$ are the number of moles of methane or CO_2 in the hydrate phase.

$$n_{CH_4}^H = n_{CH_4,ini}^V - n_{CH_4,end}^V - n_{CH_4,loss}^V \quad (A.4)$$

$$n_{CO_2}^H = n_{CO_2,ini}^V - n_{CO_2,end}^V - n_{CO_2,loss}^V \quad (A.5)$$

in which

$$n_{CH_4,ini}^V = x_{CH_4} n_{tot,ini}^V \quad (A.6)$$

$n_{tot,loss}^v$ is the amount of moles of CH_4 and CO_2 lost due to sampling.

$$n_{tot,loss}^V = \sum_{i=1}^k n_{i,loss}^V \quad (A.7)$$

$$n_{CH_4,loss}^V = \sum_{i=1}^k x_{CH_4,i} \cdot n_{i,loss}^V \quad (A.8)$$

$$n_{CO_2,loss}^V = \sum_{i=1}^k x_{CO_2,i} \cdot n_{i,loss}^V \quad (A.9)$$

$n_{tot,loss}^V$ were calculated using the Peng-Robinson EOS [102]. If the ideal gas law was used, at low pressure it gives less than 1% error respect the results calculated by Peng-Robinson EOS. However, at high pressures, it was recommended to used Peng-Robinson EOS.

$$P = \frac{RT}{V_m - b} - \frac{a(T)}{V_m(v + b) + b(V_m - b)} \quad (A.10)$$

$$a_i = 0.457235529 \frac{R^2 T_{c,i}^2}{P_{c,i}^2} \left[1 + m_i \left(1 - \sqrt{\frac{T}{T_{c,i}}} \right) \right]^2 \quad (A.11)$$

$$b_i = 0.0777960739 \frac{RT_{c,i}}{P_{c,i}} \quad (A.12)$$

were, V_m is the molar volume, $P_{c,i}$ and $T_{c,i}$ is the critical pressure and temperature for component i , a and b are coefficients in Peng-Robinson equation of state. In the mixtures, it is calculated by [136]:

A.1. CONTRIBUTION FACTOR

$$a = \sum_{i=1}^N \sum_{j=1}^N x_i x_j \sqrt{a_i a_j} (1 - k_{ij}(T)) \quad \text{A.13}$$

$$b = \sum_{i=1}^N x_i b_i \quad \text{A.14}$$

where, x_i are the mole fractions of component i and k_{ij} is the interaction parameter. The number of moles was finally calculated by:

$$n = \frac{V}{V_m} \quad \text{A.15}$$

For the calculation of the total number of moles in the gas phase at initial and at end conditions, the volume of gas phase needs to be estimated. The initial volume of the gas phase is determined by the difference of inner cell volume and the water volume. After gas hydrate formation the cell was completely filled with solid hydrates, no aqueous liquid phase was presented. The volume of the gas hydrates was larger than the volume of initial aqueous liquid phase. Assuming the expansion factor of 0.9, the volume of gas phase (V_{end}^V) at the end of hydrate formation will be $0.9V_{ini}^V$. Only for the experiment with an initial pressure of 2.5 MPa, liquid aqueous phase was still present at the end of the experiment. For this case, it was assume that $V_{end}^V = V_{ini}^V$. It should also be noted that at these low pressures where liquid aqueous phase present at end of experiments. Equation A.16 does not holds anymore. The mole of hydrate should be:

$$n_{tot}^H = n_{tot,ini}^V - n_{tot,end}^V - n_{tot,loss}^V - n_{di} \quad \text{A.16}$$

However, the solubility within the hydrate region is difficult to determine. Therefore, at 2.5 MPa, the contribution factor cannot be accurately calculated.

B

Appendix-Porous Media

B.1 Preparation of the synthetic glass beads core

The porous media core was made by uniform size glass beads. The choice of large and uniform glass-bead was made to obtain well defined properties of the core and to allow better visualisation of the gas hydrates by means of CT.

The glass beads were packed into a tube with an inner diameter of 6.0 *cm*, while shaking slightly the tube to ensure a uniform packing. At each end of the tube rubber caps were attached so that the grains could be compacted by applying a confining pressure (Figure B.1).

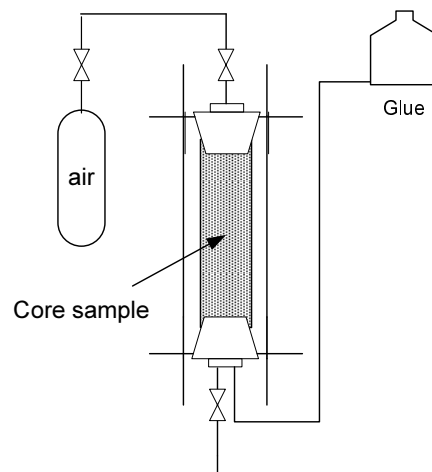


Figure B.1: Schematic drawing explaining the preparation of the glass-beads core

Glue was pumped slowly into the tube containing the glass beads through the

bottom of the tube to create a consolidated glass bead pack. After the tube was filled completely with glue, it was drained by gravity. Finally, air was flushed through the tube for 3 days to dry the glue completely. About 2.0 cm of the lower part of the core with a higher glue content was cut off.

B.2 Error Analysis on X-ray CT Images

In this appendix the error analysis of the X-Ray CT scan is discussed. In general, the intensity of a pure substance should be a constant under any condition. Therefore, the perspex tube which contains the glass beads is used as a reference material. The intensities of this tube at same location of the tube should be same. These values are used to correct for variations in the intensity.

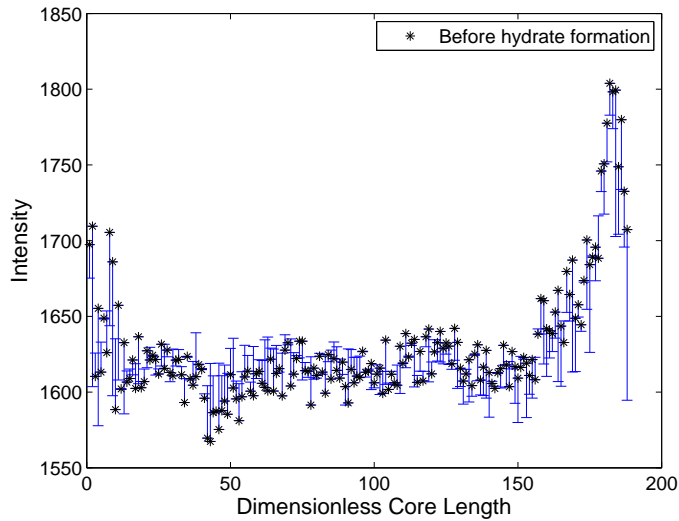


Figure B.2: Error of CT images analysed by intensity values at the various cross-sections along the core. The error is determined by comparing a reference material from duplicated scans under the same conditions before hydrate formation.

Figure B.2 shows the variation in the intensity for each cross-section slice along the core. This figure shows the difference in intensity between duplicate scans over the core length before hydrate formation. Figure B.3 shows the difference in intensity between duplicate scans after hydrate formation. Analysis of the data shows that the offset between two scans taken at the same condition before hydrate formation is ± 10 HU and for images taken after hydrate formation, the offset is ± 13 HU. Comparing the intensity of the reference material for the two scans before and after hydrate formation, an difference of ± 17 HU is

B.2. ERROR ANALYSIS ON X-RAY CT IMAGES

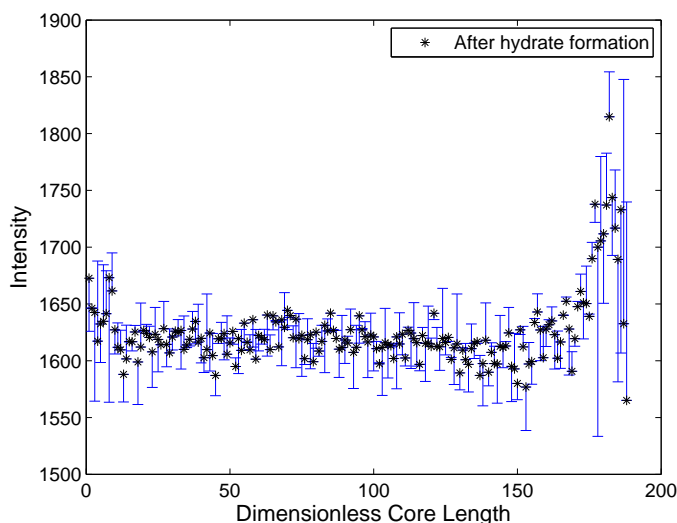


Figure B.3: Error of CT images analysed by intensity values at the various cross-sections along the core. The error is determined by comparing a reference material from duplicated scans under the same conditions after hydrate formation.

obtained. The stainless connections at both ends of the core holder induce a strong fluctuations of the intensity.

A statistical analysis was performed to investigate the intensity changes caused by gas hydrates. The intensity values were classified into 22 categories over a total range from 0 to 4000 HU . The frequencies of each of this intensity category were determined and plotted in Figure B.4.

From this plot it can be concluded that frequency of small intensities decreases after hydrate have been formed. Low intensity values are typical for gases. This suggests that the gas phase present in the core was used for hydrate formation. The frequency of the intensity category in the range between 1900 and 2000 HU increases after the formation of hydrates. It is the intensity range expected for gas hydrates. This indicates that gas hydrates have been formed in the porous media.

From the reconstructed images, the resolution is around $300 \mu m$ ($0.3 mm$). Although, the CT-images can provide information by comparing the difference of intensity and by statistical analysis of the determined value, it is still difficult to pin point distinct intensity values typical for gas hydrates. Consequently, the CT-images cannot be used (yet) as an accurate method to estimate the hydrate saturation in the core.

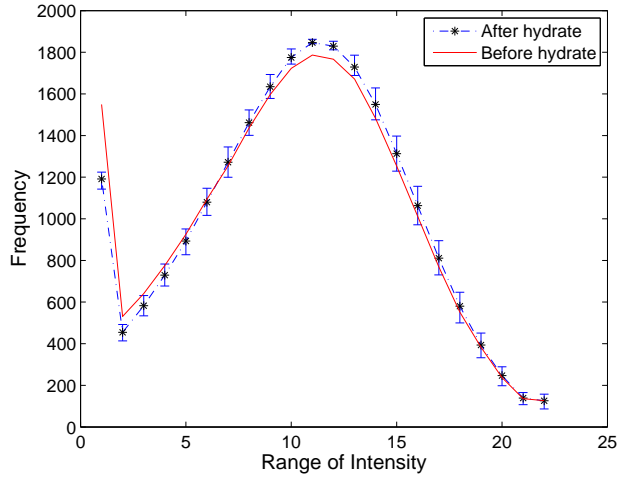


Figure B.4: Frequency of different intensity categories before and after hydrate formation. Intensity is classified into 22 categories with 1=smaller than 1000 HU , 22=larger than 3000 HU . For categories from 2-21, each category covers an intensity range of 100 HU .

B.3 Temperature Influence on Gas Hydrate Formation in Porous Media

In order to investigate how the temperature influences the gas hydrate formation in porous medium, the temperatures were varied. To avoid ice formation and CO_2 liquefaction while in the mean time maintaining the system within the phase boundary of $H - L_w - V$ equilibrium line, the temperature can only be monitored within a small range. With 1 K temperature variation, the differences in formation rate are small.

The experiments were performed at 274.15, 275.15 and 275.65 K. The initial pressure for all experiments were 3.0 MPa and the gas injection rate were 450 ml/min . Figure B.5 shows the pressure and Figure B.6 the formation rate as a function of time for gas hydrate formation at different temperatures.

The equilibrium pressure was 1.31, 1.51 and 1.63 MPa for temperature 274.15 K, 275.15 K and 275.65 K respectively. The equilibrium pressure decreased with the decrease of the temperature as expected (see the phase diagram Figure 4.1). Since the equilibrium pressure is higher at a high temperature, the time for the system to reach equilibrium is shorter. The equilibration time was found to be decreasing linearly with the temperature (as shown in the subplot in Figure B.5).

B.3. TEMPERATURE INFLUENCE ON GAS HYDRATE FORMATION IN POROUS MEDIA

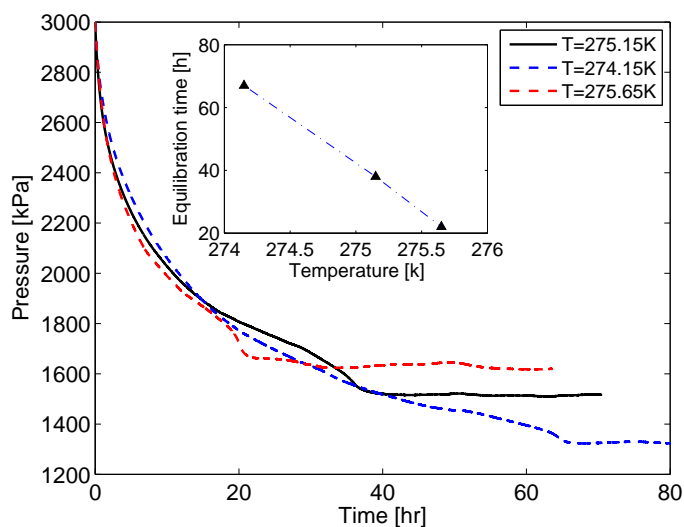


Figure B.5: Pressure decay curve for CO_2 gas hydrate formation experiments in glass bead core. Injection rates were 450 ml/min , initial pressure for all experiments were 3.0 MPa . The temperature were 274.15 K , 275.15 K and 275.65 K .

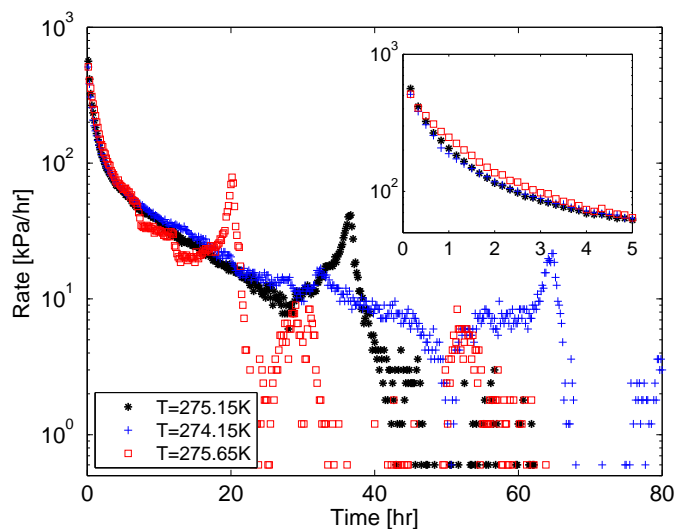
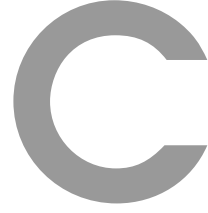


Figure B.6: Gas hydrate formation curve for CO_2 gas hydrate formation experiments in glass bead core. Injection rates were 450 ml/min , initial pressures were 3.0 MPa . The temperature were 274.15 K , 275.15 K and 275.65 K .

APPENDIX B. APPENDIX-POROUS MEDIA

As it can be seen in Figure B.6 the formation rates for the three temperatures conditions have no obvious difference in the reaction limited process. This means that the initial mass transfer of CO_2 into the other phases does not differ significantly. In the diffusion limited regime, the formation rate for $T = 275.15K$ is slightly lower than the formation rate at $T = 274.15K$, while the rate at $T = 275.65K$ is the lowest. This indicates that gas hydrate formation rate is reduced by increasing temperature. This finding is in coincidence with Barrer et al. [9, 8] who investigated gas hydrate formation from ice partials.



Appendix-Simulations

C.1 Kinetics Equation

The modelling and simulation of the gas hydrate formation are based on the Kim-Bishnoi model [63]. The gas hydrate dissociation can be write as:

$$\frac{dc_h}{dt} = k_d A_s (P_e - P_g) \quad \text{C.1}$$

where, dc_h/dt is the rate of dissociation, k_d is dissociation rate constant, A_s is the surface area, P_e is the $H - L_w - V$ equilibrium pressure and P_g is the gas pressure in gas phase.

The term k_d has an Arrhenius-type temperature dependency [63] and can be described as:

$$k_d = k_d^o e^{-\frac{E}{RT}} \quad \text{C.2}$$

where, k_d^o is the intrinsic decomposition rate constant, E is activation energy and R is the gas constant.

The hydrate surface per volume hydrate exposed to liquid phase for dissociation is described by Equation C.3 and the surface for formation is described by C.4

$$A_s = \phi_e^2 S_h S_w A_{si} \quad \text{C.3}$$

$$A_s = \phi_e S_w A_{si} + \phi_e^2 S_h S_w A_{si} \quad \text{C.4}$$

APPENDIX C. APPENDIX-SIMULATIONS

where, A_{si} is the surface area per unit volume of gas hydrates, S_w and S_h is the saturation for water and gas hydrates respectively, ϕ_e is effective porosity.

For hydrate dissociation, combining Equations C.1, C.3 and C.4 yields Equation C.5, which can be written as Equation C.6.

$$\frac{dc_h}{dt} = k_d^0 \phi_e^2 S_H S_w A_{si} e^{-\frac{E}{RT}} (P_e - P_g) \quad \text{(C.5)}$$

$$\frac{dc_h}{dt} = \frac{k_d^0 A_{si}}{\rho_h \rho_w} e^{-\frac{E}{RT}} (\phi_e S_h \rho_h) (\phi_e S_w \rho_w) (P_e - P_g) \quad \text{(C.6)}$$

where, ρ_w and ρ_h is the density of water and gas hydrates respectively. For hydrate formation can be written as Equation C.7.

$$\frac{dc_h}{dt} = \frac{k_f^0 A_{si}}{\rho_h \rho_w} e^{-\frac{E}{RT}} (\phi_e S_w \rho_w) (P_e - P_g) + \frac{k_f^0 A_{si}}{\rho_h \rho_w} e^{-\frac{E}{RT}} (\phi_e S_h \rho_h) (\phi_e S_w \rho_w) (P_e - P_g) \quad \text{(C.7)}$$

Based on Raoult's Law it can be derived that:

$$p_e x_i = y_i p \quad \text{(C.8)}$$

where x_i and y_i is the mole fraction of component i in gas phase and liquid phase respectively. And define the ratio $y_i/x_i = K$. The K value can be obtained from laboratory three phase equilibrium data (p_e). By substituting K the Equation C.8, Equation C.6 and C.7 can be rewrite as:

$$\frac{dc_h}{dt} = \frac{k_d^0 A_{si}}{\rho_h \rho_w} e^{-\frac{E}{RT}} (\phi_e S_h \rho_h) (\phi_e S_w \rho_w) \left(\frac{y_i}{x_i} p\right) \left(1 - \frac{1}{K}\right) \quad \text{(C.9)}$$

and

$$\frac{dc_h}{dt} = \frac{k_f^0 A_{si}}{\rho_h \rho_w} e^{-\frac{E}{RT}} (\phi_e S_w \rho_w) \left(\frac{y_i}{x_i} p\right) \left(\frac{1}{K} - 1\right) + \frac{k_f^0 A_{si}}{\rho_h \rho_w} e^{-\frac{E}{RT}} p_e (\phi_e S_h \rho_h) (\phi_e S_w \rho_w) \left(\frac{y_i}{x_i} p\right) \left(\frac{1}{K} - 1\right) \quad \text{(C.10)}$$

The x_i represents the mole fraction of the gas in the liquid phase. Assuming $x_i = 1$. Equation can be simplified:

$$\frac{dc_h}{dt} = \frac{k_d^0 A_{si}}{\rho_h \rho_w} e^{-\frac{E}{RT}} (\phi_e S_h \rho_h) (\phi_e S_w \rho_w) (y_i p) \left(1 - \frac{1}{K}\right) \quad \text{(C.11)}$$

and

$$\frac{dc_h}{dt} = \frac{k_f^0 A_{si}}{\rho_h \rho_w} e^{-\frac{E}{RT}} (\phi_e S_w \rho_w)(y_i p) \left(\frac{1}{K} - 1\right) + \frac{k_f^0 A_{si}}{\rho_h \rho_w} e^{-\frac{E}{RT}} p_e (\phi_e S_h \rho_h) (\phi_e S_w \rho_w)(y_i p) \left(\frac{1}{K} - 1\right) \quad \text{(C.12)}$$

The kinetic rate constant is defined as:

$$\begin{aligned} \frac{k_d^0 A_{si}}{\rho_h \rho_w} &= r_{rk1} \\ \frac{k_f^0 A_{si}}{\rho_w} &= r_{rk2} \\ \frac{k_f^0 A_{si}}{\rho_w \rho_h} &= r_{rk3} \end{aligned} \quad \text{(C.13)}$$

substituting this kinetic constant into Equation C.11 and C.12 yields:

$$\frac{dc_h}{dt} = r_{rk1} e^{-\frac{E}{RT}} (\phi_e S_h \rho_h) (\phi_e S_w \rho_w)(y_i p) \left(1 - \frac{1}{K}\right) \quad \text{(C.14)}$$

and

$$\frac{dc_h}{dt} = r_{rk2} e^{-\frac{E}{RT}} (\phi_e S_w \rho_w)(y_i p) \left(\frac{1}{K} - 1\right) + r_{rk3} e^{-\frac{E}{RT}} p_e (\phi_e S_h \rho_h) (\phi_e S_w \rho_w)(y_i p) \left(\frac{1}{K} - 1\right) \quad \text{(C.15)}$$

C.2 Correlations

C.2.1 Viscosity

The viscosity of the gas and liquid phases are described by correlations. The simulator does not have suitable correlations for CO_2 and CH_4 . Since the temperature range used in the simulations is relatively small; from 274.5 K to 291 K, thus constant values for the gas viscosity are assumed. Since no suitable correlation could be found. The liquid viscosity is calculated using Equation C.16 with values from Table C.1.

$$\mu(cp) = A_{visc} EXP(B_{visc}/T) \quad \text{(C.16)}$$

APPENDIX C. APPENDIX-SIMULATIONS

	H_2O	CO_2	CH_4
Viscosity $\mu(cp)$	0.00848	0.0147	0.0120
A_{visc}	0.0047352	0.000757	
B_{visc}	1515.7	1331.1	

Table C.1: Gas and liquid viscosity parameters

C.2.2 Heat Capacity

A constant value of $1600 J/(m^3.K)$ for the heat capacity of the hydrate phase is used. For the description of the heat release upon the phase transition from the vapour phase to the liquid phase, the vaporisation enthalpies at 298 K for water ($44.6 KJ/mole$) and for CO_2 ($5712 J/mole$) are used. The vaporisation enthalpies are a not constant, but are a function of the heat capacity of the gas and liquid.

The heat capacity of a component can be described by Eq. C.17 and parameters are listed in Table C.2.

$$C_p(T) = C_1 + C_2T + C_3T^2 + C_4T^3 \quad (C.17)$$

Phase	Constant	H_2O	CO_2	CH_4
Gas	C_1	32.2	29.3	19.3
	C_2	1.92×10^{-3}	-2.24×10^{-2}	5.21×10^{-2}
	C_3	1.06×10^{-5}	2.65×10^{-4}	1.20×10^{-5}
	C_4	-3.60×10^{-9}	-4.15×10^{-7}	-1.13×10^{-8}
Liquid	C_1	50.81069	-3553.844	-
	C_2	0.2129361	46.88128	-
	C_3	-6.31×10^{-4}	-0.201722	-
	C_4	6.48×10^{-7}	2.90×10^{-4}	-

Table C.2: Parameter and values for the calculation of heat capacity

C.2.3 Relative Permeability

To describe the multi-phase flow in the porous media, the relative permeability to the different phases with respect to the other phases needs to be defined. In this simulation the empirical relations in Equations C.18 - C.21 were used [1].

$$k_{rw} = k_{rw,iro} \cdot \left(\frac{S_w - S_{w,crit}}{1 - S_{w,crit} - S_{o,ir}} \right)^n \quad (C.18)$$

$$k_{ro,w} = k_{ro,cw} \cdot \left(\frac{S_o - S_{o,r}}{1 - S_{w,con} - S_{o,r}} \right)^n \quad \text{C.19}$$

$$k_{rog} = k_{rog,cg} \cdot \left(\frac{S_l - S_{o,r} - S_{w,con}}{1 - S_{g,con} - S_{o,r} - S_{w,con}} \right)^n \quad \text{C.20}$$

$$k_{rg} = k_{rg,cl} \cdot \left(\frac{S_g - S_{g,con}}{1 - S_{g,con} - S_{o,ir} - S_{w,con}} \right)^n \quad \text{C.21}$$

In Table C.3, the input parameters for the calculation of the relative permeability curves in Equation C.18 - C.21 were given.

Property	Value
Connate Water Saturation	0.20
Critical Water Saturation	0.20
Irreducible Oil Saturation	0.05
Residual Oil Saturation	0.05
Connate Gas Saturation	0.05
$k_{r,o}$ at Connate Water Saturation	0.80
$k_{r,w}$ at Irreducible Oil Saturation	0.80
$k_{r,g}$ at Connate Liquid Saturation	1.00
$k_{r,l}$ at Connate Gas Saturation	0.80
Exponent n	3.00

Table C.3: Parameter used for the computation of relative permeability

D

Appendix-Micro Cell

D.1 Microcell Experiments

In this work, a preliminary study on visualise CO_2 hydrate formation in small channels (which mimic the porous media) is been carried out. Images are taken using a microscope. This will also be the main future study direction.

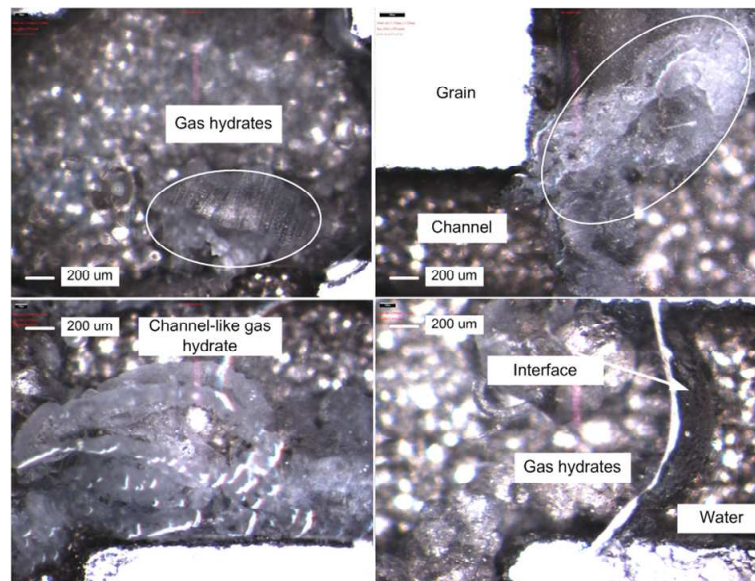


Figure D.1: Detailed view of formed CO_2 hydrates. Gas hydrates can have various appearances and location are random.

APPENDIX D. APPENDIX-MICRO CELL

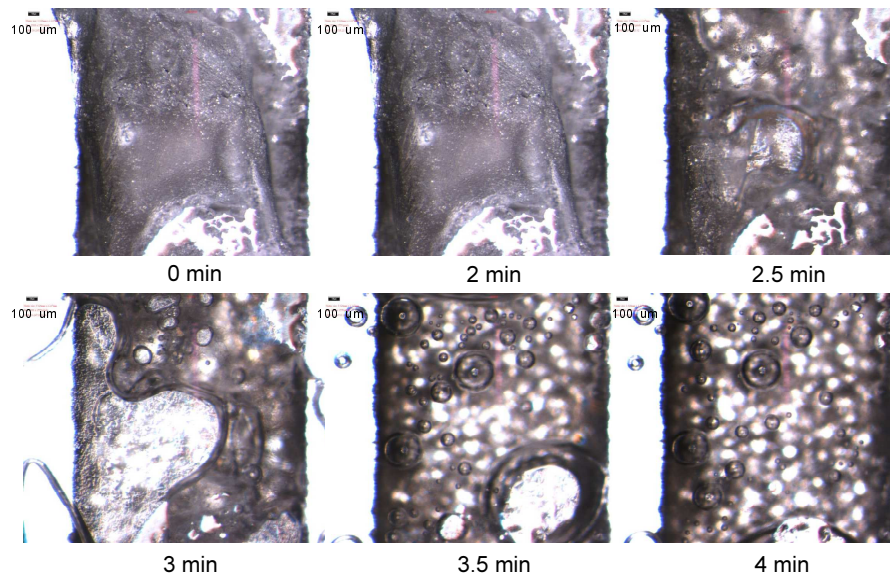


Figure D.2: Dissociation process of CO_2 hydrates in the channels. For the first two minute, no bubbles are seen. Afterwards, the dissociation is quite fast and finishes within one minute.

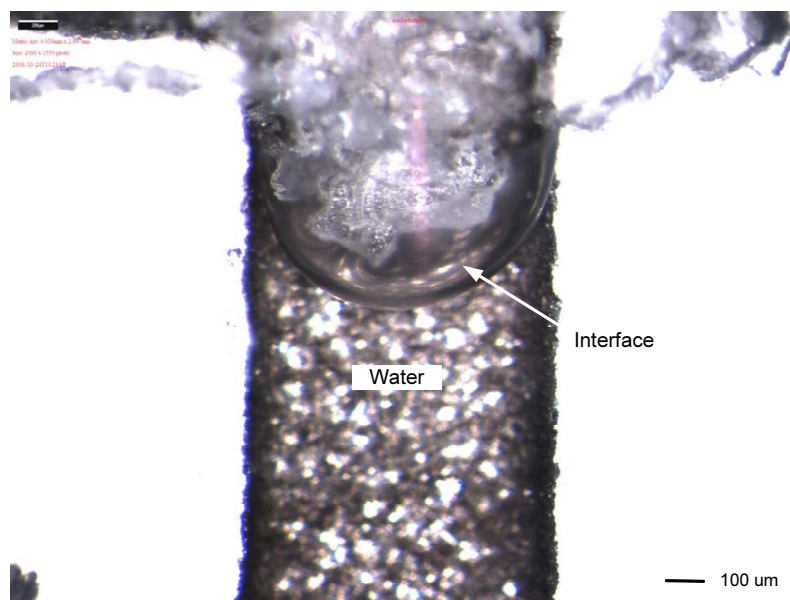


Figure D.3: The interface between aqueous phase and gas phase. Gas hydrates starts to form in the gas phase near the interface.

D.1. MICROCELL EXPERIMENTS

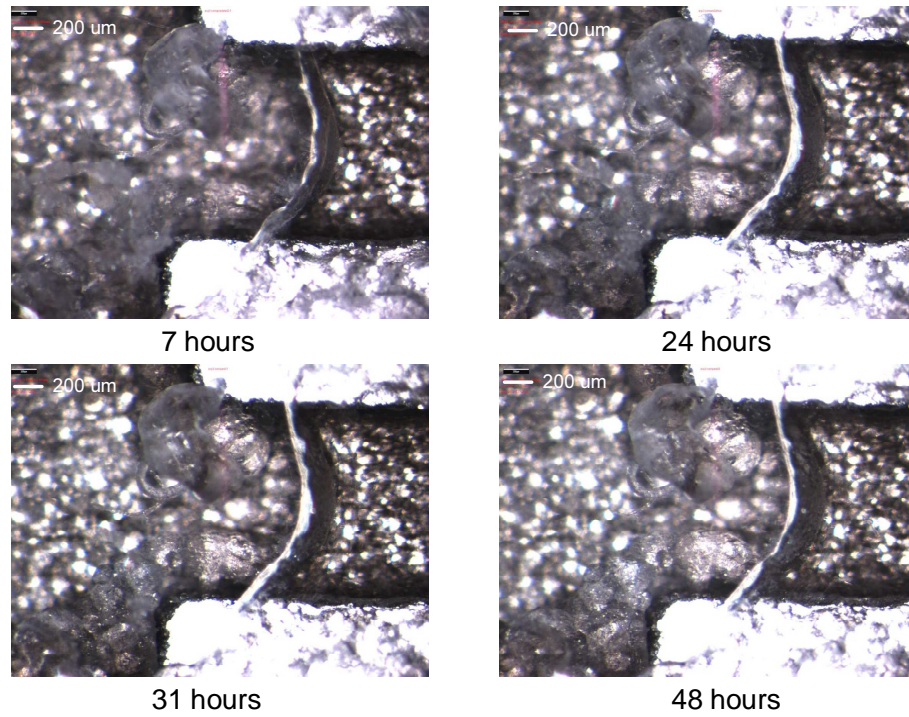


Figure D.4: Gas hydrate formation on a interface. The thickness of the hydrate layer grow with time.

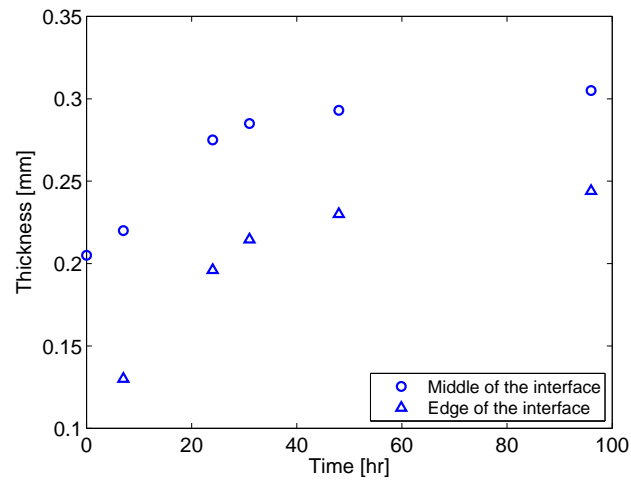


Figure D.5: Thickness gas hydrate layer as a function of time. Data is gained by determined thickness of layer by image analysis based on Figure D.4.

Nomenclature

General

a	interaction parameter, PR EOS [-]
A_p	Surface of the particles [m^2]
A_s	Surface area per unit volume [m^2/m^3]
A_{si}	Surface area per unit volume of the hydrate [m^2/m^3]
b	covolume PR EOS [-]
C_{ij}	Langmiur constant [$1/Pa$]
D_{in} :	Diameter of porous core [m]
E :	X-ray photon energy [keV]
E_a	Activation energy [$kJ/gmol$]
f	Fugacity [Pa]
f_{eq}	Fugacity at equilibrium [Pa]
g	Gibbs energy [$kcal/mol$]
h_f	Heat of formation [kJ/kg]
k	Permeability [m^2]
k	Combined rate parameter [$mol/m^2.Pa.s$]
k_B	Boltzmann constant [J/k]
K_d	Dissociation rate constant [$mol/(m^2.Pa.s)$]
K_f	Formation rate constant [$mol/(m^2.Pa.s)$]
k_{ij}	binary interaction parameter [-]
L :	Length of the core [m]
L_s :	Slice thickness of CT scan [m]
m	shape factor [-]
$m_{w,o}$:	Mass of outflow water [kg]
$m_{w,i}$:	Mass of inflow water [kg]
n :	Number of moles [$mole$]

APPENDIX D. APPENDIX-MICRO CELL

P_{ini}	Initial pressure [MPa]
P_{eq}	Equilibrium pressure [MPa]
$P_{1/2}$	Half-decay pressure [MPa]
P_c	critical pressure [Pa]
q	hydration number [-]
Q	Flow Rate [ml/s]
R	Gas constant [J/K · mol]
S_w	Water saturation [-]
S_h	Gas hydrate saturation [-]
S_g	Gas saturation [-]
$t_{s,1/2}$	Scaled half-decay time [s]
$t_{1/2}$	Half-decay time [s]
t_{tr}	Time to reach steady-state nucleation [s]
t_n	Time for the actual nucleation [s]
t_g	Time for crystals to detectable sizes [s]
T	Temperature [K]
T_c	critical temperature [K]
V	volume [m^3]
V_p	Volume of Porous Space [m^3]
v_j	Ration of cavities [-]
V_m	molar volume [m^3/mol]
$w(r)$	Potential energy [J]
x	mole fractions in gas phase [-]
y_i	mole fractions in liquid phase [-]
Z	Atomic Number [-]

Greek

ϑ_{ij}	Fraction of cavity j occupied by gas i [-]
γ	Order of reaction with respect of pressure [-]

μ	Chemical potential [J/mol]
α	contribution factor [-]
ϕ	Porosity [-]
ρ	Density [kg/m^3]
$\mu :$	Viscosity of Fluid [$pa \cdot s$]
$\alpha :$	Attenuation Coefficient [-]

Phases

$H :$	Hydrate
$L :$	Liquid
$I :$	Ice
$V :$	Gas
$Q :$	Quadruple point

Bibliography

- [1] Advanced process and thermal reservoir simulator. In *CMG STARS manual*. Computer Modelling Group Ltd. Calgary, Canada, 2008.
- [2] R. Anderson, M. Llamedo, B. Tohidi, and R.W. Burgass. Characteristics of clathrate hydrate equilibria in mesopores and interpretation of experimental data. *Journal of Physical Chemistry B*, 107(15):3500–3506, 2003.
- [3] R. Anderson, M. Llamedo, B. Tohidi, and R.W. Burgass. Characteristics of clathrate hydrate equilibria in mesopores and interpretation of experimental data. *Journal of Physical Chemistry B*, 107(15):3507–3514, 2003.
- [4] R. Anderson, H. Mozaffar, and B. Tohidi. Development of a crystal growth inhibition based method for the evaluation of kinetic hydrate inhibitors. In *The 7th International Gas Hydrate Conference, Edinburgh*, 2011.
- [5] I. Aya, K. Yamane, and H. Nariai. Solubility of co2 and density of co2 hydrate at 30 mpa. *Energy*, 22(2-3):263 – 271, 1997.
- [6] B.A. Baldwin, J. Stevens, J. Howard, A. Graue, B. Kvamme, E. Aspenes, G. Erslund, J. Husebø, and D. Zornes. Using magnetic resonance imaging to monitor ch4 hydrate formation and spontaneous conversion of ch4 hydrate to co2 hydrate in porous media. *Magnetic Resonance Imaging*, 27:720–726, 2009.
- [7] L. Ballard and E.D. Sloan. The next generation of hydrate prediction. *Fluid Phase Equilibrium*, 216:257–270, 2003.
- [8] R.M. Barrer and D.J. Ruzicka. Non-stoichiometric clathrate compounds of water. part 4.kinetics of formation of clathrate phases. *Transactions of the Faraday Society*, 58:2262–2271, 1962.
- [9] R.M. Barrer and W.I. Stuart. Proceedings of the royal society. 1958.
- [10] A. Beer. Determination of the absorption of red light in coloured liquids. *Annalen der Physik und Chemie*, 86:78–88, 1852.
- [11] M.E. Benesh. Patent no. 2270016. 1942.
- [12] D. Berner. The marine transportation of natural gas in hydrate form. In *Second International Offshore and Polar Engineering Conference*, 1992.
- [13] P.R. Bishnoi, A.K. Gupta, P. Englezos, and N. Kaloferakis. *Fluid Phase Equilibrium*, 53(97), 1989.
- [14] P.G. Brewer, F.M. Orr, G. Friederich, K.A. Kvenvolden, and D.L. Orange. Gas hydrate formation in the deep sea: in situ experiments with controlled release of methane natural gas and carbon dioxide. *Energy and Fuels*, 12:183, 1998.
- [15] B.A. Buffett and O.Y. Zatsepina. Formation of gas hydrate from dissolved gas in natural porous media. *Marine Geology*, 164:69–77, 2000.

BIBLIOGRAPHY

- [16] P.C. Carman. *Flow of Gases Through Porous Media*. Academic Press, new york edition, 1956.
- [17] G.J. Chen and T.M. Guo. Thermodynamic modelling of hydrate formation based on new concepts. *Fluid Phase Equilibrium*, 122:43, 1996.
- [18] G.J. Chen and T.M. Guo. A new approach to gas hydrate modelling. *Chemical Engineering Journal*, 71:145, 1998.
- [19] M. Clarke and P.R. Bishnoi. Determination of the intrinsic kinetics of co₂ gas hydrate formation using in situ particle size analysis. *Chemical Engineering Science*, 60:695–709, 2005.
- [20] M.A. Clarke and P.R. Bishnoi. Determination of the activation energy and intrinsic rate constant of methane gas hydrate decomposition. *The Canadian Journal of Chemical Engineering*, 79(1):143–147, 2001.
- [21] M.A. Clarke and P.R. Bishnoi. Determination of the intrinsic rate constant and activation energy of co₂ gas hydrate decomposition using in-situ particle size analysis. *Chemical Engineering Science*, 59(14):2983–2993, 2004.
- [22] W.F. Claussen. *Journal of Chemical Physics*, 19:662, 1951.
- [23] W.F. Claussen. *Journal of Chemical Physics*, 19:1425, 1951.
- [24] W.F. Claussen and M.F. Polgase. *Journal of the American Chemical Society*, 74:4817, 1952.
- [25] M.B. Clennel, M. Hovland, J.S. Booth, P. Henry, and W.J. Winters. Formation of natural gas hydrates in marine sediments 1. conceptual model of gas hydrate growth conditioned by host sediment properties. *Journal of Geophysical Research*, 104(B10):22985–22003, 1999.
- [26] N. Daraboina, J. Ripmeester, V.K. Walker, and P. Englezos. Multi-scale assessment of the performance of kinetic hydrate inhibitors. In *The 7th International Gas Hydrate Conference, Edinburgh*, 2011.
- [27] W.M. Deaton and E.M. Frost Jr. *Gas hydrates and their relation to the operation of natural-gas pipe lines*. U.S. Bureau of Mines Monograph, 1946.
- [28] J.H. Van der Waals and J.C. Platteeuw. Clathrate solutions. *Advances in Chemical Physics*, 2(1):1–57, 1959.
- [29] P.D. Dholabhai, N. Kalogerakis, and P.R. Bishnoi. *SPE Production and Facilities*, 185, 1993.
- [30] P.D. Dholabhai, N. Kalogerakis, and P.R. Bishnoi. *Canadian Journal of Chemical Engineering*, 71:68, 1993.
- [31] Z. Duan and R. Sun. A model to predict phase equilibrium of ch₄ and co₂ clathrate hydrate in aqueous electrolyte solutions. *American Mineralogist*, 91(8-9):1346–1354, 2006.

-
- [32] J. Dvorkin, M.B. Helgerud, W.F. Waite, S.H. Kirby, and A. Nur. Introduction to physical properties and elasticity models. In *In M.D. Max ED. Natural Gas Hydrate in Oceanic and Permafrost Environments*, pages 245–260, 2000.
- [33] P. Englezos. Nucleation and growth of gas hydrate crystals in relation to kinetic inhibition. *Revue de l'institut Francis du Petrole*, 51(6):789–795, 1996.
- [34] P. Englezos, N. Kalogerakis, P.D. Dholabhai, and P.R. Bishnoi. Kinetics of formation of methane and ethane gas hydrates. *Chemical Engineering Science*, 42(11):2647–2658, 1987.
- [35] P. Englezos, N. Kalogerakis, P.D. Dholabhai, and P.R. Bishnoi. Kinetics of gas hydrate formation from mixtures of methane and ethane. *Chemical Engineering Science*, 42(11):2659–2666, 1987.
- [36] G. Ersland, J. Husebø, A. Graue, B.A. Baldwin, J. Howard, and J. Stevens. Measuring gas hydrate formation and exchange with co₂ in bentheim sandstone using mri tomography. *Chemical Engineering Journal*, 158:25–31, 2010.
- [37] G. Ersland, J. Husebø, A. Graue, and B. Kvamme. Transport and storage of co₂ in natural gas hydrate reservoirs. *Energy Procedia*, 1:3477–3484, 2009.
- [38] M. Faraday and H. Davy. On fluid chlorine. *Philosophical Transactions of the Royal Society of London*, 113:160–165, 1823.
- [39] G. Genov, W.F. Kuhs, D.K. Staykova, E. Goreschnik, and A.N. Slamatin. Experimental studies on the formation of porous gas hydrates. *American Mineralogist*, 89:1228–1239, 2004.
- [40] J.W. Gibbs. *The Collected Works of J. Willard Gibbs. Vol I, Thermodynamics*. Yale University Press, New Haven, Connecticut, 1928.
- [41] G.D. Ginsburg and V.A. Soloviev. Submarine gas hydrate estimation: theoretical and empirical approaches. In *Proceedings of Offshore Technology Conference*. Houston, TX, vol. 1 513-518, 1995.
- [42] M. Golombok, E. Ineke, J.C.R. Luzardo, Y. He, and P. Zitha. Resolving co₂ and methane hydrate formation kinetics. *Environmental Chemistry Letters*, 7(4):325–330, 2009.
- [43] J. Gopalakrishnan. *New Directions in Solid State Chemistry*. Cambridge University Press, 1997.
- [44] A. Graue, B. Kvamme, B.A. Baldwin, J. Stevens, J. Howard, E. Aspenes, G. Ersland, J. Husebø, and D. Zornes. Mri visualisation of spontaneous methane production from hydrates in sandstone core plugs when exposed to co₂. *SPE Journal*, 13(2):146–152, 2008.
- [45] J.-S. Gudmundsson and A. Borrehaug. Frozen hydrate for transportation of natural gas. In *2nd International Conference of Natural Gas Hydrates*, pages 415–422. Toulouse, France, 1996.
-

BIBLIOGRAPHY

- [46] J.-S. Gudmundsson and M Parlaktuna. Storage of natural gas at refrigerated conditions. In *AICHE Spring National Meeting*, 1992.
- [47] E.G. Hammerschmidt. Formation of gas hydrates in natural gas transmission lines. *Industry Engineering Chemistry*, 26(8):851–855, 1934.
- [48] Y.P. Handa and D. Stupin. Thermodynamic properties and dissociation characteristics of methane and propane hydrates in 70 radius silica gel pores. *Journal of Physical Chemistry*, 96(21):8599–8963, 1992.
- [49] S. Hashemi, A. Macchi, S. Bergeron, and P. Servio. Prediction of methane and carbon dioxide solubility in water in the presence of hydrate. *Fluid Phase Equilibria*, 246:131–136, 2006.
- [50] Y. He, E.S.J. Rudolph, P.L.J. Zitha, and M. Golombok. Kinetics of co2 and methane hydrate formation: An experimental analysis in the bulk phase. *Fuel*, 90:272–279, 2011.
- [51] R.W. Henning, A.J. Schultz, V. Thieu, and Y. Halpern. Neutron diffraction studies of co2 clathrate hydrate: Formation from deuterated ice. *Journal of Physical Chemistry A*, 104:5066–5071, 2000.
- [52] K.C. Hester, S.N. White, E.T. Peltzer, P.G. Brewer, and E.D. Sloan. Raman spectroscopic measurement of synthetic gas hydrates in the ocean. *Marine Chemistry*, 98:304, 2006.
- [53] G.D. Holder and G.C. Grigoriou. *Journal of Chemical Thermodynamics*, 12:1093, 1980.
- [54] G.D. Holder and J.H. Hand. *AICHE Journal*, 28:440–447, 1982.
- [55] M. Holland, P. Schultheiss, J. Roberts, and M. Druce. Observed gas hydrate morphologies in marine sediments. In *Proceedings of the 6th international Conference on Gas Hydrates (ICGH 2008)*, 2008.
- [56] R.H. Jacoby. Vapor-liquid equilibrium data for use of methanol in preventing gas hydrate. In *Gas Hydrocarbon Control conference, University of Oklahoma, Norman*, 1953.
- [57] G.A. Jeffrey. Hydrate inclusion compounds. *Journal of Inclusion Phenomena and Macrocyclic Chemistry*, 1(3):211–222, 1984.
- [58] E.D. Sloan. Jr. *Clathrate Hydrates of Natural Gases*. Marcel Dekker, first edition, 1990.
- [59] E.D. Sloan. Jr. *Clathrate Hydrates of Natural Gases*. Marcel Dekker, second edition, 1998.
- [60] S. Kang, Y. Seo, and W. Jang. Kinetics of methane and carbon dioxide hydrate formation in silica gel pores. *Energy Fuels*, 23(7):3711–3715, 2009.
- [61] D.L. Katz and R.L. Lee. Gas hydrate and their prevention. In *Natural Gas Engineering Production and Storage, Chapter 5, McGraw-Hill, New York*, 1990.

-
- [62] T. Kawamura, T. Komai, Y. Yamamoto, K. Nagashima, K. Ohga, and K. Higuchi. Growth kinetics of co₂ hydrate just below melting point of ice. *Journal of Crystal Growth*, 234:220, 2002.
- [63] H.C. Kim, P.R. Bishnoi, R.A. Heidemann, and S.S.H. Rizvi. Kinetics of methane hydrate decomposition. *Chemical Engineering Science*, 42(7):1645–1653, 1987.
- [64] R.A. Kini, S.F. Dec, and E.D. Sloan. Methane + propane structure ii hydrate formation kinetics. *Journal of Physical Chemistry A*, 108:9550–9556, 2004.
- [65] W.G. Knox, M. Hess, G.E. Jones, and H.B. Smith. The hydrate process. *Chemistry Engineering Progress*, 57(2):66–71, 1961.
- [66] C.A. Koh. Toward a fundamental understanding of natural gas hydrates. *Chemical Society Reviews*, 31:157–167, 2002.
- [67] C.A. Koh, C.C. Savidge, and C.C. Tang. *Journal of Physical Chemistry*, 100:6412, 1996.
- [68] C.A. Koh, R.E. Westacott, W. Zhang, K. Hirachand, J.L. Creek, and A.K. Soper. Mechanisms of gas hydrate formation and inhibition. *Fluid Phase Equilibrium*, 194-197:134–151, 2002.
- [69] B. Kvamme and H. Tanaka. Thermodynamic stability of hydrates for ethane, ethylene and carbon dioxide. *Journal of Physical Chemistry*, 99(18):7114–7119, 2002.
- [70] K.A. Kvenvolden. Methane hydrates - a major reservoir of carbon in the shallow geosphere. *Chemical Geology*, 71:41–51, 1988.
- [71] S.D. Larson. *Ph.D. Thesis*. University Michigan, 1955.
- [72] J.D. Lee, R. Susilo, and P. Englezos. Kinetics of structure h gas hydrate. *Energy and Fuels*, 19:1008–1015, 2005.
- [73] Y. Makogon. *Hydrates of Hydrocarbons*. PennWell, Oklahoma, 1997.
- [74] Y.F. Makogon. Hydrate formation in the gas-bearing beds under permafrost conditions. *Gazovaya Promyshlennost*, (5):14–15, 1965.
- [75] M.B. Malegaonkar, P.D. Dholabhai, and P.R. Bishnoi. Kinetics of carbon dioxide and methane hydrate formation. *The Canadian Journal of Chemical Engineering*, 75(6):1090–1099, 1997.
- [76] S. Marinhas, A. Delahaye, L. Fournaison, D. Dalmazzone, W. Fürst, and J-P. Petitet. Modelling of the available latent heat of a co₂ hydrate slurry in an experimental loop applied to secondary refrigeration. *Chemical Engineering and Processing*, 45:184–192, 2006.
- [77] D.R. Marshall, S. Saito, and R. Kobayashi. Hydrates at high pressures: Part i. methane-water, argon-water, and nitrogen-water systems. *AIChE Journal*, 10(2):202–205, 1964.
-

BIBLIOGRAPHY

- [78] Y. Masuda, M. Kurihara, and T. sato. A field-scale simulation study on gas productivity of formations containing gas hydrates. Fourth International Conference on Gas Hydrates, Yokohama, Japan, 2002.
- [79] P.L. McGuire and L. Alamos. Recovery of gas from hydrate deposits using conventional technology. In *SPE Unconventional Gas Recovery Symposium, Pittsburgh, Pennsylvania*, 1982.
- [80] V. Mckoy and O. Sinanoglu. Theory of dissociation pressure of some gas hydrates. *Journal of Chemical Physics*, 38(12), 1963.
- [81] A.V. Milkov, R. Sassen, I. Novikova, and E. Mikhailov. Gas hydrates at minimum stability water depths in the gulf of mexico: Significance togeohazard assessment. In *Transactions Gulf Coast Association of Geological Societies*, 2000.
- [82] B. Miller and E.R. Strong. *Proceedings - American Gas Association*, 27(80), 1945.
- [83] G. Moridis, J. Apps, K. Pruess, and L. Mye. Eoshydra: a tough2 module for ch₄-hydrate release and flow in the subsurface. In *Berkeley National Laboratory*, 2000.
- [84] G.J. Moridis, T.S. Collett, R. Boswell, M. Kurihara, M.T. Reagan, C. Koh, and E.D. Sloan. Towards production from gas hydrates: current status, assessment of resources and simulation-based evaluation of technology and potential. SPE Unconventional Reservoir Conference, Colorado, U.S., 2008.
- [85] G.J. Moridis and M.B. Kowalsky. *Gas Production from Unconfined Class 2 Hydrate Accumulations in the Oceanic Subsurface*, in book *Economic Geology of Natural Gas Hydrates*. Kluwer Academic/Plenum Publishers, 2006.
- [86] G.J. Moridis and M.T. Reagan. Gas production from class 2 accumulation in the permafrost. SPE Annual Technical Conference and Exhibition, 2007.
- [87] G.J. Moridis and M.T. Reagan. Strategies for gas production from an oceanic class 3 hydrate accumulations. Offshore Technology Conference, Houston, Texas, USA, 2007.
- [88] G.J. Moridis and E.D. Sloan. Gas production potential of disperse low-saturation hydrate accumulations in oceanic sediments. *Energy Conversion and Management*, 48(6):1834–1849, 2007.
- [89] A.S. Myerson. *Handbook of Industrial Crystallization*. Butterworth-Heiermann, 1993.
- [90] S. Nakano and K. Ohgaki. Relative cage occupancy of co₂ methane mixed hydrate. *Journal of Chemical Engineering of Japan*, 33(3):554–556, 2000.
- [91] P.H. Nelson. Pore-throat sizes in sandstones, siltstones, and shales. *AAPG Bulletin*, 95:1448–1453, 2011.
- [92] H.J. Ng and D.B. Robinson. *Fluid Phase Equilibrium*, 21:145, 1985.
- [93] H.J. Ng and D.B. Robinson1971. *Gas Proc. Assn. Rsch. Rpt*, 66, 1983.

-
- [94] R.B. Nielse and R.W. Bucklin. Why not use methanol for hydrate control. *Hydrocarbon Process*, 62(4):71–78, 1983.
- [95] B.A. Nikitin. *Izv. Akad. Nauk SSSR*, 1:39, 1940.
- [96] F. Ning, Y. Yu, S. Kjelstrup, T.J.H. Vlught, and K. Glavatskiy. Mechanical properties of clathrate hydrates: status and perspectives. *Energy and Environment Science*, 2012.
- [97] K. Ohgaki, K. Takano, H. Sangawa, T. Matsubara, and S. Nakano. Methane exploitation by carbon dioxide from gas hydrates-phase equilibria for co₂-ch₄ mixed hydrate system. *Journal of Chemical Engineering of Japan*, 29(3):478–483, 1996.
- [98] J.S. Parent and P.R. Bishnoi. Investigation into the nucleation behaviour of methane gas hydrates. *Chemical Engineering Communications*, 144:51–64, 1996.
- [99] J.A. Riomeester, T.A. Tse, C.I. Ratcliffe, and B.M. Powell. *Nature*, 325:135, 1987.
- [100] O.L Roberts, E.R Brownscombe, and L.S. Howe. *Oil and Gas Journal*, 39:37–40, 1940.
- [101] D.B. Robinson and B.R. Mehta. *Journal of Canadian Petroleum Technology*, 10(33), 1971.
- [102] D.B. Robinson and D.Y. Peng. The characterization of the heptanes and heavier fractions for the gpa peng-robinson programs. In *Research Report PR-28*. Gas processors association, 1978.
- [103] J.L. De Roo, C.J. Peters, R.N. Lichtenthaler, and G.A.M. Diepen. Occurrence of methane in hydrate-bearing sediments and under saturated solutions of sodium chloride and water in dependence of temperature and pressure. *AIChE Journal*, 29:651–657, 1983.
- [104] S. Saito, D.R. Marshall, and R. Kobayashi. Hydrates at high pressures: Part ii. application of statistical mechanics to the study of the hydrates of methane, argon, and nitrogen. *AIChE Journal*, 10(5):734–740, 1964.
- [105] W.K. Sawyer, C.M. Boyer, J.H. Frantz Jr., and A.B. Yost. Comparative assessment of natural gas hydrate production models. In *SPE/CERI Gas Technology Symposium, 3-5 April 2000, Calgary, Alberta, Canada*, 2000.
- [106] X. Wang A.J schultz and Y. Halpern. Kinetics of methane hydrate formation from polycrystalline deuterated ice. *Journal of Physical Chemistry A*, 106:7304–7309, 2000.
- [107] Y. Seo and H. Lee. Hydrate phase equilibria of the carbon dioxide, methane and water system. *Journal of Chemistry Engineering Data*, 46:381–384, 2001.
- [108] Y. Seo and H. Lee. Multiple-phase hydrate equilibria of the ternary carbon dioxide, methane and water mixtures. *Journal of Physical Chemistry B*, 105:10084–10090, 2001.
- [109] P.J. Sheskin. *Handbook of parametric and nonparametric statistical procedures*. CRC Press, 2004.
-

BIBLIOGRAPHY

- [110] P. Skovborg, H.J. Ng, P. Rasmussen, and U. Mohn. Measurement of induction times for the formation of methane and ethane gas hydrates. *Chemical Engineering Science*, 48(3):445–453, 1993.
- [111] E.D. Sloan and C.A. Koh. *Clathrate Hydrates of Natural Gases*. CRC Press, third edition, 2007.
- [112] E.D. Sloan, K.A. Sparks, and J.J. Johnson. *Industrial Engineering Chemistry Research*, 26:1173, 1987.
- [113] V.A. Soloviev. Global estimation of gas content in submarine gas hydrate accumulation. *Russian Geology and Geophysics*, 43:609–624, 2002.
- [114] Y. Song, B. Chen, M. Nishio, and M. Akai. Measurement of clathrate hydrate precipitation from CO₂ solution by nondestructive method. *American Mineralogist*, 89:1247, 2004.
- [115] E. Spangenberg, J. Kulenkampff, R. Naumann, and J. Erzinger. Pore space hydrate formation in a glass bead sample from methane dissolved in water. *Geophysical Research Letters*, 32:L24301, 2005.
- [116] D.K. Staykova, W.F. Kuhs, A.N. Slamatin, and T. Hansen. Formation of porous gas hydrates from ice powders: diffraction experiments and multistage model. *Journal of Physical Chemistry B*, 107:10299–10311, 2003.
- [117] L.A. Stern, S.H. Kirby, W.B. Durham, S. Circone, and W.F. Weite. Laboratory synthesis of pure methane hydrate suitable for measurement of physical properties and decomposition behaviour. pages 232–348, 2000.
- [118] F.H. Stillinger. Water revised. *Science*, 209(4455):451–457, 1980.
- [119] S. Subramannian and E.D. Sloan. Molecular measurements of methane hydrate formation. *Fluid Phase Equilibria*, 158-160:813–820, 1999.
- [120] R. Susilo, J.A. Ripmeester, and P. Englezos. Characterization of gas hydrate with pXRD, DSC, NMR, and Raman spectroscopy. *Chemical Engineering Science*, 62:3930, 2007.
- [121] W.J.A.M. Swinkels and R.J.J. Drenth. Thermal reservoir simulation model of production from naturally occurring gas hydrate accumulations. *SPE Reservoir Evaluation and Engineering*, 3(6):559–566, 2000.
- [122] J.L. Thakore and G.D. Holder. Solid-vapor azeotropes in hydrate-forming systems. *Industrial Engineering Chemistry Research*, 26:462–469, 1987.
- [123] B. Tohidi, R. Anderson, M.B. Clennell, R.W. Burgass, and A.B. Biderkab. Visual observation of gas hydrate formation and dissociation in synthetic porous media by means of glass micro models. *Geology*, 29:867–870, 2001.
- [124] B. Tohidi, R. Anderson, M.B. Clennell, J. Yang, A. Bashir, and R.W. Burgass. Application of high pressure glass micromodels to gas hydrate studies. In *Proceeding of the Fourth International Conference on Gas Hydrates, Yokohama*, 2002.

-
- [125] B. Tohidi, A. Dannesh, and A. Todd. *Chemical Engineering Research and Design*, 73:464, 1995.
- [126] D.J. Turner, R.S. Cherry, and E.D. Sloan. Sensitivity of methane hydrate phase equilibria to sediment pore size. *Fluid Phase Equilibria*, 228-229:505–510, 2005.
- [127] D.J. Turner and E.D. Sloan. Hydrate phase equilibria measurements and prediction in sediments. In *Proceedings of the Fourth International Conference on Gas hydrate*, 2002.
- [128] T. Uchida, T. Ebinuma, and T. Ishizaki. Dissociation condition measurements of methane hydrate in confined small pores of porous glass. *Journal of Physical Chemistry B*, 103:3659–3662, 1999.
- [129] T. Uchida, S. Takeya, E.M. Chuvilin, R. Ohmura, J. Nagao, V.S. Yakushev, V.A. Istomin, H. Minagawa, T. Ebinuma, and H. Narita. Decomposition of methane hydrates in sand, sandstone, clays, and glass beads. *Journal of Geophysical Research*, 109(B5206), 2004.
- [130] K.A. Udachin, C.I. Ratcliffe, and J.A. Ripmeester. A dense and efficient clathrate hydrate structure with unusual cages. *Nature*, 40(7):1303–1305, 2001.
- [131] M. Uddin and D. Coombe. Co₂ hydrate formation in geological reservoir by injection of co₂. In *Canadian International Petroleum Conference, Calgary, Alberta, Canada*, 2007.
- [132] M. Uddin, D.A. Coombe, D.A. Law, and W.D. Gunter. Numerical studies of gas-hydrates formation and decomposition in a geological reservoir. SPE Gas Technology Symposium, 2006.
- [133] A. van Cleeff and G.A.M. Diepen. *Recueil des Travaux Chimiques*, 79:582, 1960.
- [134] M.M. Mooijer van ven Heuvel. Phase behaviour and structural aspects of ternary chalthrate hydrate systems. In *Delft University of Technology, PhD dissertation*, 2004.
- [135] P. Villard. *Compt. Rend.*, 106:1602, 1888.
- [136] S. Vitu, R. Privat, J.N. Jaubert, and F. Mutelet. Predicting the phase equilibria of co₂ + hydrocarbon systems with the ppr78 model (pr eos and kij calculated through a group contribution method). *Journal of Supercritical Fluids*, 45:1–26, 2008.
- [137] M. von Stackelberg. *Naturwiss*, 36(327):359, 1949.
- [138] M. von Stackelberg and H.R. Müller. *Naturwiss*, 38:456, 1951.
- [139] M. von Stackelberg and H.R. Müller. *Journal of Chemical Physics*, 19:1319, 1951.
- [140] V.P. Voronov, E.E. Gorodetskii, and S.S. Safonov. Thermodynamic properties of methane hydrate in quartz powder. *Journal of Physical Chemistry B*, 45:86–96, 2007.

BIBLIOGRAPHY

- [141] A. Vysniauskas and P.R. Bishnoi. A kinetics study of methane hydrate formation. *Chemical Engineering Science*, 38(7):1061–1072, 1983.
- [142] A. Vysniauskas and P.R. Bishnoi. Kinetics of ethane hydrate formation. *Chemical Engineering Science*, 40(2):299–303, 1985.
- [143] W.F. Waite, B.J. deMartin, S.H. Kirby, and J. Pinkston. Thermal conductivity measurements in porous mixtures of methane hydrate and quartz sand. *Geophysical Research Letters*, 29:2229, 2002.
- [144] W.F. Waite, W.J. Winters, and D.H. Mason. Methane hydrate formation in partially water-saturated ottawa sand. *American Mineralogist*, 89:1202–1207, 2004.
- [145] N.C. Wardlaw and J.P. Cassan. Oil recovery efficiency and the rock-pore properties of some sandstone reservoirs. *Canadian Petroleum Geology*, 27(2):117–138, 1979.
- [146] O. Yamamuro and H. Suga. Thermodynamic studies of clathrate hydrates. *Journal of Thermal Analysis*, 35:2025–2064, 1989.
- [147] S.O. Yang, S.H. Cho, H. Lee, and C.S. Lee. Measurement and prediction of phase equilibria for water + methane in hydrate forming conditions. *Fluid Phase Equilibria*, 185(1-2):53–63, 2001.
- [148] S.O. Yang, I.M. Yang, Y.S. Kim, and C.S. Lee. Measurement and prediction of phase equilibria for water+co2 in hydrate forming conditions. *Fluid Phase Equilibrium*, 175:75–89, 2000.
- [149] O.Y. Zatsepina, D. Riestenberg, S.D. McCallum, M. Gborigi, C. Brandt, B.A. Buffett, and T.J. Phelps. Influence of water thermal history and over pressure on co2-hydrate nucleation and morphology. *American Mineralogist*, 89:1245–1249, 2004.
- [150] P.L.J. Zitha, Q.P. Nguyen, P.K. Currie, and M.A. Buijse. Coupling of foam drainage and viscous fingering in porous media revealed by x-ray computed tomography. *Transport in Porous Media*, 64:301–313, 2006.